DESIGN OF POTENTIOSTAT AND FLUIDIC CHAMBER FOR BIOSENSING DENGUE DETECTION

BY

NUR HANISAH BINTI AZMI

A dissertation submitted in fulfilment of the requirement for the degree of Master of Science in Engineering

Kulliyyah of Engineering
International Islamic University Malaysia

AUGUST 2024

ABSTRACT

The World Health Organization (WHO) identifies dengue as one of the top ten threats to global health. Statistics in Malaysia show a 148.4 % rise in dengue cases in 2022. Delay in dengue diagnosis may affect severity and mortality of the patient. Early and rapid dengue diagnosis is critical for clinical management, epidemiological strategies and appropriate patient care. There are limitations in both conventional and modern dengue diagnostics. Currently, Rapid Test Kits (RTK) produce fast results and can be used for detection of dengue but cannot detect the patient's susceptibility to dengue haemorrhagic fever and dengue shock syndrome. Reverse Transcription Polymerase Chain Reaction (RT-PCR) tests can distinguish different dengue variants but are time consuming and costly. In this work, an alternative technique using an Integrated Electrochemical Quartz Crystal Microbalance (IEQCM) biosensor with a potentiostat. This rapid and early detection method senses NS1 antigen, provides electronic readouts, and has the potential to identify different dengue variants. Potentiostats have been widely used for electrochemical detection but some of them are bulky, expensive and not suitable for Point-of-Care applications. For this work a portable and flexible potentiostat has been proposed. Unlike traditional rigid potentiostats, this design was fabricated on a flexible printed circuit board. The fabricated potentiostat can perform Cyclic Voltammetry (CV) measurements and experimental results produced ΔE_p of 0.132 V, which is similar to the voltage produced by a commercial potentiostat, EmStat Pico. Next, Electrochemical Impedance Spectroscopy (EIS) measurements were done on the IEQCM sensor to detect NS1 dengue antigen. This detection was performed using EmStat Pico and it measures biological reactions between the biorecognition element (NS1 antibody) and NS1 antigen of dengue samples. The EIS measurement showed the lowest Limit of Detection (LoD) is 2.31 ng/mL and Limit of Quantitation (LoQ) is 6.99 ng/mL. When compared with previous work, with an absolute error of ~ 5 %. This indicates that the design potentiostat is a viable tool for dengue diagnosis.

خلاصة البحث

تعتبر منظمة الصحة العالمية حمى الضنك واحدة من التهديدات العشرة الأولى على الصحة العالمية، وأظهرت الإحصائيات في ماليزيا ارتفاعاً بنسبة 148.4% في حالات حمى الضنك في عام 2022. وقد يؤدي التأخير في تشخيص حمى الضنك إلى زيادة شدة المرض وازدياد خطر الوفاة، لذلك يعدّ التشخيص المبكر والسريع لحمى الضنك أمراً بالغ الأهمية للإدارة السريرية والاستراتيجيات الوبائية والرعاية المناسبة للمرضى. وهناك محددات في كل من التشخيص التقليدي والتشخيص الحديث لحمى الضنك، ففي الوقت الحالي، يمكن الحصول على نتائج سريعة باستخدام مجموعات الاختبار السريع (RTK)، حيث يمكن استخدامها للكشف عن حمى الضنك، ولكنها لا تستطيع اكتشاف قابلية المريض للتعرض للإصابة بحمى الضنك النزفية ومتلازمة صدمة حمى الضنك. إنّ اختبارات النسخ العكسي لتفاعل سلسلة بوليمراز (RT-PCR) يمكنها تمييز الأشكال المختلفة لحمّى الضنك، ولكنها مكلفة، وتستغرق وقتاً طويلاً. وفي هذه الدراسة، تم اقتراح تقنية بديلة تستخدم المستشعر الحيوي لتوازن بلور الكوارتز الكهروكيميائي المدمج (IEQCM)، إضافة إلى جهاز التحكم بالجهد (potentiostat). وطريقة الكشف السريع والمبكر هذه تستشعر مستضد (NS1)، وتوفر قراءات إلكترونية، ولديها القدرة على تحديد الأشكال مختلفة من حمى الضنك. وقد تم استخدام أجهزة التحكم بالجهد على نطاق واسع للكشف الكهروكيميائي، ولكن بعضها كبير الحجم، ومكلف، وغير مناسب لتطبيقات نقطة الرعاية. وفي هذه الدراسة، تم اقتراح جهاز تحكم بالجهد محمول ومرن، على عكس أجهزة التحكم بالجهد الصلبة التقليدية، حيث تم تصنيع هذا التصميم على لوحة دوائر مطبوعة مرنة. وجهاز التحكم بالجهد المصنَّع في هذه الدراسة يمكنه إجراء قياسات الجهد الدوري (CV)، حيث كانت قيمة فرق الجهد (ΔE_p) التي تم الحصول عليها من النتائج التجريبية 0.132 فولت، وهي مشابهة لقيمة الجهد الذي ينتجه جهاز التحكم بالجهد (EmStat Pico). بعد ذلك، تم إجراء قياسات التحليل الطيفي للمقاومة الكهروكيميائية (EIS) على مستشعر (IEQCM) للكشف عن مستضد حمى الضنك (NS1)، حيث تم إجراء هذا الكشف باستخدام جهاز التحكم بالجهد (EmStat Pico) الذي يقيس التفاعلات الحيوية بين عنصر التعرف الحيوي (الجسم المضاد) (NS1) وبين مستضد (NS1) لعينات حمى الضنك. وقد أظهر قياس (EIS) أنّ الحد الأدنى للكشف (LoD) مقداره 2.31 نانوغرام/ مل، وأنّ الحد الأقصى للكمية (LoQ) مقداره 6.99 نانوغرام/ مل. وبالمقارنة مع الأعمال السابقة، كان مقدار الخطأ المطلق 5٪ تقريباً، مما يشير إلى أنّ تصميم جهاز التحكم بالجهد المقترح هو أداة قابلة للتطبيق لتشخيص حمى الضنك.

APPROVAL PAGE

I certify that I have supervised and read this study and that in my opinion, it conforms to acceptable standards of scholarly presentation and is fully adequate, in scope and quality, as a dissertation for the degree of Master of Science in Engineering.

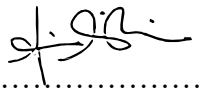

…….
Anis Nurashikin Nordin
Supervisor

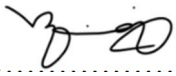

…….
Rosminazuin Ab. Rahim
Co-Supervisor

…….
Aliza ‘Aini Md Ralib @ Md Raghib
Co-Supervisor

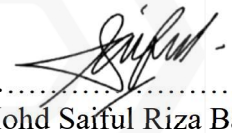

…….
Mohd Saiful Riza Bashri
Co-Supervisor

I certify that I have read this study and that in my opinion it conforms to acceptable standards of scholarly presentation and is fully adequate, in scope and quality, as a dissertation for the degree of Master of Science in Engineering.

…….
Hasmah Mansor
Examiner

…….
Norhayati Soin
External Examiner

This dissertation was submitted to the Department of Electrical and Computer Engineering and is accepted as a fulfilment of the requirement for the degree of Master of Science in Engineering.

…….
Othman Omran Khalifa
Head, Department of Electrical and Computer Engineering

This dissertation was submitted to the Kulliyyah of Engineering and is accepted as a fulfilment of the requirement for the degree of Master of Science in Engineering.

…….
Khairul Azami Sidek
Dean, Kulliyyah of Engineering

DECLARATION

I hereby declare that this dissertation is the result of my own investigations, except where otherwise stated. I also declare that it has not been previously or concurrently submitted as a whole for any other degrees at IIUM or other institutions.

Nur Hanisah Azmi

Signature……  …… Date…….18/08/2024……

INTERNATIONAL ISLAMIC UNIVERSITY MALAYSIA

DECLARATION OF COPYRIGHT AND AFFIRMATION OF FAIR USE OF UNPUBLISHED RESEARCH

DESIGN OF POTENTIOSTAT AND FLUIDIC CHAMBER FOR BIOSENSING DENGUE DETECTION

I declare that the copyright holder of this dissertation are jointly owned by the student and IIUM.

By signing this form, I acknowledged that I have read and understand the IIUM Intellectual Property Right and Commercialization policy.

Affirmed by Nur Hanisah Azmi

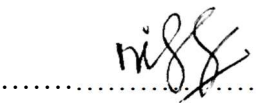

…… Signature

……18/08/2024……. Date

This dissertation is dedicated to my parents for laying the foundation of what I turned out to be in life.

ACKNOWLEDGEMENTS

All glory is due to Allah, the Almighty, whose Grace and Mercies have been with me throughout the duration of my programme. Although it has been tasking, His Mercies and Blessings on me ease the herculean task of completing this dissertation.

I am most indebted to my supervisor, Prof. Dr. Anis Nurashikin Nordin, whose enduring disposition, kindness, promptitude, thoroughness and friendship have facilitated the successful completion of my work. I put on record and appreciate her detailed comments, useful suggestions and inspiring queries which have considerably improved this dissertation. Her brilliant grasp of the aim and content of this work led to his insightful comments, suggestions and queries which helped me a great deal. Despite her commitments, she took time to listen and attend to me whenever requested. The moral support she extended to me is in no doubt a boost that helped in building and writing the draft of this research work. I am also grateful to my co-supervisor, Dr. Rosminazuin Ab. Rahim, Dr. Aliza 'Aini Md Ralib @ Md Raghib and Dr. Mohd Saiful Riza Bashri whose support and cooperation contributed to the outcome of this work.

Lastly, my gratitude goes to my beloved parents and family; for their prayers, understanding and endurance while away.

Once again, we glorify Allah for His endless mercy on us one of which is enabling us to successfully round off the efforts of writing this dissertation. Alhamdulillah.

TABLE OF CONTENT

LIST OF TABLES

LIST OF FIGURES

LIST OF EQUATIONS

CHAPTER 1

INTRODUCTION

1.1 INTRODUCTION

Dengue is a mosquito-borne tropical disease with a rapid increase in the number of dengue fever cases worldwide. It threatens about 40 % of the world's population which is around 3 billion people and spreads throughout more than 100 countries worldwide with tropical and subtropical regions being most greatly impacted, with 100-400 million individuals getting infected each year (Nanaware et al., 2021). The World Health Organization (WHO) identifies dengue as one of the top ten threats to global health earlier in 2019. WHO has released an update on the dengue situation in Malaysia as of December 2022, illustrated in Figure 1.1 (World Health Organization (WHO), 2022). Statistics show that during epidemiological week 51 of 2022, about 2,018 dengue cases were reported bringing the total number of recorded dengue cases for the year to 64,078 cases. This represents a shocking 148.4 % increase over the 25,794 cases reported during the same time in 2021. 50 deaths due to dengue fever had been reported as of epidemiological week 51 in 2022, compared to 19 deaths during the same period in 2021.

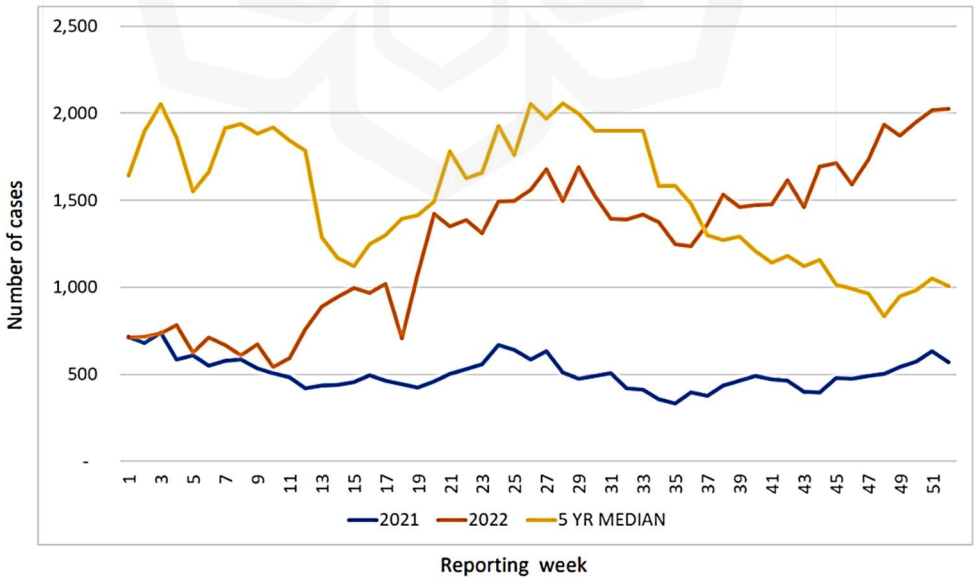

Figure 1.1: Dengue cases reported from 2021 to 2022 in Malaysia (World Health Organization (WHO), 2022).

The primary vectors that transmit the dengue virus are female mosquitoes mainly of the species Aedes aegypti and Aedes albopictus. Diseases like chikungunya, yellow fever and Zika are all spread by these kinds of mosquitoes. Dengue fever is caused by a virus of the Flaviviridae family called dengue virus (DENV). There are five strains of the virus, five unique but closely related serotypes namely DENV-1, DENV-2, DENV-3, DENV-4 and the latest serotypes is DENV-5 which has been announced in October 2013 (Mustafa et al., 2015; Sabir et al., 2021). Dengue infection can occur up to five times with different dengue serotypes, but severe complications and mortality are predicted with each consecutive infection. Infection with one serotype often gives lifetime immunity to that type, but only temporary immunity to the others. According to Singhal et al., severe dengue fever is caused by infection from a serotype of dengue virus during secondary infection (re-infection) that is different from the serotype associated with primary infection (Singhal et al., 2020).

Dengue begins abruptly following a standard incubation period of 5 – 7 days and progresses through the febrile, critical and convalescent stages in primary and secondary dengue infection as seen in Figure 1.2 (Stiba, 2015). Lathika et al. mentioned that during the early febrile phase of dengue infection after onset of symptoms, the single-positive stranded Ribonucleic Acid (RNA) virus secretes high concentrations of the dengue Non-Structural glycoprotein 1 (NS1) antigens (Lathika et al., 2021). While Lovera et al. stated that antibodies such as Immunoglobulin M (IgM) become detectable in the febrile phase of infection, whereas Immunoglobulin G (IgG) emerges in the critical phase of primary infection and during the early stages of secondary infection (Lovera et al., 2019). Severe dengue can occur during primary dengue infection but most commonly occurs among patients with secondary infections with a significant mortality risk. There is currently no effective vaccine to prevent dengue because the existing vaccine against dengue, Dengvaxia is only effective on seropositive individuals who have previously had a dengue virus infection but had a higher risk of developing more severe dengue on those seronegative individuals (Thomas & Yoon, 2019).

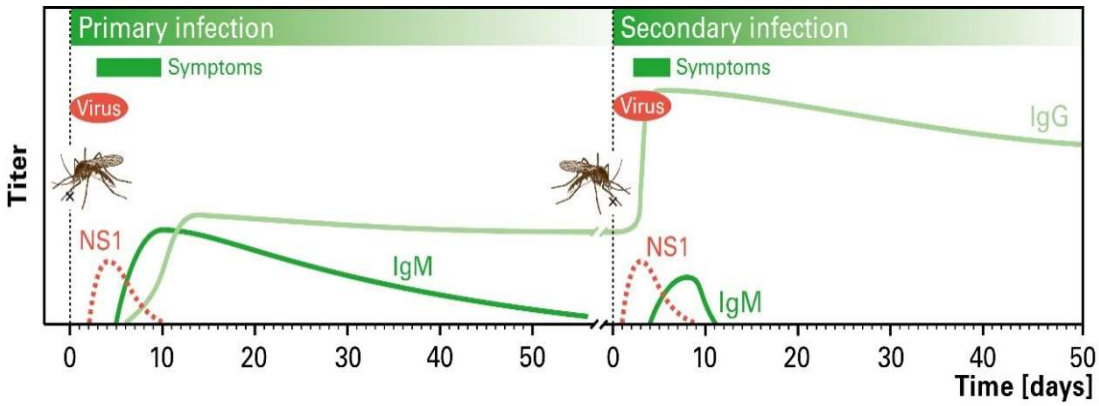

Figure 1.2: Primary and secondary dengue virus infection (Stiba, 2015).

Early and rapid dengue diagnosis is critical for clinical management, epidemiological strategies and appropriate patient care. Anusha et al. presented a wide range of dengue detection methods including both traditional and modern approaches as seen in Figure 1.3 (Anusha et al., 2019). In conventional methods, Rapid Test Kits (RTK) can be used for detection of dengue but cannot detect a patient's susceptibility to dengue haemorrhagic fever and dengue shock syndrome and may produce false positive results (Yan et al., 2020). Reverse Transcription Polymerase Chain Reaction (RT-PCR) tests can distinguish different dengue variants but are time consuming and costly (Sampaio et al., 2022). An enzyme-linked immunosorbent assay (ELISA) test can detect IgG and IgM antibodies produced in response to dengue viral infection in the blood but it requires expensive equipment and trained users for analysis as well as time consuming (Parkash et al., 2021; Sampaio et al., 2022). An alternative to this is the use of electrochemical biosensors with potentiostats which provide electronic readouts to determine the presence of different dengue variants. Biosensors have long been used to drive innovation in the worlds of industry and research and have aided breakthroughs of electrochemistry for over a century due to its real-time measurement, low-cost and high efficiency relative to traditional methods (Cagnani et al., 2022).

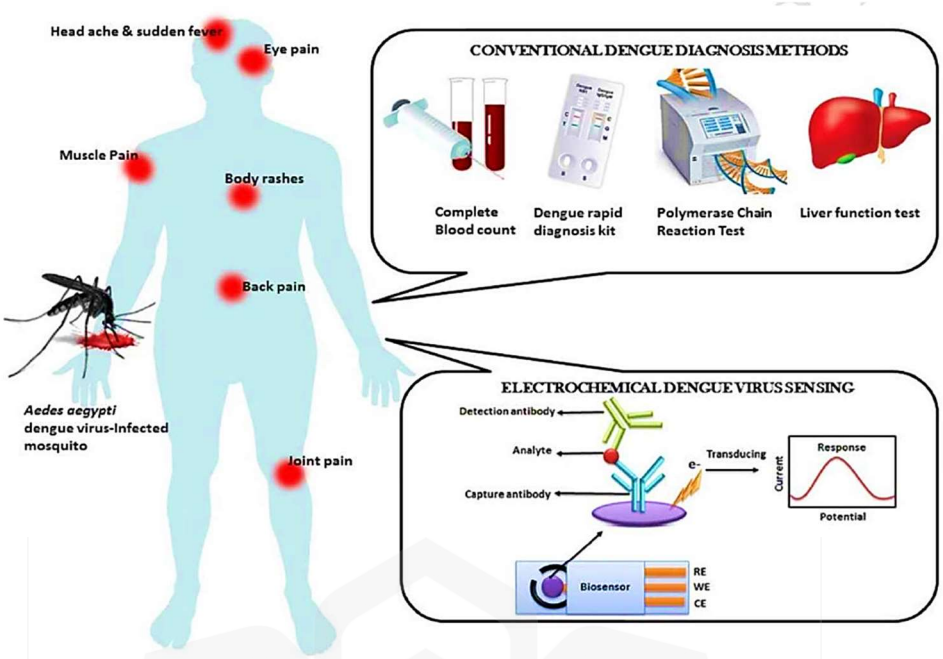

Figure 1.3: Schematic representation of dengue virus infection, symptoms, conventional and electrochemical diagnosis method (Anusha et al., 2019).

Electrochemical biosensors, piezoelectric biosensors and optical biosensors are among the biosensor techniques used in biosensing applications as shown in Figure 1.4. Electrochemical measurement and analytical techniques using potentiostat can measure biological or chemical responses by generating electrochemical signals proportional to the concentration of an analyte to guarantee accurate cell conditioning and signal processing (Abdullah et al., 2019). Integrated Electrochemical Quartz Crystal Microbalance (IEQCM) biosensor is a combination of piezoelectric and electrochemical biosensors monitors the change in mass or electron transfer of layers adhering to the surface of a quartz crystal substrate for dengue diagnosis (A. A. Zainuddin et al., 2019). Potentiostat is an element of choice in biosensing applications due to the high demand of higher-accuracy, higher-precision and higher performance instruments. It has been widely used for electrochemical detection but some of them are bulky, expensive and impractical for Point-of-Care (PoC) applications. This research presents the use of an electrochemical biosensor with portable potentiostat and fluidic chamber in biosensing application for early and rapid dengue virus variants detection.

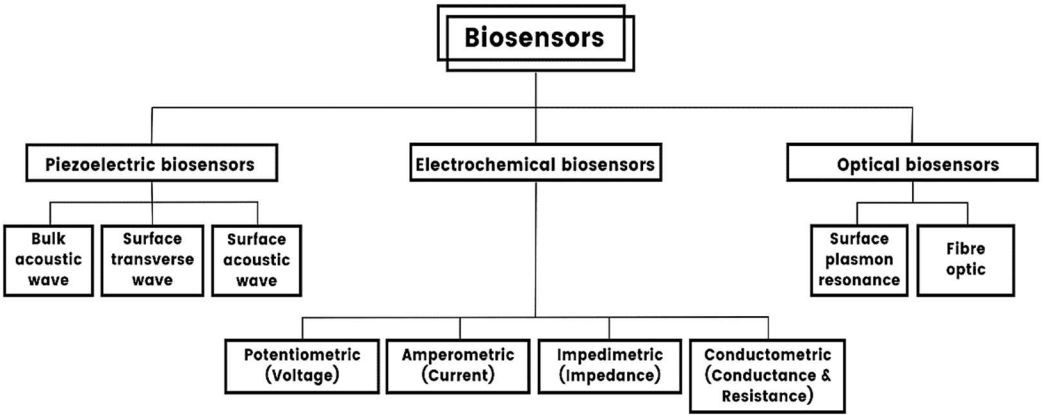

Figure 1.4: Classification of biosensors based on the transduction method or nature to their biological component.

1.2 PROBLEM STATEMENT

Early dengue identification and prompt initiation of appropriate treatment to the patients are vital for successful management of severe dengue virus infections and epidemiological strategies improvement. One of the leading causes of dengue-related deaths is the inability to detect a patient's susceptibility to dengue haemorrhagic fever and dengue shock syndrome, and early diagnosis is the main solution (Raafat et al., 2019). In conventional methods, although virological and serological tests are now still being utilized for dengue fever diagnosis, it was observed that no single measure such as the RTK, RT-PCR and ELISA has met the ideal requirements with high sensitivity and specificity, as well as being rapid and affordable (Yan et al., 2020; Parkash et al., 2021; Sampaio et al., 2022).

Conventional methods such as RT-PCR and ELISA are time consuming as it requires a lot of sequential steps, thermal cycling, large sample volumes, reagents, high end laboratory facilities and well-trained staff (Parkash et al., 2021; Sampaio et al., 2022). RT-PCR, primarily used for detecting nucleic acids like RNA can distinguish different dengue variants but requires assay time of 48-72 hours five days after the initial diagnosis and costs around RM 170 - RM 190 per person (Laurent Bleu Medical Clinic, 2021; Doğan et al., 2022; Qualitas Health Malaysia, 2023). ELISA can identify IgG and IgM antibodies produced in response to dengue virus infection after 14 days

post symptom onset and its assay time may extend up to 26 hours, with kits priced at approximately RM 458.15 (Cook et al., 2021; Parkash et al., 2021; Quick Lab, 2024). RTK tests may produce fast in just 30 minutes - 2 hours and cost around RM 50 - RM 60 but have limited sensitivity, specificity and may yield false positives. In addition, it cannot detect susceptibility of dengue patients to dengue haemorrhagic fever and dengue shock syndrome (Yan et al., 2020; Laurent Bleu Medical Clinic, 2021; Qualitas Health Malaysia, 2023).

An alternative to this conventional method is the use of electrochemical biosensors with potentiostats for early, accurate, rapid and variant dengue detection. Potentiostats have been widely used for electrochemical detection but some of them are bulky with approximately 520 mm x 160 mm x 420 mm size, expensive and impractical for Point-of-Care applications (Alao, 2018; Environmental Expert, n.d.). This challenge is similar to the limitations observed in conventional RT-PCR and ELISA methods, which are laboratory-based and non-portable (J. J. Tsai et al., 2019). Electrochemical biosensors, when compared to commercial ELISA, displayed a high specificity as well as a high sensitivity with a low Limit of Detection (LoD) (Parkash et al., 2021).

IEQCM is one of the electrochemical sensors that is capable of being reused (Wasilewski et al., 2022). IEQCM is reusable for a specific number of cycles, given appropriate care and handling. An IEQCM biosensor with portable potentiostat and miniaturized fluidic chamber has been proposed for early and rapid detection of different NS1 dengue variants. The portability of the proposed potentiostat and fluidic chamber are ideal for PoC diagnostics, enabling patients to monitor health conditions with minimal supervision. NS1 antigen detection is particularly advantageous in early infection compared to IgG and IgM antibody detection, enhancing the efficiency for rapid diagnosis and enabling the identification of different dengue variants.

1.3 RESEARCH OBJECTIVES

The main objective of this research is to design an integrated readout circuit and fluidic chamber for biosensing applications which can be specified as follows:

i. Design and development of a portable potentiostat system for the Integrated Electrochemical Quartz Crystal Microbalance (IEQCM) that can perform Cyclic Voltammetry (CV).
ii. Design and development of a fluidic chamber for integration with IEQCM and potentiostat.
iii. Testing and benchmarking of the completed prototype with commercial potentiostat and with previous research work on dengue detection.

1.4 RESEARCH METHODOLOGY

The methodology employed in this project includes the development and fabrication of both portable potentiostat and fluidic chamber systems that occur concurrently before the integration of both systems as a single dengue diagnostic device. The final result of the research was obtained using the designed potentiostat and the commercialized potentiostat, EmStat Pico integrated together with the fluidic chamber and IEQCM sensor. Surface bio-functionalization was modified on IEQCM sensor for the attachment of the NS1 antibody-antigen of the dengue samples. Testing was done on the potentiostat system using electrochemical measurements such as Cyclic Voltammetry (CV) and Electrochemical Impedance Spectroscopy (EIS). The methodology of the whole system can be visualized by the following flowchart in Figure 1.5.

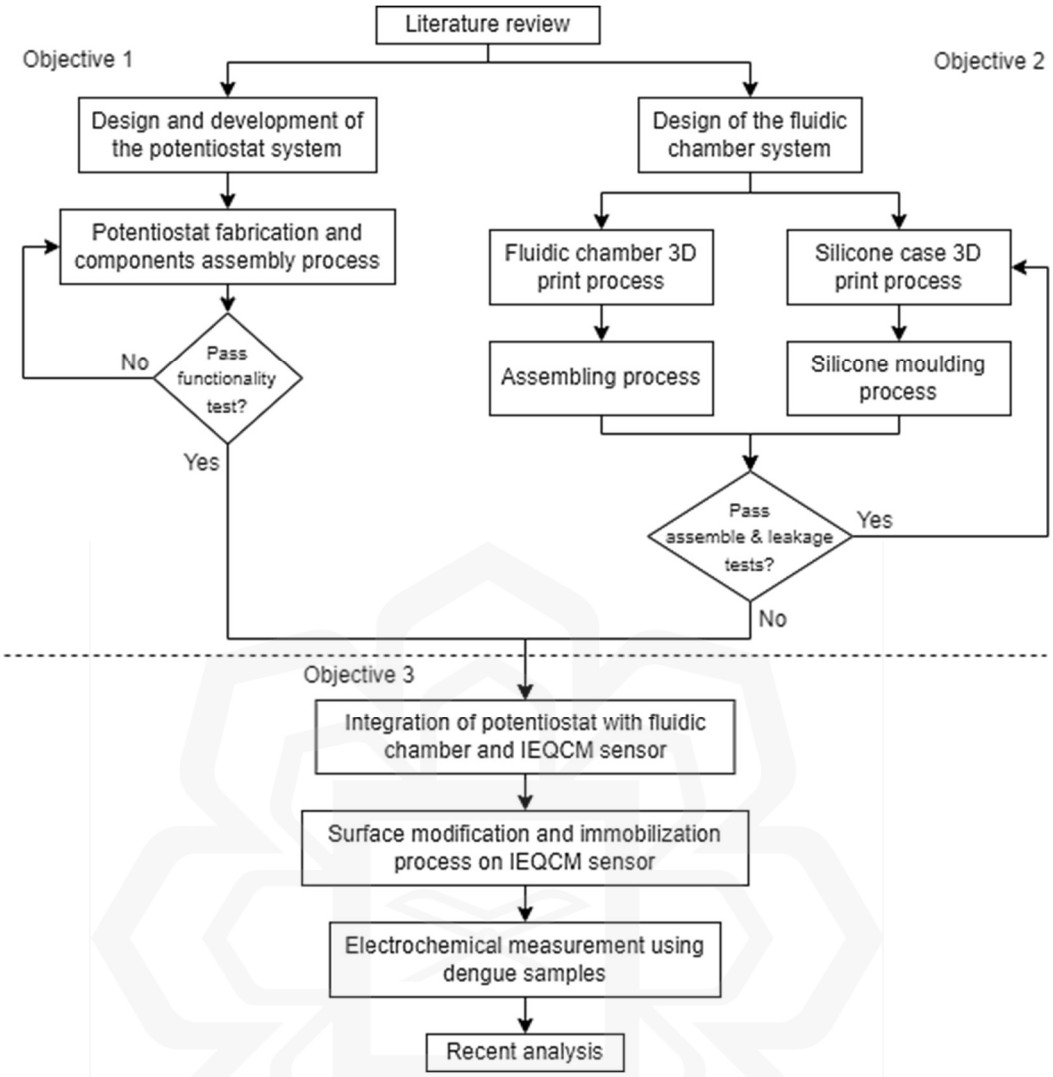

Figure 1.5: Flowchart of the research methodology.

1.5 RESEARCH SCOPE

The focus of this research is to minimize the spread of dengue virus using potentiostats for early diagnosis of dengue fever. Recent advancements in technology have discovered potentiostats as a viable tool for detecting and quantifying viruses with rapid detection, lower costs but higher sensitivity and selectivity that are on par with or better than the traditional diagnostic method. This studies emphasis on the development of a potentiostat system as a Point-of-Care (PoC) dengue diagnostics in a single board together with IEQCM. This research also focuses on the fabrication of the 3-dimensional (3D) printed fluidic chamber to hold the IEQCM sensor during electrochemical measurement.

Several biosensors are used in biosensing applications such as electrochemical biosensors, piezoelectric biosensors and optical biosensors. The QCM sensor used in this research is mainly designed as a piezoelectric biosensor but has been integrated with electrochemical biosensor to become an IEQCM biosensor with dual functionalities. Electrochemical measurement is an element of choice in this research instead of mass sensing for dengue detection. However, the design of the IEQCM biosensor is not included in the scope of this study. The simulation of the electrochemical measurement is also not within the scope of the study.

1.6 ORGANIZATION OF DISSERTATION

The introduction of this research which includes background, problem statement, objectives, methodology and scope of research is presented in Chapter One. The literature review of biosensors such as conventional and modern method of dengue detection and types of existing potentiostats and its basic principles which includes the past related works done by various researchers in developing dengue sensors are reviewed in Chapter Two. In Chapter Three, the methodology of theoretical and novel design of the proposed potentiostat using IEQCM sensor are discussed. Fabrication, characterization and verification process of the potentiostat system and the preliminary results using dengue samples are summarized in Chapter Four. Finally, Chapter Five concludes this research.

CHAPTER 2

LITERATURE REVIEW

2.1 INTRODUCTION TO DENGUE

This chapter explores in depth the facts and various methods of dengue detection which includes both traditional and modern approaches. It is a known fact that dengue fever is caused by dengue virus (DENV). DENV is a single-stranded positive-sense RNA virus that is enclosed and almost spherical in form which can be seen in Figure 2.1. The viral genome consists of the ORF encoding polyprotein that acts as a template for the translation of three structural proteins Capsid (C), Pre-Membrane (PrM), and Envelope (E) and seven non-structural proteins (NS1, NS2A, NS2B, NS3, NS4A, NS4B, NS5) that are essential for viral replication (Nanaware et al., 2021). This RNA virus secretes Non-Structural 1 (NS1) glycoprotein antigens into the blood during the early stages of dengue infection. Individuals who have been infected with dengue have B-cells that secrete antibodies that bind to E and NS1 proteins as well as peptides produced from the PrM protein. B-cells are a type of white blood cell that produces antibodies that are proteins. These antibodies bind to pathogens or foreign substances like viruses, preventing them from accessing normal cells and protecting the host from infection. DENV can be transmitted to humans by the bite of an infected Aedes species mosquito (Ae. aegypti or Ae. albopictus). Codeço et al. emphasized that the transmission cycle of dengue virus is shown in Figure 2.2 where it may spread from infected female mosquitoes to humans and from infected humans to mosquitoes, but it is not contagious from one person to another (Codeço et al., 2018).

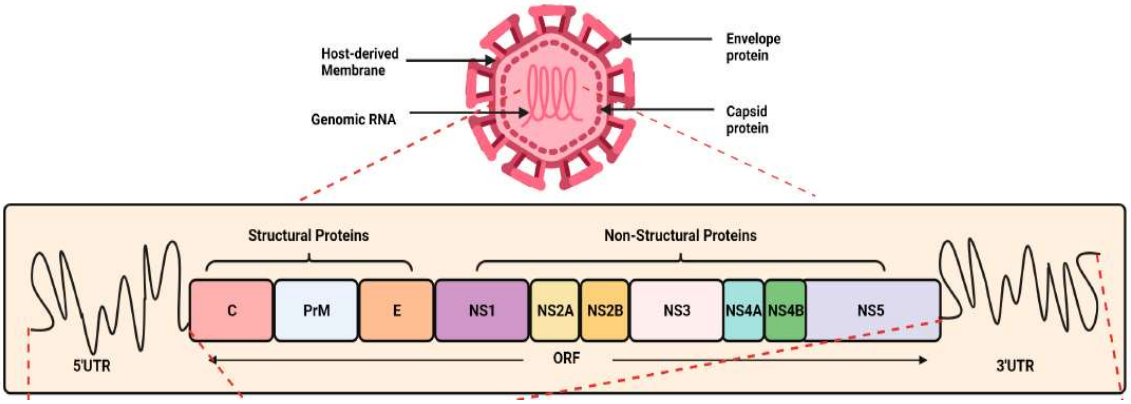

Figure 2.1: Structural organization of dengue virus genome (Nanaware et al., 2021).

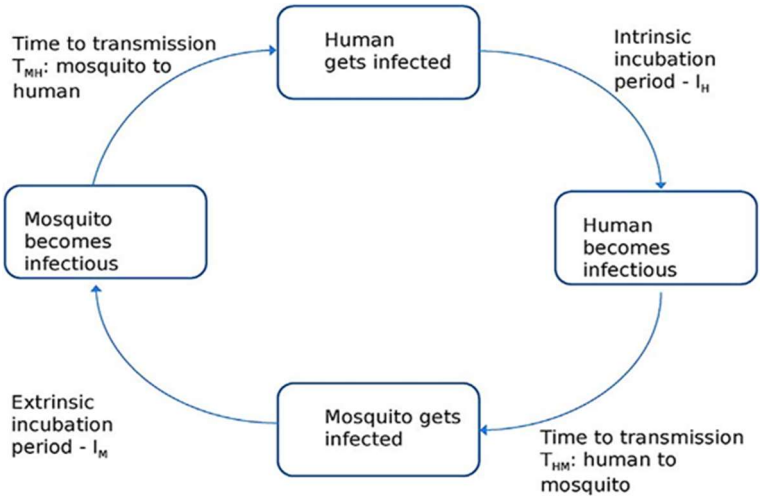

Figure 2.2: Transmission cycle of dengue virus to humans (Codeço et al., 2018).

Dengue is an endemic disease in Southeast Asia and is widespread throughout the tropical and subtropical regions where the risk of dengue varies locally depending on local climatic, socioeconomic and environmental factors. Ryan et al. studied that Ae. aegypti is likely to spread particularly in tropical zones with warm and urban environments as its nature is more heat-tolerant while Ae. albopictus transmission potential is likely to rise substantially in subtropical zones that occur in suburban and rural areas due to its more heat-limited feature (Ryan et al., 2019). Reforestation, climate change, global warming, and lax mosquito control regulations are some of the causes contributing to the increase in dengue rate. Dengvaxia vaccines have been licensed in 20 tropical and subtropical countries for dengue treatment, however they have failed to deliver complete immunity in seropositive individuals and have increased the risk in seronegative individuals when compared with unprotected seronegative individuals (Anasir et al., 2020).

Most dengue cases are asymptomatic but as illustrated in Figure 2.3, it can turn to symptomatic infection that can advance from mild Dengue Fever (DF) to severe Dengue Haemorrhagic Fever (DHF) with a high chance of fatality if not treated effectively (Wang et al., 2020). DF includes a high fever with symptoms like headache, nausea, rash and others. These symptoms can often deteriorate into life-threatening DHF with warning signs such as severe stomach pain, persistent vomiting, breathing problems and many more (Nanaware et al., 2021). Dengue infection occurs erratically after a standard incubation time and advances through the febrile, critical, and

convalescent phases in both primary and secondary dengue infection. Defervescence signals the beginning of the crucial phase of dengue, where the majority of dengue patients recover during this stage but severe dengue patients will become critically ill. The severity of the dengue infection, as well as any medications administered during the febrile and critical phases will impact how well the patient recovers during the convalescent period.

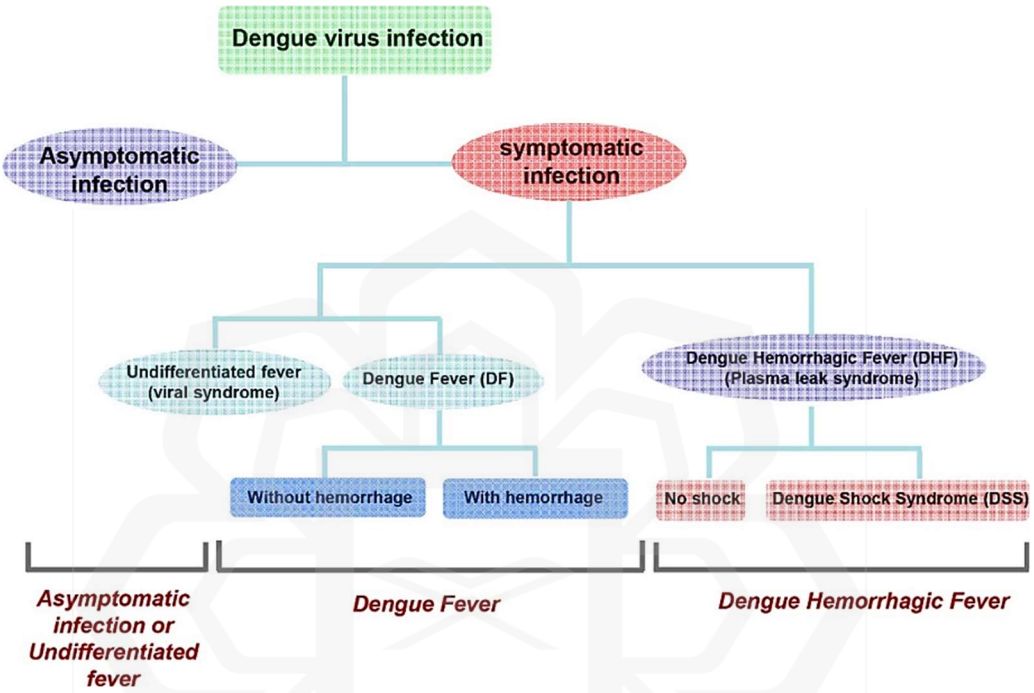

Figure 2.3: Classification of dengue virus infection (Wang et al., 2020).

Delay in dengue diagnosis may affect severity and mortality of the patient. The standard and most widely used clinical diagnostic procedures for dengue detection are virological tests performed during the early stages of infection or serological testing conducted at the end of the acute phase of infection. However, Rapid Test Kits (RTK) cannot determine a patient's vulnerability to dengue haemorrhagic fever or dengue shock syndrome which also may produce false positive results, Reverse Transcription Polymerase Chain Reaction (RT-PCR) tests are time consuming and expensive while Enzyme-Linked Immunosorbent Assay (ELISA) is time consuming, requires professional use and costly (Yan et al., 2020; Parkash et al., 2021; Sampaio et al., 2022). An alternative to the standard dengue diagnosis is the use of electrochemical biosensors which are the analytical system of choice in medical diagnostics when rapid and on-site results are required (Wongkaew et al., 2019). Potentiostats have been widely utilized

for electrochemical detection of different dengue variants, although some of them are large, expensive, and unsuitable for Point-of-Care applications. As a result, the goal of this chapter is to tackle the problem with existing dengue diagnosis tools by developing a portable potentiostat with an electrochemical biosensor for early and variant dengue detection.

2.2 METHOD OF DENGUE DETECTION

2.2.1 Conventional Method

It is essential to detect dengue virus immediately in the early phase of infection to prevent it from progressing into a severe one in a matter of time. Figure 2.4 depicts the direct and indirect approaches for dengue detection known as virological and serological diagnosis respectively (Erba Mannheim, 2018). Virological diagnosis has a high likelihood of detecting the specific dengue virus type, while serological diagnosis has a high chance of being detected. Virological tests including virus isolation, genome detection and antigen test have better specificity initially during the acute phase of the dengue infections and serological tests for dengue virus-specific antibodies are more practical to detect primary or secondary infections in their early stages but have low specificity.

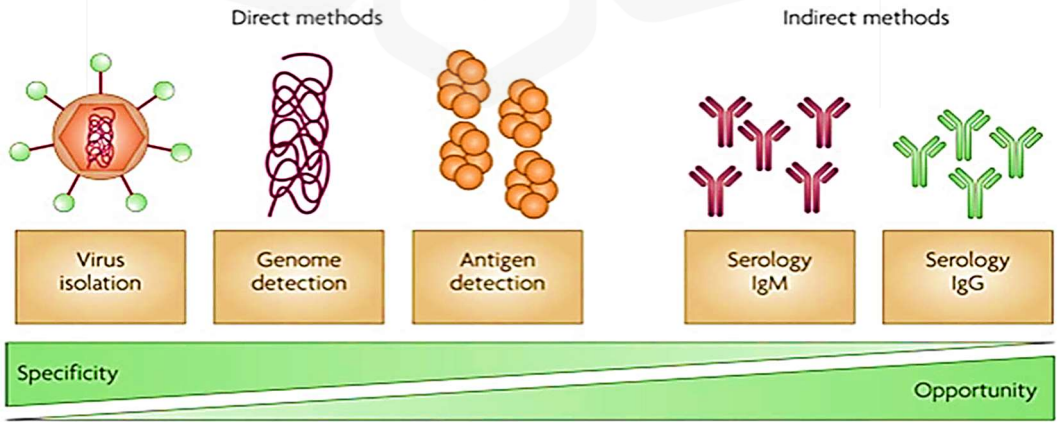

Figure 2.4: Direct and indirect methods for dengue diagnostics (Erba Mannheim, 2018).

2.2.1.1 Virological Test

Virus isolation, genome detection and antigen detection directly test for elements of the virus. Both virus isolation and genome detection were tested using the RT–PCR method. Virus isolation is the gold standard as it is a simple, reliable and commonly used approach for dengue virus diagnosis that provides the most accurate result especially when serum samples are acquired up to five days after the onset of illness (Muller et al., 2017). Virus isolation has high specificity when done during the acute phase of infection before the presence of antibodies and when the amount of virus titre in serum or blood is high but it is tedious as it requires sophisticated laboratory equipment and well-trained staff.

The Flaviviridae viral family consists of four genera of enfolded viruses having a single-stranded ribonucleic acid (RNA) genomic sequence that is positive in sense (Hegde & Bhat, 2022). Dengue genome detection is the most reliable viral infection diagnostic method that focuses on detecting the viral genome or its specific segment and it may distinguish dengue serotypes resulting in better specificity when integrated with real-time technologies. Unfortunately, this approach cannot be used once the virus in the blood has completely degraded and it also necessitates specialized operators and costly reagents, limiting its applicability. Generally, RT-PCR test costs around RM 170 – RM 190 per person and requires assay time of 48 - 72 hours (Laurent Bleu Medical Clinic, 2021; Doğan et al., 2022; Qualitas Health Malaysia, 2023).

The Non-Structural (NS1) protein is a glycoprotein produced in the cells of people infected with dengue (Hegde & Bhat, 2022). The NS1 antigen test using ELISA has been widely used as a diagnostic for early identification of dengue disease notably during primary and secondary dengue infections before the emergence of antibodies. Even though these technologies for dengue diagnosis have been established and are commercially available, extensive validation has revealed that they have a low sensitivity for NS1 detection and necessitates consecutive laboratory investigations to identify the dengue virus which is time-consuming (Izuan Abdul Rashid & Azah Yusof, 2018).

2.2.1.2 Serological Test

Dengue virus-specific antibodies such as Immunoglobulin M (IgM) or Immunoglobulin G (IgG) are formed after an acute phase of dengue infection and can be detected using serological tests. ELISA is the most frequently used approach as it may confirm the presence of a recent or past infection by measuring IgM and IgG antibodies and it have easy processes, reasonable sensitivity and provides quick outcomes compared to techniques such as nucleic acid detection where it requires health professional and laboratory instrument (Raafat et al., 2019). Identification of IgG and IgM antibodies using ELISA requires assay time up to 26 hours, with kits priced at approximately RM 458.15 (Cook et al., 2021; Parkash et al., 2021; Quick Lab, 2024). ELISA demands a high level of expertise to run specific equipment leading to higher expenses.

2.2.2 Modern Approach

2.2.2.1 Biosensing Technique

Recent studies have suggested the use of biosensors as a novel dengue diagnosis tool which are advantageous over traditional approaches. The benefits and drawbacks of traditional approaches have been comprehensively examined in terms of sensitivity, accuracy, rate of detection, detection limit, and ability to be used in clinical applications (Eivazzadeh-Keihan et al., 2019). Biosensor applications are used to increase the accuracy and efficiency of monitoring biological reactions used in medical science, pollutant detection, plant biology, food safety, and drug discovery (Chadha et al., 2022). An alternative to this conventional method is the use of electrochemical biosensors with potentiostats for early, rapid and variant dengue detection. Reusability of biosensors in an application is crucial to enhance the efficiency of diagnosis and IEQCM is one of the electrochemical sensors that is capable of being reused (Wasilewski et al., 2022).

2.2.3 Summary of Method for Dengue Detection

Table 2.1: Summary of dengue detection method.

Research Work	Approach	Contributions	Limitations
Clinical and Laboratory Diagnosis of Dengue Virus Infection (Muller et al., 2017); Dengue detection: Advances and challenges in diagnostic technology (Hegde & Bhat, 2022); Laboratory Diagnosis and Potential Application of Nucleic Acid Biosensor Approach for Early Detection of Dengue Virus Infections (Izuan Abdul Rashid & Azah Yusof, 2018).	Conventional Method: Virus isolation; genome detection; antigen test.	• Simple, reliable and commonly used. • High specificity for early phase dengue virus diagnosis. • Commercially available at a reasonable price.	• Necessitate well-trained personnel. • Time-consuming. • Require high-cost facilities. • Low sensitivity of NS1 detection.
A review of dengue diagnostics and implications for surveillance and control (Raafat et al., 2019).	Conventional Method: Serological diagnosis.	• Easy processes. • Reasonable sensitivity. • Provide quick outcomes.	• Demand high expertise. • Higher expenses. • Limited availability.
Dengue virus: a review on advances in detection and trends – from conventional methods to novel biosensors (Eivazzadeh-Keihan et al., 2019).	Modern Approach: Biosensing technique.	• High accuracy and efficiency of monitoring biological reactions. • Used in illness monitoring and disease markers.	• Detection limit. • Detection time. • Specificity limitation.

2.3 INTRODUCTION TO BIOSENSORS

2.3.1 Basic Principles of Biosensors

Innumerable researchers have studied this before, and so have other neoteric researchers; but it was first developed by Leland C. Clark, Jr in 1956 (Bhalla et al., 2016). Biosensor is an analytical device that measures biological or chemical reactions and converts it into an electrical signal. Figure 2.5 depicts a typical biosensor which includes analyte, bioreceptor, transducer and signal output (Kim et al., 2019). An element of interest that requires identification is referred to as an analyte. A bioreceptor includes enzymes, cells, aptamers, Deoxyribonucleic Acid (DNA) and antibodies is a molecule that detects the analyte. Transducers transform one type of energy into another by converting a bio-recognition event into a quantifiable signal. Electronic part analyses and displays the transduced signal made up from complicated electronic circuitry that performs signal conditioning functions such as amplification and digital signal conversion. The display is a combination of hardware and software that delivers user-friendly biosensor results in numeric, visual, tabular, or graphic form. Among the biosensor approaches utilized in biosensing applications are electrochemical biosensors, piezoelectric biosensors and optical biosensors. Electrochemical biosensors are the analytical system of choice when rapid and on-site results are required in dengue diagnostics.

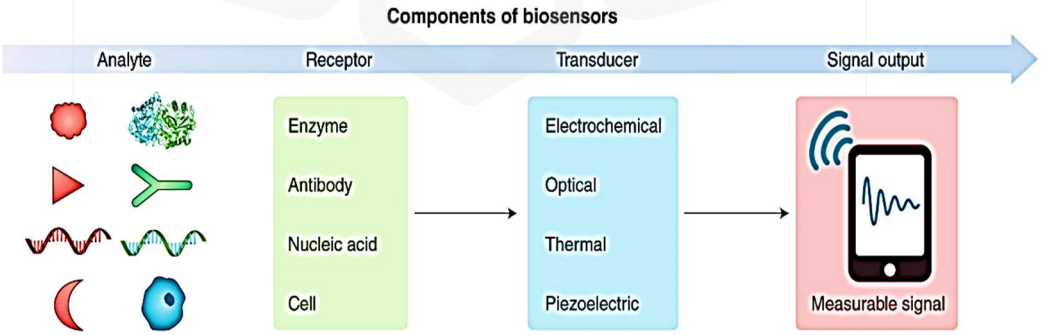

Figure 2.5: A typical biosensor system (Kim et al., 2019).

2.3.2 Electrochemical Biosensor

Electrochemical biosensor is a device that connects a chemically selective layer which is the recognition element to an electrochemical transducer that converts the chemical signal into an electrical signal and provides information about the composition of a system in real time. In fact, the electrochemical biosensor was the first commercially available biosensor which works by consuming or producing ions or electrons during electrochemical interactions between immobilised bioreceptors and target analytes. Potential and current are the electrochemical parameters of solution that can be used to determine the presence of analytes. Electrochemical biosensors are usually made up of a three-electrode system. The three-electrode arrangement is appropriate for monitoring signal responses such as current or impedance coming from oxidation-reduction (redox) species in electrochemical cells. Figure 2.6 shows the conventional three-electrode setup and commercial screen-printed electrodes used in electrochemical measurements (Damiati & Schuster, 2020). The three-electrode configuration system in electrochemical cells includes a working electrode (WE), counter electrode (CE) and reference electrode (RE) and is often used in electrochemistry experiments.

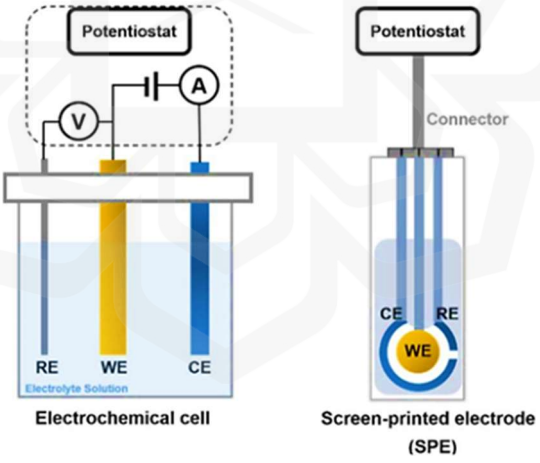

Figure 2.6: The conventional three-electrode setup and commercial screen-printed electrodes in electrochemical measurements (Damiati & Schuster, 2020).

Most chemical reactions occur on the surface of WE and CE is used to flow the electric current in this system. The potential difference between WE and CE is measured with respect to the RE and RE is used to adjust the ohmic drop between WE and RE, as the current is pushed to flow between WE and CE. The measured potential

is the result of ions passing between these electrodes in the electrolyte solution. On the surface of the WE and CE, positive and negative ions will combine to create an electric double layer (EDL). As a result of the change in electron-transfer kinetics of redox processes in the EDL region, changes in impedance, current, and capacitance can be evaluated. Potentiometric, amperometric, impedimetric and conductometric are the major types of electrochemical biosensors that are further described in Table 2.2.

Table 2.2: Types of electrochemical biosensors.

Type of Biosensors	Sensor Working Principle	Measured Parameter
Potentiometric	Potentiometric biosensors measure the changes in potential ofan electrode immersed in the solution measured between reference potential and measured potential between analyte and a sensitive surface and potential proportional to the electrochemical concentration (Ding & Qin, 2020).	Oxidation and reduction potential (Voltage).
Amperometric	Amperometric biosensors measure the changes in current intensity from electroactive element generation by applying a constant potential (Bollella & Gorton, 2018).	Electric current.
Impedimetric	Impedimetric biosensors measure the changes in chargeconductance and capacitance at the sensor surface by applying a small amplitude sinusoidal voltage signal to the system. The molecule-to-molecule interaction on the electrode surface obstructs electron flow, resulting in an increase in impedance measurement based on the voltage/current ratio (Preuß et al., 2020).	Impedance.
Conductometric	Conductometric biosensors identify the changes in the electrical conductivity or resistivity of the solution after any reaction. Sinusoidal voltage is commonly used to reduce undesirable effects like double layer capacitance (Soldatkina et al., 2018).	Conductance and resistance.

2.3.2.1 Screen Printed Electrode (SPE)

Screen-printed electrodes (SPEs) are electrochemical measurement devices printed with several types of ink on plastic or ceramic surfaces which enable speedy in-situ examination with great repeatability, sensitivity and accuracy. Reduced graphene oxide was used as a carbon-based nanomaterial in Screen-Printed Carbon Electrodes (SPCEs) while gold was used in Screen-Printed Gold Electrodes (SPGEs). Both SPEs are intended for the development of biosensors with microvolumes and better electrochemical active areas. SPCEs and SPGEs are great platforms for decentralised assays or the development of biosensors and they can be used for electrochemical measurement by dropping or dipping them in solution. The SPCEs electrode was made of carbon for the working and counter electrodes, whereas silver or gold is used for the reference electrode (DropSens, n.d.-a). The working and counter/auxiliary electrodes of the SPGEs electrode are created out of gold, whereas the reference electrode is made of silver (DropSens, n.d.-b). Figure 2.7 shows the commercial Metrohm SPCEs and SPGEs made from ceramic substrate with dimensions of 33.0 mm x 10.0 mm x 0.5mm (Barton et al., 2016).

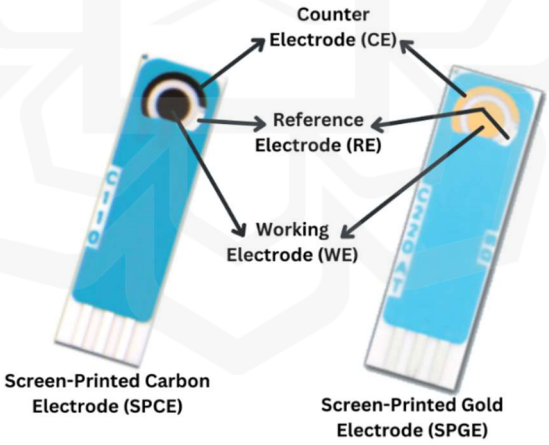

Figure 2.7: The commercial Metrohm SPCE and SPGE (DropSens, n.d.-a; DropSens, n.d.-b).

2.3.2.2 Integrated Electrochemical Quartz Crystal Microbalance (IEQCM)

The Quartz Crystal Microbalance (QCM) is a piezoelectric biosensor which is a mass sensing device that can sense slight changes in mass on a coated surface of the quartz

crystal. A QCM biosensor calculates the mass variation per unit area by measuring the change in frequency of a quartz crystal resonator. However, recent studies have discovered the Integrated Electrochemical Quartz Crystal Microbalance (IEQCM) biosensor which is a combination of piezoelectric and electrochemical biosensors. This sensor consists of three identical quartz crystal microbalance and electrochemical biosensors placed as a radial array on a single substrate that provides dual functionalities in a single measurement platform. Each electrochemical sensor was made of the three-electrode configuration system, working electrode (WE), counter electrode (CE) and reference electrode (RE). It is ideal for monitoring signal responses from electron transfer during redox reactions. IEQCM has been one of the choices amongst other sensors due to its high stability, sensitivity and conductivity as it was made from gold. IEQCM is capable of being reused given appropriate care and handling (Wasilewski et al., 2022). Figure 2.8 indicates the design of an IEQCM sensor having WE and CE constructed of gold on a single quartz substrate with a diameter of approximately 14mm and the optimal radius between each single sensor about 6.0 mm which is specifically used for early dengue diagnosis (A. A. Zainuddin et al., 2019).

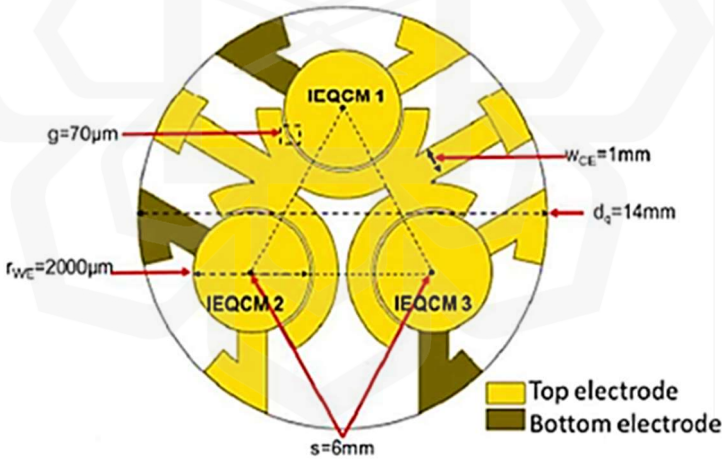

Figure 2.8: The Integrated Electrochemical Quartz Crystal Microbalance (IEQCM) sensor (A. A. Zainuddin et al., 2019).

2.3.3 Electrochemical Measurement

Electrochemical measurements are carried out in an electrochemical cell, which consists of two or more electrodes and electrical circuitry for controlling and measuring current and potential. Normally, three electrodes are used in a typical electrochemical

cell. The working electrode has a voltage that is sensitive to the concentration of the analyte. The counter electrode completes the electrical circuit and serves as a reference for measuring the potential of the working electrode. The counter electrode's potential should ideally remain constant so that any changes in the overall cell potential can be assigned to the working electrode. If the potential of the counter electrode is not constant, a reference electrode will be used with a constant potential. These experiments are based on Ohm's equation, which states that a current (I), passing through a resistance (R), generates a potential (E).

$$E = IR \qquad \text{(Equation 2.1)}$$

The charge transfer resistance (R_{ct}) and kinetics of the redox reaction process can be quantitatively examined using electrochemical detection methods such as Electrochemical Impedance Spectroscopy (EIS) and Cyclic Voltammetry (CV). Potassium ferrocyanide solution is widely employed as a redox couple in electrochemical studies to explore the kinetics of heterogeneous electron transfer reactions in terms of current and impedance changes owing to changes in electrode surface area. When antigens and antibodies of dengue samples are deposited at the working electrode during electrochemical measurements, electrochemical reactions occur, obstructing current flow through the electrode and electrolyte system. This behaviour demonstrates a change in current density and impedance as a result of changes in surface area in the electrode and electrolyte system.

Electrochemical measurement theoretical data can be obtained from the commercialized EmStat Pico development kit through the PSTrace software. EmStat Pico is an embedded electrochemistry with a miniaturized, software enabled, potentiostat system on module. A small system on module (SOM) potentiostat with dimension of 30.5 mm x 18.0 mm x 2.6 mm, the EmStat Pico is the result of a collaboration between Analog Devices and PalmSens BV (Stratmann, 2019). In this research, CV and EIS are the electrochemical measurement of choice measured using the EmStat Pico development kit as displayed in Figure 2.9 that will be used as benchmark result for the designed potentiostat.

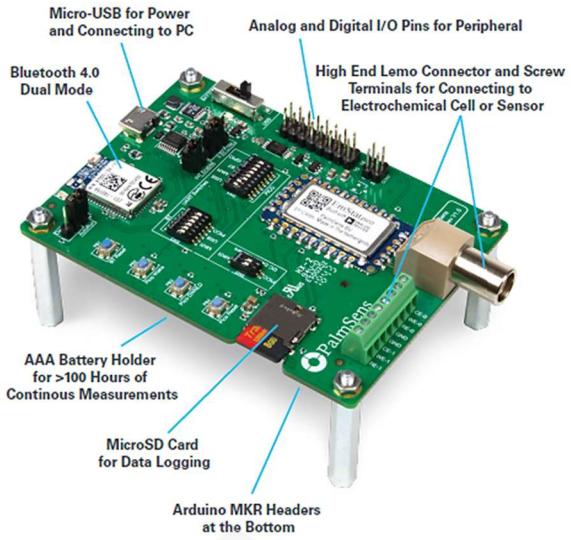

Figure 2.9: EmStat Pico development board (Stratmann, 2019).

2.3.3.1 Cyclic Voltammetry (CV)

Cyclic Voltammetry (CV) is an electrochemical technique used for measuring the current response of a redox active solution. It is performed by changing the voltage of a working electrode and then measuring the current. From CV plot, electrochemical reversibility, electrokinetic behaviour and electrochemical stability of the electron transfer on the electrode-electrolyte interface can be studied. Electron transfer properties are mainly represented by the linear fit on the graph of a peak current (I_{pa}) against the root-squared scan rate ($v^{1/2}$). Figure 2.10 (a, b) demonstrates CV plots at various scan rate, ranging from 50 mV/s to 1000 mV/s and plots of I_{pa} with $v^{1/2}$ to differentiate between the adsorption-controlled and diffusion-controlled processes of the redox reaction that took place at the electrode-electrolyte interface (A. A. Zainuddin, 2020). The anodic peak changes with scan rate and square root of scan rate, the anodic and cathodic peak current plots were linearly dependent on $v^{1/2}$ with a significant correlation coefficient ($R^2 \approx 1$), indicating that the redox process is diffusion-controlled. The electron transfer behaviour can be described as follow:

- Diffusion: Variation of current peaks plots were linearly dependent on $v^{1/2}$.
- Adsorption: Variation of current peaks are linear with the scan rate.
- Molecules in solution: Variation of the current peaks is linear with $v^{1/2}$.

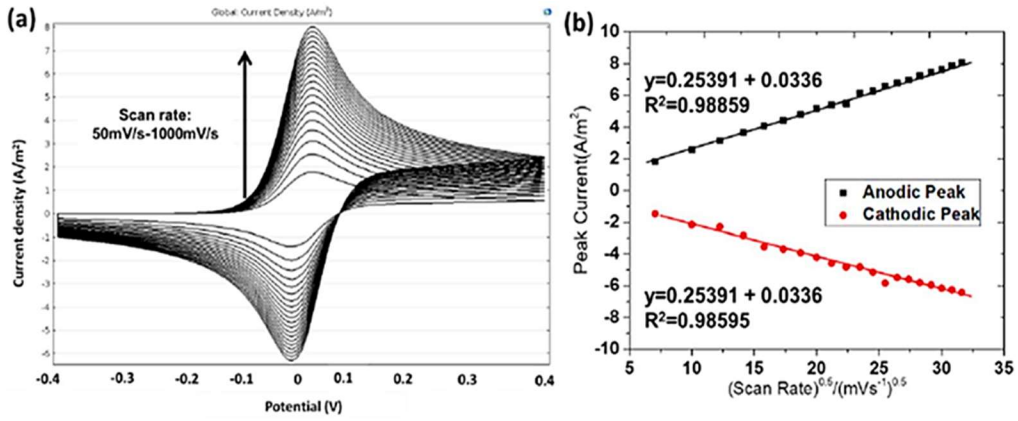

Figure 2.10: (a) CV measurement at different scan rate (b) Plots of the anodic and the cathodic peak currents (I_{pa}) against root-squared scan rate ($v^{1/2}$) (A. A. Zainuddin, 2020).

Electrochemical reversibility of a redox couple is related to the electron transfer rate at the electrode-electrolyte interface which can be determined from the peak-to-peak potential (ΔE_p) separation from the CV plot. The peak current on a CV graph represents an electrode's electron-transfer ability with a greater peak current implying that more electrons get transferred from the solution to the electrode and vice versa. The formula for the peak-to-peak potential (ΔE_p):

$$\Delta E_p = E_{pa} - E_{pc} \qquad \text{(Equation 2.2)}$$

where E_{pa} and E_{pc} are the anodic and cathodic peak potential respectively. Ideal values of ΔE_p are shown below (Graham, 2018) (Benoudjit, 2021):

- Reversible: $\Delta E_p \approx 0.06V$.
- Quasi-reversible: $\Delta E_p > 0.06V$ (with presence of both peaks).
- Irreversible: $\Delta E_p < 0.06V$ (with absence of peak for reverse scan).

Another important aspect of determining a system's electrochemical reversibility is by observing the dependence of anodic (E_{pa}) and cathodic peak potentials (E_{pc}) to the log scan rate as seen in Figure 2.11. E_{pa} shifts towards more positive potential and E_{pc} towards more negative potential when the scan rate increases for all electrodes. As a result, a reversible electrochemical process was considered with the electrochemical processes adhering to the Randles-Sevcik theory for a diffusion-controlled reaction to the electrode surface.

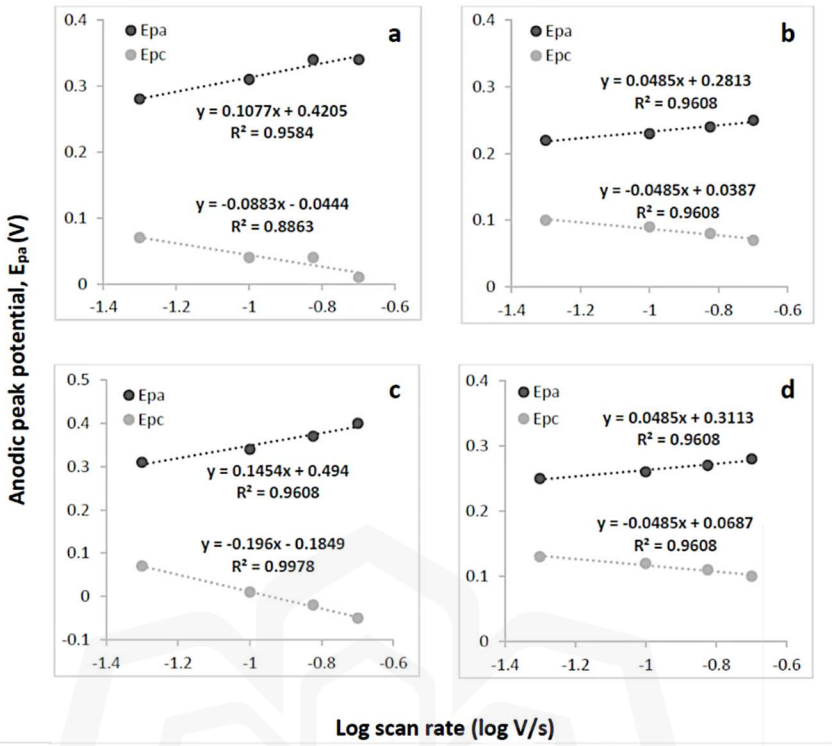

Figure 2.11: Anodic peak potential (E_{pa}) against log scan rate graph (Benoudjit, 2021).

2.3.3.2 Electrochemical Impedance Spectroscopy (EIS)

Electrochemical impedance spectroscopy (EIS) is an electrochemical technique for determining impedance in relation to the frequency of the alternating current potential. In a direct current (DC) system, resistance is the ratio of voltage or potential to current, whereas in an alternating current (AC) system, impedance is the ratio of potential to current. The potentiostat can determine impedance by applying a sinusoidal potential to the working electrode and measuring the output voltage (A. A. Zainuddin, 2020). It calculates real part (Z') and imaginary part (Z'') to represent the impedance (Z) of an electrochemical system and Nyquist plot graphically displays this impedance data (A. A. Zainuddin, 2020). The real and imaginary parts of impedance are related to the magnitude and phase of the impedance, respectively.

The three-electrode arrangement in electrochemical cells is ideal for monitoring signal responses from electron transfer processes during oxidation reduction (redox)

reactions that take place at the surface of WE as shown in Figure 2.12 (Magar et al., 2021). Most chemical reactions occur on the surface of WE and CE is used to flow the electric current in this system. The potential difference between WE and CE is measured with respect to the RE where RE is used to adjust the ohmic drop between WE and RE, as the current is pushed to flow between WE and CE. The measured potential is the result of ions passing between these electrodes in the electrolyte solution.

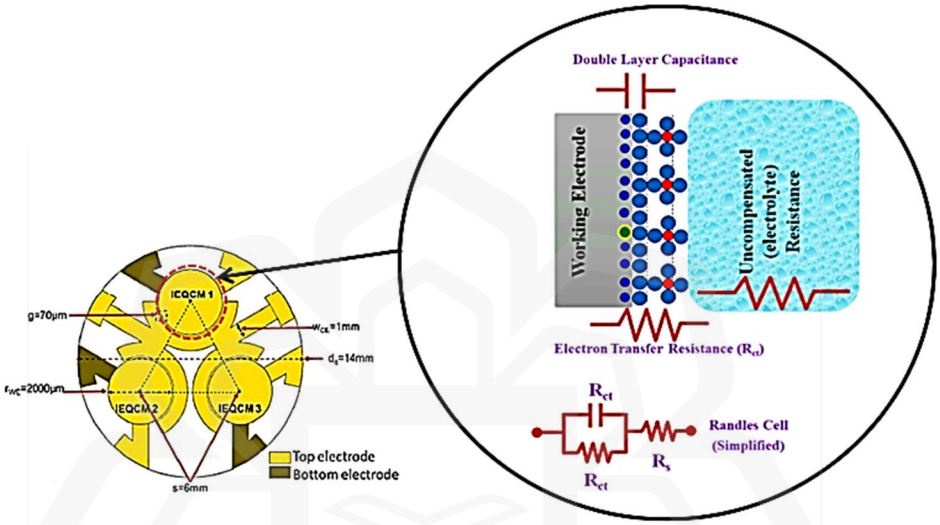

Figure 2.12: A representation of the electron transfer on the surface of a working electrode (WE) during redox reactions (A. A. Zainuddin, 2020; Magar et al., 2021).

Figure 2.13 (a) shows the Nyquist plot and the usage of Randle's equivalent circuit in Figure 2.13 (b) which act as a basic model to depict a solution resistance (R_s), double layer capacitance (C_{dl}) and charge transfer resistance (R_{ct}) (Lasia, 1999; A. A. Zainuddin, 2020). The C_{dl} and R_{ct} values are calculated to indicate how the electrode surface changes over time. These values alter when the capacitance of the electrode surface changes. The Warburg impedance (W) in this system is low because it does not contribute significantly to the overall impedance. The impedance of the Randle's equivalent circuit in Figure 2.13 (b), is defined as:

$$Z(j\omega) = R_s + \frac{1}{\frac{1}{R_{ct}} + j\omega C_{dl}} \qquad \text{(Equation 2.3)}$$

With these ideal or distributed impedance elements placed in series or parallel with each other, these equivalent circuits are used to approximate the experimental impedance data.

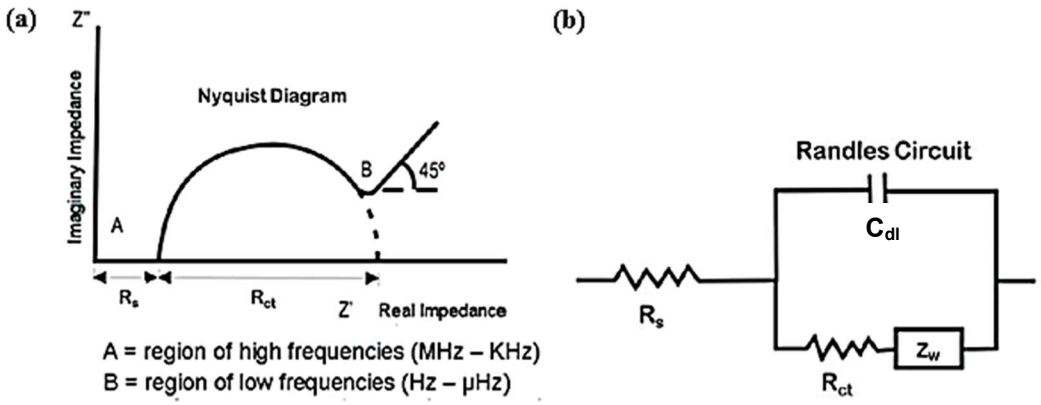

Figure 2.13: (a) Nyquist plot of EIS and (b) Randle's equivalent circuit (A. A. Zainuddin, 2020).

2.4 POTENTIOSTAT FOR POINT-OF-CARE (POC) DIAGNOSTICS

Potentiostat is an essential analytical tool for biosensing application that requires potentiometric signals to measure the reaction between analyte and a surface and potential proportional to the electrochemical concentration in the three-electrode electrochemical system (Yao et al., 2020). This instrument is essential in modern electrochemical research since it allows researchers to investigate reaction pathways in redox chemistry and other chemical phenomena. Potentiostats are used to control most electroanalytical experiments and are commonly used to test for electrochemically active compounds and microbes in solution. The development of potentiostat is important in the fields of healthcare, wearables, environment and many more. However, current existing laboratory potentiostats are normally bulky in size with complex processes and high maintenance cost. There is a high demand of a low-cost and low-power potentiostat development board that is on par with the laboratory-based potentiostat outcomes (Bezuidenhout et al., 2017). Some potentiostat use the IEQCM biosensor for the combination of detection methods which include simultaneous monitoring of mass change performed in parallel with Cyclic Voltammetry (CV) or Electrochemical Impedance Spectroscopy (EIS) measurements as Point-of-Care (PoC) diagnostics (A. A. Zainuddin et al., 2019).

2.4.1 Metrohm Autolab PGSTAT302N

In recent years, electrochemistry has become more significant in novel applications such as biosensors. The Metrohm Autolab PGSTAT302N potentiostat/galvanostat in Figure 2.14 (a, b) represents the most comprehensive and advanced electrochemical instrumentation that is suitable for all electrochemical applications (Alao, 2018). EIS is a powerful technique for the characterization of electrochemical systems. Additionally, it has been widely employed as a tool for analysing the mechanisms involved in electrodeposition, electro dissolution, passivity and corrosion investigations, ion transport across membranes, semiconductor interface research and biosensor development. The compliance voltage and bandwidth of this premium, high current potentiostat/galvanostat are 30 V and 1 MHz respectively. The maximum current is 2 A and current resolution is 30 fA at a current range of 10 nA. The current range may be expanded to 20 A with the BOOSTER20A. The input impedance may be generated with an output impedance more than 1 TOhm and the potential range is around 10 V with a potential precision of 0.3 µV.

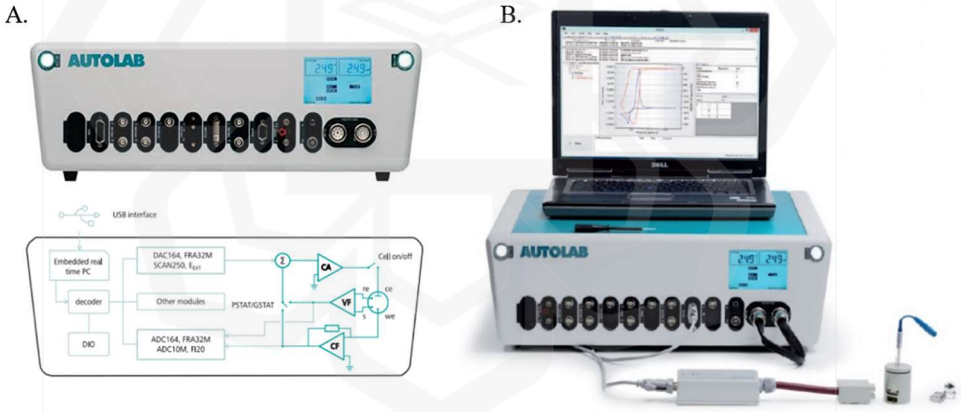

Figure 2.14: (a) The functional diagram of the Autolab potentiostat and (b) the Autolab potentiostat (Alao, 2018).

The potentiostat/galvanostat is a basic instrument that may be used to perform all fundamental electrochemical procedures including Chronoamperometry (CA), Square Wave Voltammetry (SWV), Differential Pulse Voltammetry (DPV) and Cyclic Voltammetry (CV). The FRA32M module allows EIS measurements and enables one to conduct potentiostatic and galvanostatic impedance measurements across a broad frequency range of 10 Hz to 32 MHz but restricted to 1 MHz (University of Antwerp,

n.d.). The input range is approximately 10 V with an AC amplitude of 0.0002 - 0.35 times current range in galvanostatic mode and 0.2 mV to 0.35 Vrms in potentiostatic mode. However, this laboratory sized potentiostat is large with approximately 520.0 mm x 160.0 mm x 420.0 mm in size with high maintenance cost and complex processes (Environmental Expert, n.d.).

2.4.2 ABE-Stat: A Fully Open-Source and Versatile Wireless Potentiostat Project Including Electrochemical Impedance Spectroscopy

ABE-Stat is a small and flexible potentiostat device that comes with software to do numerous standard electrochemical tests, as well as designs and source code that are freely accessible for direct use or adaptation (Jenkins et al., 2019). ABE-Stat is a potentiostat network configurable through a series of high impedance electronically addressable analogue switches, significant attention to isolating noise of digital sections of the device from sensitive analogue signals and use of ADS1220, a high-resolution sensors 24-bit Sigma-Delta Analogue to Digital Converter (ADC) and AD5061, a 16-bit Digital to Analogue Converter (DAC) communicating to the microcontroller through the Serial Peripheral Interface (SPI). ABE-Stat incorporates the capability of conducting EIS measurements across a wide frequency spectrum of 0.1 Hz to 100 kHz and a large range of impedance values with any of four available peak AC amplitudes (100 mV, 50 mV, 20 mV or 10 mV). The Abe-Stat schematic diagram and complete device can be seen on Figure 2.15 (a, b).

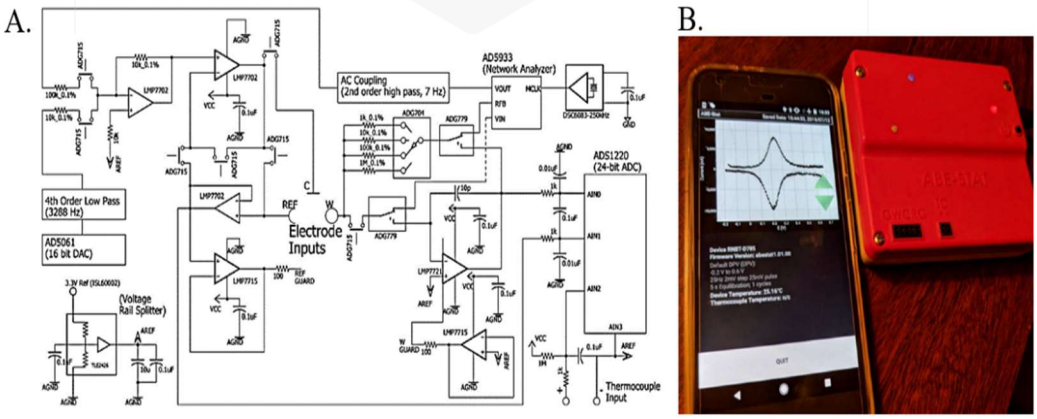

Figure 2.15: (a) The full schematic diagram of the ABE-Stat and (b) the ABE-Stat device interfaced wirelessly to Android apps on smartphones (Jenkins et al., 2019).

The integration of a network analyser chip, AD5933 and modification of the control amplifier network to permit EIS over the spectrum from 0.1 Hz to 100 kHz with arbitrary bias and any of four pre-programmed AC amplitudes is the fundamental novelty of the ABE-Stat analogue network. ABE-Stat is also completely wirelessly enabled through Wi-Fi or Bluetooth and offers an Android interface. The ESP8266 Wi-Fi microcontroller system with embedded Wi-Fi radio, 80 MHz 32-bit CPU, and 4 MB of flash/programmable memory was utilised for system control that also includes a traditional serial Bluetooth module for easy interface with a custom Android app (Jenkins et al., 2019). Setting the states of eight analogue switches through Inter-Integrated Circuit (I^2C) communication allows for the configuration of the electrode network and the composition of the control signal. Additionally, the I^2C port is utilized to manage and read data from the network analyser AD5933. ABE-Stat may be powered directly by a single-cell lithium battery for totally portable operation. However, this device still requires some improvement design with respect to current noise on the ADC control amplifier for voltammetric applications and consistency of EIS measurements.

2.4.3 MiniStat: Development and Evaluation of a Mini-Potentiostat for Electrochemical Measurements

An opportunity has emerged to push electrochemical analysis approaches out of the lab and into new application areas necessitating the development of potentiostat to be portable which enables simple hands-on, embeddable which enables long-term in situ assays and affordable which enables numerous parallel and large-scale tests. MiniStat is a Mini-Potentiostat that enables a range of electrochemical tests to be carried out on a miniaturized, inexpensive device powered by batteries (Adams et al., 2019). The feature of a potentiostat might vary substantially depending on the primary purpose of the device. The primary design objectives of MiniStat are to provide a tool suitable for broad electrochemical analysis in a smaller package size into a single footprint of 27.0 mm x 20.0 mm while keeping manufacturing simplicity and utilizing low-cost discrete components as shown in Figure 2.16 (a, b, c) (Adams et al., 2019).

The MiniStat uses the Microchip Technology ATxmega32E5 microcontroller, the low-power, 32 MHz, 8/16-bit with upgraded Reduced Instruction Set Computing (RISC) based-architecture. This microcontroller includes an internal real-time clock, two 16-bit timer/counters, 26 programmable input/output lines, and 32 KB of flash with additional features of a 12-bit Analog-to-Digital Converters (ADC) and 12-bit Digital-to-Analog Converters (DAC). The Atxmega32E5 is suited for a low-power testing device like the MiniStat because of these qualities. The programming language used to program MiniStat is the C programming language.

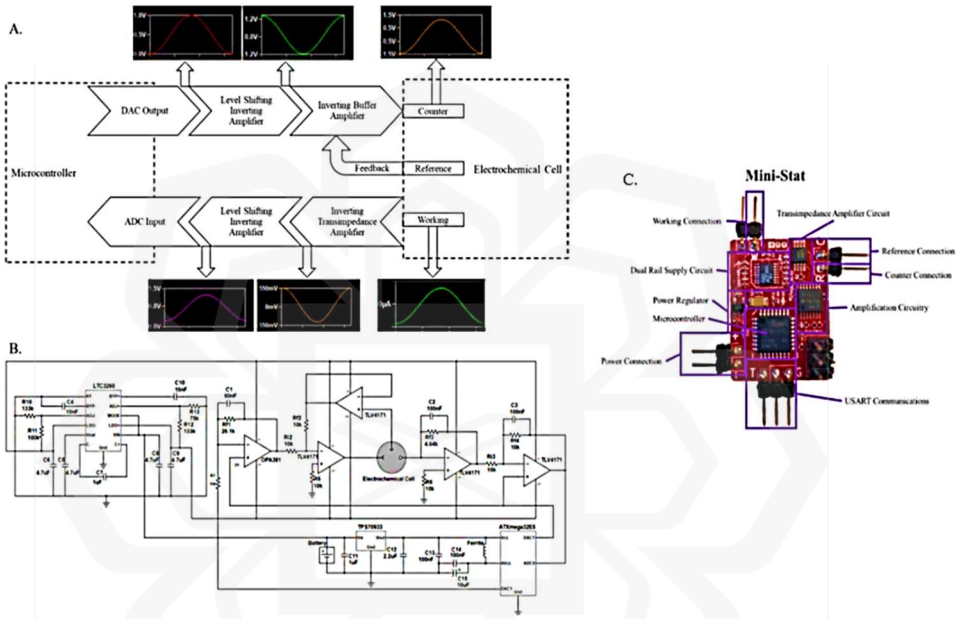

Figure 2.16: (a) The functional diagram of the MiniStat, (b) the full circuit diagram of the MiniStat and (c) the MiniStat device (Adams et al., 2019).

This article provided an overview of how experimental techniques that are traditionally restricted to expensive, large-footprint laboratory equipment may be applied in a low-cost, small-footprint device. This MiniStat device provides a variety of electrochemical experiments such as ChronoAmperometry (CA), Cyclic Voltammetry (CV) and anodic stripping Square Wave Voltammetry (SWV) with accurate results. However, there are a few drawbacks of this MiniStat as it is only intended to be used in circumstances when a full-sized lab potentiostat is impractical or impossible, but it cannot completely replace the laboratory potentiostat. The MiniStat also lacks the extremely advanced software found on the majority of laboratory-grade

potentiostats that utilized a wide range of various experiment kinds, but the MiniStat requires more time to transition between experiment types (Adams et al., 2019).

2.4.4 SIMstat: Hardware Design Considerations for Implementing a Low-Cost, Portable Potentiostat

Development of open-source designs and advancement in microelectronics has now made the potentiostat evolve to be more affordable and portable than tabletop models. This research studies on the design and development for a low-cost and portable potentiostat termed "SIMstat". SIMstat is a new low-cost potentiostat designed by Cook which is mainly intended to speed up the design and implementation of a new low-cost potentiostat and as a source of information for electrical engineers to learn about electrochemical concepts for circuit design (J. Cook, 2020). Figure 2.17 (a, b, c) exhibits the whole functional system of SIMstat.

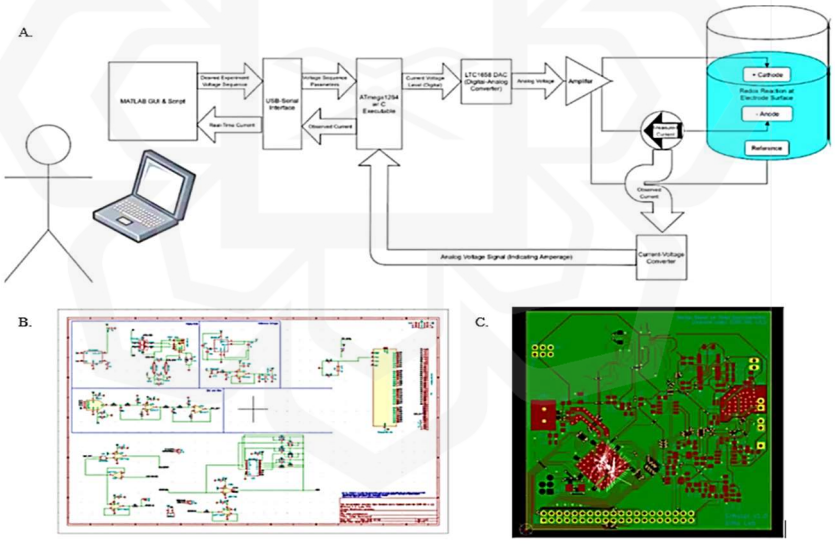

Figure 2.17: (a) SIMstat overall block diagram, (b) draft of SIMstat KiCad schematic design and (c) draft of SIMstat PCB schematic and layout (J. Cook, 2020).

Resolution was a key constraint of pre-existing prototypes in any low-cost potentiostat configuration. The LTC-1658 was utilized because the interfaces between the analogue and digital components are the Analog-to-Digital Converters (ADCs) and Digital-to-Analog Converters (DACs) with a resolution of 14 bits. The ATmega1284

microcontroller was recommended to connect to this device because it features an external clock source with clock rates close to 20 MHz, a second USART module for connecting to the DAC with 10-bit ADC, and a serial-interface compatible USART module. Future work of this study is to interface firmware development with MATLAB (J. Cook, 2020).

This SIMstat has not yet finalized its design but it was intended to carry out Cyclic Voltammetry (CV) tests using three electrodes in real-time and validate its performance with a tabletop potentiostat. The existing potentiostats that are currently in use are not enhanced by the SIMstat design shown in this article. However, the significant effort made to produce SIMstat is to speed up the creation of upcoming inexpensive potentiostats and as a starting point for those who wish to learn more about both electrochemical principles and electrical design (J. Cook, 2020).

2.4.5 KickStat: A Coin-Sized Potentiostat for High-Resolution Electrochemical Analysis

Electrochemical sensor research has increased in response to the need for wearable and point-of-care medical devices which can now monitor a wider variety of biological substances. The development of novel biosensors requires smaller apparatus capable of performing very sensitive amperometric measurements in order to transition from the benchtop to fully portable devices. This study developed KickStat, a coin-sized miniature potentiostat that enables high-resolution electrochemical analysis without the use of complex electronics as displayed in Figure 2.18 (a, b, c) (Hoilett et al., 2020).

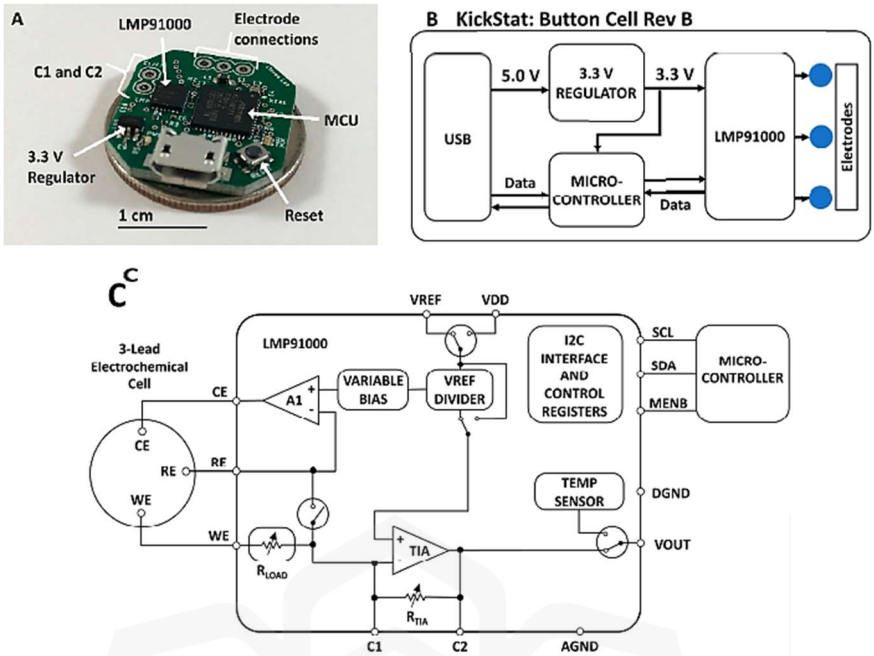

Figure 2.18: (a) Photograph of the assembled KickStat, (b) functional block diagram of KickStat and (c) block diagram of the LMP91000 chip (Hoilett et al., 2020).

KickStat combines a 3-electrode system with the compact size of an integrated LMP91000 programmable potentiostat chip with an inbuilt voltage reference generator. On a specially made 21.6 mm x 20.3 mm circuit board, the ARM Cortex-M0+ SAMD21 microcontroller is merged with the computing capability of the LMP91000 (Hoilett et al., 2020). SAMD21 32-bit microcontroller with on-board debugger (nEDBG), six serial communication modules (SERCOM) configurable as UART/USART, SPI or I^2C, three 16-bit timer/counters, 32-bit Real-Time Clock and calendar, 20 PWM channels, one 14-channel 12-bit ADC, one 10-bit DAC. KickStat managed to accomplish a high-resolution voltage increment and an instrumental limit of detection in a coin-sized form factor by integrating onboard signal processing via the SAMD21. KickStat was coded using Arduino which utilized the C/C++ programming language.

The findings indicate that KickStat is comparable to a high-resolution monitoring of aptamer-based biosensors using Cyclic Voltammetry (CV) and Square Wave Voltammetry (SWV) as well as the general electrochemical measurements like Chronoamperometry (CA) and Normal Pulse Voltammetry (NPV) that is equivalent with high-end benchtop potentiostat. An expensive module-oriented potentiostat like

the EmStat Pico is bigger in size and higher in cost making KickStat more appropriate in wearable and other portable applications (Hoilett et al., 2020; Stratmann, 2019).

2.4.6 Flexible Potentiostat Readout Circuit Patch for Electrochemical and Biosensor Applications

A miniaturized potentiostat readout circuit patch is designed and fabricated on a flexible polyimide substrate using easily accessible electronics for electrochemical or biosensors application (Escobedo et al., 2020). The patch is flexible and portable in contrast to the traditional bulky electrochemical measurement equipment as seen in Figure 2.19 (a). A printed thick film potentiometric pH sensor with a platinum counter electrode was used to monitor pH in a buffer solution to show its capabilities (6 - 8 pH values). The acquired results are consistent with those obtained from a commercially available potentiostat utilized for benchmarking.

A potentiostat is simply an electrical circuit made up of four major components, the control amplifier, electrometer, I/V converter and signal source as analyzed in Figure 2.19 (b) (Escobedo et al., 2020). OPA2227 precision bipolar operational amplifiers are used in this design for the electrometer, control amplifier and I/V converter. These devices run on a 5 V dual supply voltage, necessitating the use of a voltage inverter based on the ADM660 integrated circuit to derive the negative voltage (-5 V) from a 5 V positive supply. The ADM660 was chosen for its low quiescent current (600 A) and simple inverter arrangement, which requires just two external capacitors. This patch includes plans to integrate a microcontroller-based circuit for conversion and communication in the future (Escobedo et al., 2020).

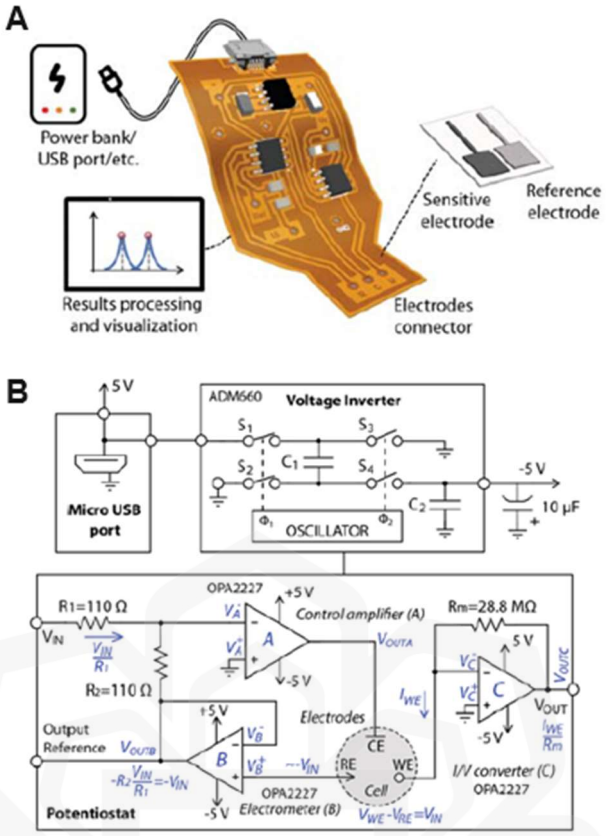

Figure 2.19: (a) Overview of the potentiostat readout circuit patch system, (b) block diagram of the complete readout system (Escobedo et al., 2020).

2.4.7 Summary of Existing Potentiostats

Table 2.3: Summary of existing potentiostats.

Research Work	Approach	Contributions	Limitations
Online Condition Monitoring of Lithium-Ion and Lead Acid Batteries for Renewable Energy Applications (Alao, 2018).	• Equipped with FRA32M module for EIS measurements, enabling potentiostatic and galvanostatic impedance measurements in the frequency range of 10 Hz to 32 MHz. • The maximum current is 2 A and current resolution is 30 fA at a current range of 10 nA with potential range around 10 V with a potential precision of 0.3 μV.	• A basic laboratory electrochemical instrumentation. • Able to perform most fundamental electrochemical procedures CA, SWV, DPV and CV.	• Compact but bulky size. • Involves a complex operating procedure. • High maintenance cost.
ABE-Stat: A Fully Open-Source and Versatile Wireless Potentiostat Project Including Electrochemical Impedance	• Utilizes the high-resolution sensor ADS1220 (24-bit ADC) and AD5061 (16-bit DAC) and integrated with the AD5933 network analyzer chip. • Wirelessly enabled through WiFi or Bluetooth and offers an Android interface.	• Small and flexible potentiostat device. • Offers standard electrochemical tests such as CV, DPV and EIS. • Free accessible designs and source code.	• High noise on the ADC control amplifier. • Wireless functionality unverified. • Inconsistency of EIS measurements.

Spectroscopy (Jenkins et al., 2019).			
MiniStat: Development and Evaluation of a Mini-Potentiostat for Electrochemical Measurements (Adams et al., 2019).	• Powered by the Microchip Technology ATxmega32E5 microcontroller, low-power, 32 MHz, 8/16-bit with upgraded reduced instruction set computing (RISC) based-architecture.	• Miniaturized, inexpensive and battery powered device designed for low-power testing. • Provides a variety of electrochemical tests such as CA, CV and SWV.	• Not suitable as a lab potentiostat replacement. • Lacks the advanced software found in most laboratory potentiostats. • Requires more time to switch between experiment types.
SIMstat: Hardware Design Considerations for Implementing a Low-Cost, Portable Potentiostat (Cook, 2020).	• Incorporates LTC-1658, a 14-bit digital-to-analog converter (DAC) integrated with ATmega1284 microcontroller with 20 MHz external clock source. • Have a second USART module for connecting to the DAC with 10-bit ADC, and a serial-interface compatible USART module.	• Cost-effective potentiostat designed to expedite new low-cost potentiostat designs. • Serve as a resource in circuit design. • Expected to carry out CV measurement.	• The design is currently under finalization. • The existing potentiostats do not incorporate the improvements offered by this design.

Kickstat: A Coin-Sized Potentiostat for High-Resolution Electrochemical Analysis (Hoilett et al., 2020).	• Uses LMP91000 programmable chip integrated with ARM Cortex-M0+ SAMD21 32-bit microcontroller. • Six serial communication modules (SERCOM) configurable as UART/USART, SPI or I^2C, 16-bit timer/counters, one 14-channel 12-bit ADC, one 10-bit DAC.	• Miniaturized potentiostat that enables high-resolution electrochemical analysis without complex electronics. • Able to run CV, SWV, CA and NPV.	• Possesses limitations in electrochemical analysis due to its small size.
Flexible Potentiostat Readout Circuit Patch for Electrochemical and Biosensor Applications (Escobedo et al., 2020).	• Potentiostat readout circuit patch made up of control amplifier, electrometer, I/V converter and signal source. • The electrometer, control amplifier, and I/V converter utilize the OPA2227 op-amplifiers known for low offset voltage.	• Miniaturized and flexible potentiostat readout circuit. • Enable pH measurement.	• Lacks microcontroller-based circuit, limiting capabilities beyond pH measurements.

2.5 SURFACE BIO-FUNCTIONALIZATION

2.5.1 Type of Biological Recognition Element

Potentiostat measures biological or chemical reactions between a chemically selective layer which is the bio-recognition element (NS1 antibody) to the target analytes (NS1 antigen) using an electrochemical biosensor and translates the responses into an electrical signal to provide details on the composition of the dengue samples. Analyte, bio-recognition element, transducer and signal output are four basic elements that make up a typical electrochemical biosensor (Kim et al., 2019; Liu et al., 2020). Bio-recognition elements include enzymes, cells, aptamers, deoxyribonucleic acid (DNA) and antibodies that detect and bind specifically to the analyte. Nucleic acid-based and protein-based bio-recognition elements that can selectively bind to the target analyte as shown in Figure 2.20 are extensively used in microfluidic biosensors (Liu et al., 2020; Loo et al., 2023).

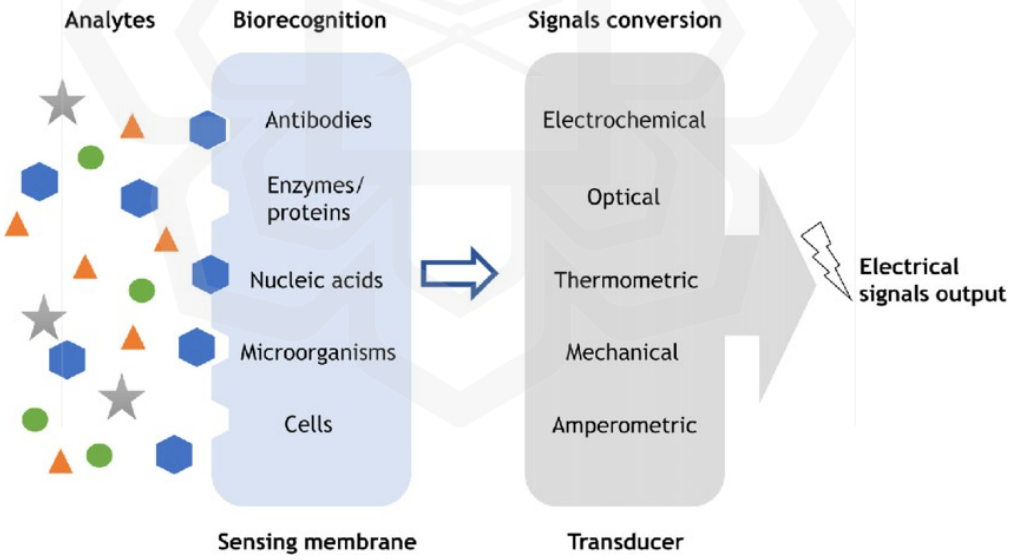

Figure 2.20: Types of bio-recognition elements (Liu et al., 2020).

2.5.2 Surface Modification and Immobilization Techniques

Surface bio-functionalization is the process of modifying the surface characteristics of an electrode that have a wide range of applications in fundamental and applied

electrochemistry research. Electrode surfaces can be functionalized with molecules that have specific physical, chemical or biological functionalities to strongly attach a biorecognition element which binds to the analyte selectively. The bioreceptor components can be immobilized on gold working electrode surfaces using a variety of methods including self-assembled monolayers (SAMs) (Drobysh et al., 2022; Tricase et al., 2022; A. Zainuddin et al., 2022). SAMs are thin molecular layers that build on an electrode surface from chemical solution by adsorption. The three most important components of the SAMs structure, as shown in Figure 2.21 are the head-group, backbone, and end-group (Bobb-Semple et al., 2019; Singh et al., 2020). Their formation is facilitated by a certain functional group that has a great affinity to the surface of the electrode resulting in a microscopic superlattice structure of layers. Thiol adsorption begins with the self-assembly of alkanethiols on gold surfaces, proceeds with thiol group (-SH) physisorption, chemisorption and the breakage of the S-H bond (Sakellari et al., 2020). The headgroup S molecule coats the gold surface, while the alkyl chains that are usually utilized as backbones are tightly packed and form the monolayer via van der Waals interactions (Bobb-Semple et al., 2019; Li et al., 2019).

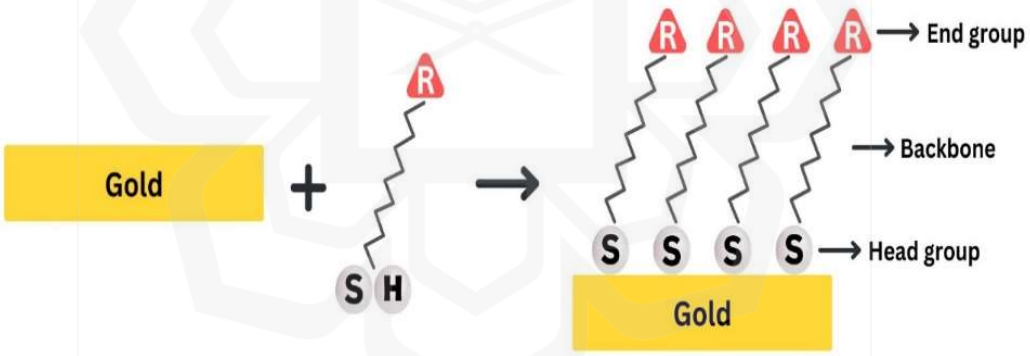

Figure 2.21: Construction of SAM on gold electrode.

SAMs are often formed on gold electrode surfaces using 11-mercaptoundecanoic acid (11-MUA) which has long alkane chains and carboxyl-containing thiols that are densely packed. The formation of SAMs can be accomplished by immobilising 5 mM 11-MUA on a gold film (T. C. Tsai et al., 2019). SAMs can also be modified with absolute ethanol containing 10mM 11-MUA or a binary mixture of 2.5 mM 11-MUA and 7.5 mM 6-mercaptohexanol (6-MCH) or in a solution of 10 mM 11-MUA for 1 hour at room temperature on gold surfaces pre-cleaned with PBS and

ethanol (Kilic et al., 2018; Thébault et al., 2022). Immobilisation of 20 mM 11-MUA in ethanol for 12 hours can also be done on a gold surface cleaned with ethanol, acetone and deionized water and rinsed with ethanol to remove unbound 11-MUA molecules or treated with a mixture of 20 mM 11-MUA and 3-mercapto propionic acid (MPA) at a ratio of 1:9 overnight at room temperature (Lathika et al., 2021; Narayan et al., 2019). SAMs may also be produced on gold surfaces with aqueous and ethanol solutions containing 50 mM mercaptoacetic acid (MAA) or an ethanol solution having the same quantity of 11-MUA (Raymundo-Pereira et al., 2021).

The carboxylic acid terminated group on the modified electrodes for NS1 antibody attachment are normally activated by n-(3-dimethylaminopropyl)-n-ethylcarbodiimide (EDC) and n-hydroxysuccinimide (NHS) or sulfo-NHS (N-hydroxysulfosuccinimide). Sulfo-NHS are more likely preferable than NHS esters as it is relatively water soluble and longer lived and hydrolyses more slowly in water. This functionalization step aims to create –COOH terminal end which covalently binds with the amine group of antibodies. Carboxylic groups from the SAMs were activated in a mixture of 0.4 M EDC and 0.1 M NHS in the ratio of 1:1 for 15 to 30 minutes for activation of SAMs surface which contrast with EDC/NHS mixture formulated by Yang that use 0.1 M EDC and 0.4 M NHS dissolved in the sodium acetate (NaOAc) buffer for 10 minutes at room temperature (Narayan et al., 2019; Raymundo-Pereira et al., 2021; Yang et al., 2018).

Subsequent surface activation on SAMs can also be done in a solution containing a mixture of 0.15 M EDC and 0.03M NHS at a ratio of 1:1 for 1 hour at room temperature and the substrate is washed with phosphate buffer saline (PBS) to remove any traces of EDC and NHS (Lathika et al., 2021). 50 mM EDC and 30 mM sulfo-NHS prepared in MES pH 4.7 and incubated at room temperature for 1 hour to form an active layer and the activated surface was rinsed twice with PBS to remove the unreacted EDC/sulfo-NHS (Jampasa et al., 2019). The SAM functionalized surfaces can be activated in 0.05 M EDC and 0.025M NHS prepared in PBS for 15 minutes to activate the amines or in a 10 mM PBS solution with pH 6 containing 2 mM of EDC and 5 mM of sulfo-NHS for 30 minutes or in a solution of 10 mM EDC and 20 mM NHS in milliQ water for 90 minutes all at room temperature (Ekici et al., 2022; Stanković et al., 2020; Thébault et al., 2022).

Next step is the incubation of the anti-NS1 antibody on the enhanced SAM-EDC/NHS surface for NS1 antigen-antibody binding. Dengue virus type 2 E-proteins monoclonal antibodies (IgM) with a concentration of 1 mg/ml can be purchased from life science suppliers such as Meridian Life Science, Sigma-Aldrich or Abcam (Omar et al., 2020). The modified SAM-EDC/NHS gold surfaces were immersed with anti-NS1 antibody diluted with PBS at a ratio of 1:10 incubated at 4 °C for 3 hours and rinsed with PBS to remove unbound antibodies (Lathika et al., 2021). Immobilization of the anti-NS1 antibody was performed by 10 µg/mL anti-NS1 on the electrode surface and incubated in a moist chamber for 1 hour at room temperature (Mendonça et al., 2021). The modified SAM-EDC/NHS electrode can also be functionalized with specific capture anti-dengue NS1 IgG 0.1 mg/mL for 1 hour at room temperature and washed with PBS for unbound antibodies removal (Sinawang et al., 2016).

The deactivation of the unbound active sites of remaining NHS esters on the SAM-EDC/NHS-NS1Antibody surface can be blocked by ethanolamine (ETA) solution. Addition of 1 M ETA solution for 5 minutes and rinsing the surface thoroughly with deionized water was done to block unreacted compounds modified on SAM-EDC/NHS-NS1Antibody surface (A. A. Zainuddin et al., 2019). The remaining NHS ester can also be deactivated using ETA in a pH -8.5 solution incubated for 5 minutes (Narayan et al., 2019). The active sites from the SAM can be blocked using a solution containing 0.1 M or 1.0 mM of ETA solution for 1 hour to wash and remove non-specific adsorption on SAM-EDC/NHS-NS1Antibody surface (Raymundo-Pereira et al., 2021; Yang et al., 2018).

Finally, the remaining free reactive carboxylic groups were blocked with 50 mM glycine prepared in 0.1 M of citrate phosphate buffer (pH 5.5) (Mendonça et al., 2021). Glycine is used to block nonspecific sites on the surface of the electrode by immersing the modified SAM-EDC/NHS-NS1Antibody-ETA electrodes in 5mM of glycine solution in PBS for 30 minutes (A. Zainuddin et al., 2022). NS1 concentration can be detected about 0.04 – 2 µg/mL in primary infection, but only 0.01 – 2 µg/mL for secondary infection in the acute phase of dengue infection (Khristunova et al., 2020). Different NS1 antigen concentrations of 10, 50, 100, 500, 1000 and 2000 ng/mL were prepared on the sensor interface at room temperature for 30 minutes in pH 7.4 for NS1 antigen detection (A. A. Zainuddin et al., 2019).

2.5.3 Summary of Surface Bio-Functionalization Process

Table 2.4: Summary of surface bio-functionalization process.

Research Work	Approach	Functions
Self-assembled monolayer (SAM) using 11-mercaptoundecanoic acid (11-MUA) (Tsai et al., 2019; Kilic et al., 2018; Thébault et al., 2022; Lathika et al., 2021; Narayan et al., 2019; Raymundo-Pereira et al., 2021).	• 5 mM 11-MUA on a gold film. • 10 mM 11-MUA or a binary mixture of 2.5 mM 11-MUA and 7.5 mM 6-6-MCH in absolute ethanol. • 10 mM 11-MUA for 1 hour at room temperature. • 20 mM 11-MUA in ethanol for 12 hours. • A mixture of 20mM 11-MUA and 3-mercapto propionic acid (MPA) at a ratio of 1:9 overnight at room temperature. • Mixture of 50 mM mercaptoacetic acid (MAA) or an ethanol solution having the same quantity of 11-MUA.	Form a thiol terminated self-assembly monolayer (SAM) modifying the gold surface to strongly attach a biorecognition element (NS1 antibody) that binds to the analyte (NS1 antigen) selectively.
Activation of SAM by n-(3-dimethylaminopropyl)-n-ethylcarbodiimide (EDC) and n-hydroxysuccinimide (NHS) or sulfo-NHS (N-hydroxysulfosuccinimide)	• A mixture of 0.4 M EDC and 0.1 M NHS in the ratio of 1:1 for 15 to 30 minutes. • 0.1 M EDC and 0.4 M NHS dissolved in the sodium acetate (NaOAc) buffer for 10 minutes at room temperature.	Activate the carboxylic acid terminated group on the modified SAM surface for NS1 antibody attachment.

(Narayan et al., 2019; Raymundo-Pereira et al., 2021; Yang et al., 2018 Lathika et al., 2021; Jampasa et al., 2019; Ekici et al., 2022; Stanković et al., 2020; Thébault et al., 2022).	• A mixture of 0.15 M EDC and 0.03 M NHS at a ratio of 1:1 for 1 hour at room temperature and washed with phosphate buffer saline (PBS) • 50 mM EDC and 30 mM sulfo-NHS prepared in MES pH 4.7 and incubated at room temperature for 1 hour and rinsed twice with PBS. • 0.05 M EDC and 0.025 M NHS prepared in PBS for 15 minutes at room temperature. • 10 mM PBS solution with pH 6 containing 2 mM of EDC and 5mM of sulfo-NHS for 30 minutes at room temperature. • 10 mM EDC and 20mM NHS in milliQ water for 90 minutes at room temperature.	
Anti-NS1 antibody incubation (Lathika et al., 2021; Mendonça et al., 2021; Sinawang et al., 2016).	• Anti-NS1 antibody diluted with PBS at a ratio of 1:10 incubated at 4 °C for 3 hours and rinsed with PBS. • 10 µg/mL anti-NS1 incubated on the electrode surface in a moist chamber for 1 hour at room temperature. • 0.1 mg/mL anti-dengue NS1 IgG 0.1 mg/mL functionalized for 1 hour at room temperature and washed with PBS.	Incubation of the anti-NS1 antibody on the enhanced SAM-EDC/NHS surface for NS1 antigen-antibody binding.
Deactivation of the unbound active sites by ethanolamine (ETA) (A. A. Zainuddin et al., 2019; Narayan et al., 2019;	• Addition of 1 M ETA solution for 5 minutes and rinsing the surface thoroughly with deionized water. • ETA in a pH -8.5 solution incubated for 5 minutes. • A solution containing 0.1 M or 1.0 mM of ETA solution for 1 hour.	Deactivate the unbound active sites of remaining NHS esters on the SAM-EDC/NHS-NS1Antibody surface.

Raymundo-Pereira et al., 2021; Yang et al., 2018).		
Block other nonspecific sites by glycine (Mendonça et al., 2021; A. Zainuddin et al., 2022).	• 50 mM glycine prepared in 0.1 M of citrate phosphate buffer (pH 5.5). • 5 mM of glycine solution in PBS for 30 minutes.	Block the remaining free reactive carboxylic groups.
NS1 antigen detection (Khristunova et al., 2020; A. A. Zainuddin et al., 2019).	• 0.04 – 2 µg/mL of NS1 concentration can been detected in primary dengue infection, but only 0.01 – 2 µg/mL for secondary dengue infection • Different NS1 antigen concentrations of 10, 50, 100, 500, 1000 and 2000 ng/mL were incubated at room temperature for 30 minutes in pH 7.4.	Ensure that the NS1 antibodies bind specifically to the targeted NS1 antigens.

2.6 FLUIDIC CHAMBER SYSTEM

Fluidic systems have become a significant tool for engineering microenvironments in controlled biological research which encompasses instruments and procedures for regulating and manipulating fluids on a tiny scale with great precision. Non-turbulent, highly ordered fluid flow systems are frequently used in biosensing applications to detect antibodies against viruses (Muzammil et al., 2021). This system interprets tiny quantities of analyte via the channels to examine the behaviour of the virus captured by the transducer and signal output. Open and closed channel systems are the most common types of fluidic systems. Closed fluidic systems typically consist of channels and structures covered by a lid, ensuring a contained and controllable environment, whereas open fluidics expose the liquid to the atmospheric environment and may not be externally controlled. Even though the use of open channel systems is easy to fabricate and maintain, a closed system is more preferable in a biosensing application to ensure that the analyte is contained in a controllable environment (Oliveira et al., 2019).

Printed circuit board (PCB) technology and 3D printed fluidic chamber implies the integration of microfluidics and electronics in biosensing applications. However, the biocompatibility of the involved materials has to be examined if they are in contact with biological elements (Urbano-Gámez et al., 2021). The importance of three-dimensional (3D) printing techniques has bloomed as a possible alternative to existing techniques for microfluidic devices fabrication in recent years as the designs can be modified and reprinted (Nielsen et al., 2020). It is a rapidly growing technology that best fits for biological applications. Other essential advantages of 3D printed devices are quick fabrication, easy accessibility, processing of varied materials and sustainability. Fused Deposition Modelling (FDM) and Stereolithography (SLA) is the most common, affordable and easily accessible 3D printing technique that utilizes a variety of materials (Piironen et al., 2020). Numerous plastic materials are available for 3D printing such as Acrylonitrile Butadiene Styrene (ABS) because it is a biocompatible 3D printable polymer material (Pokharna et al., 2021). This means that 3D printed fluidic chambers made from ABS material when in contact with biological elements will not elicit toxicity on the biological systems making it suitable for functional prototypes.

2.7 CHAPTER SUMMARY

This chapter provides an overview of various methods used in dengue diagnosis, encompassing traditional techniques such as virus isolation, genome detection, antigen tests, and serological diagnosis, as well as modern biosensing approaches. Biosensing techniques that implement the use of potentiostat in electrochemical biosensing applications are (Alao, 2018), (Jenkins et al., 2019), (Adams et al., 2019), (Cook, 2020), (Hoilett et al., 2020) and (Escobedo et al., 2020). However, both traditional and current (RT-PCR and ELISA) methods for dengue detection have detection limits, are time consuming, expensive, and have limited specificity and sensitivity. To address these challenges, this research proposes a biosensing system that uses a portable potentiostat integrated with fluidic chamber and IEQCM sensor inspired by (Hoilett et al., 2020). This biosensing system has high accuracy and is cost-effective for early dengue detection. Surface bio-functionalization techniques were studied to optimize NS1 antibody-antigen attachment on gold surface electrodes. The 3D printed fluidic chamber was designed to ensure a confined and biocompatible environment. The proposed portable potentiostat system with IEQCM sensor offers a portable, sensitive and selective alternative, focusing on NS1 antigen detection for rapid dengue diagnosis.

CHAPTER 3

RESEARCH METHODOLOGY

3.1 INTRODUCTION

This chapter highlights the design and development of a potentiostat and fluidic chamber using an array of Integrated Electrochemical Quartz Crystal Microbalance (IEQCM) biosensor for dengue detection. This includes the design and development of potentiostat systems using Altium Designer software. The electrochemical measurement, specifically Cyclic Voltammetry (CV) program was designed using Arduino software. These studies also include the design of a fluidic chamber for the IEQCM biosensor designed using SolidWorks. Once the fabrication of both potentiostat and fluidic chamber systems has completed, they will undergo a testing process accordingly. The functionality and leakage tests will be done on the potentiostat and the fluidic chamber respectively to ensure that both devices can be integrated together for further dengue sample testing. However, due to the limitation of the designed potentiostat that can only perform CV measurement, the commercial EmStat Pico potentiostat was utilized for the EIS measurement of the dengue samples.

Figure 3.1 shows the research methodology flowchart of the designed dengue detection system. The designed potentiostat was integrated together with the fluidic chamber and IEQCM sensor. Next, the functionality of this system was tested via CV measurements. Once the IEQCM sensor is confirmed to be working, the next step was to perform EIS measurements using the commercial, EmStat Pico potentiostat. Surface bio-functionalization was done to strongly attach a bio-recognition element onto the IEQCM sensor. The bio-recognition element used in this work was the NS1 antibody which selectively binds to the analyte, the NS1 antigen of dengue samples. The EmStat Pico potentiostat will translate the responses obtained from the dengue samples and produce a Nyquist plot.

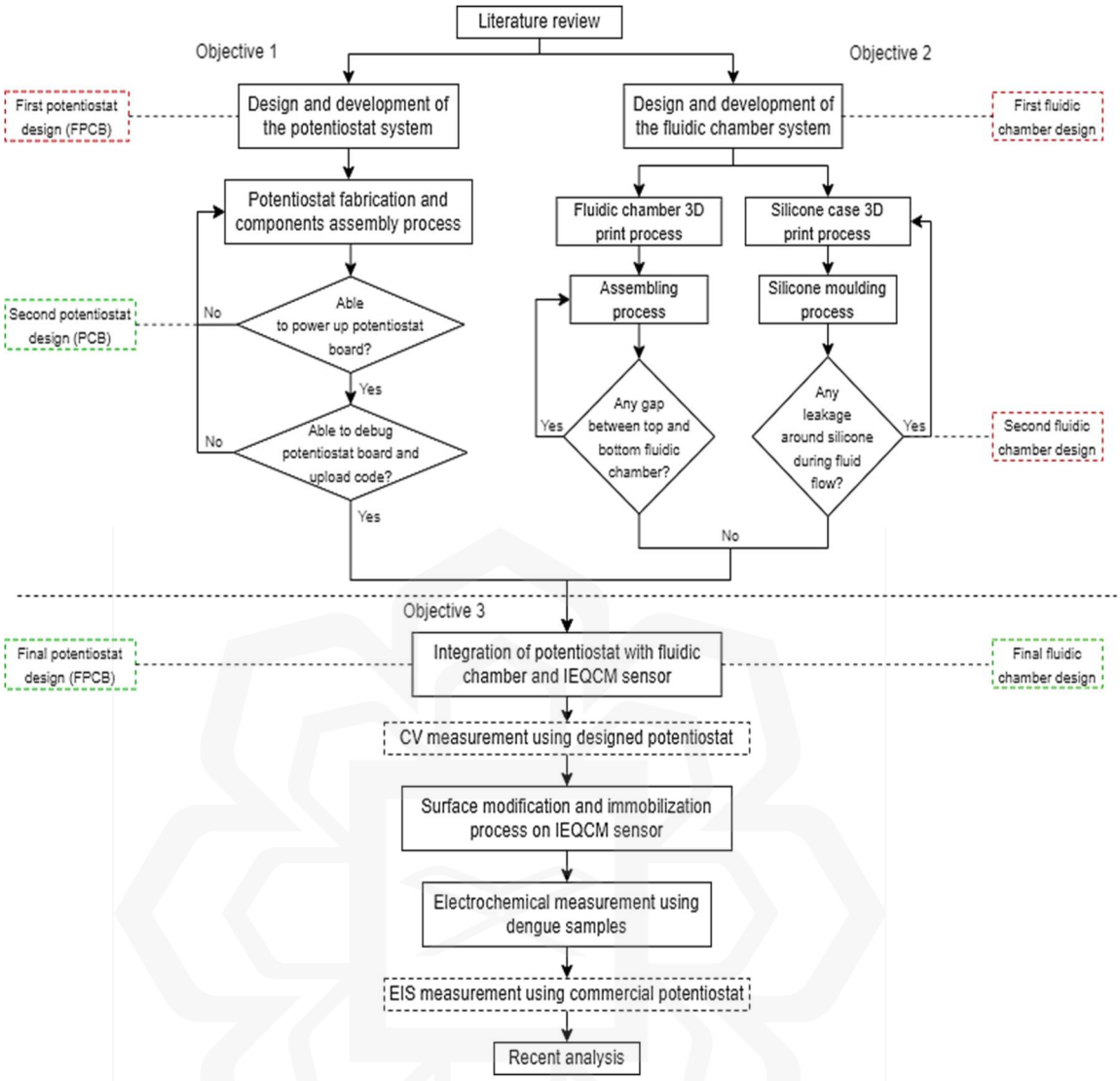

Figure 3.1: Research methodology flow chart for the dengue detection potentiostat system (Refer to Fig. 4.1 for detailed potentiostat and fluidic chamber designs).

3.2 RESEARCH DESIGN

The research design comprises three main parts namely the design of the potentiostat, the software and the fluidic chamber design.

3.2.1 Potentiostat Design

3.2.1.1 Design Specifications

The design of the proposed potentiostat system includes both potentiostat and fluidic chamber systems. There are three versions of the potentiostat design, the first design was fabricated on a flexible printed circuit board (FPCB) while the second design was on rigid PCB but the final design was fabricated on FPCB. This research is a collaboration with Jabil Circuit, an expert in flexible printed electronics. The first design was fabricated on a FPCB but failed to power up. To facilitate troubleshooting, the second design was fabricated by PCBWay on rigid PCB for faster customization and flexibility. However, the final design was returned to Jabil Circuit that specialized in FPCB, aligning with the main objective of flexible potentiostat circuit. The flowchart of the potentiostat design was shown in Figure 3.2.

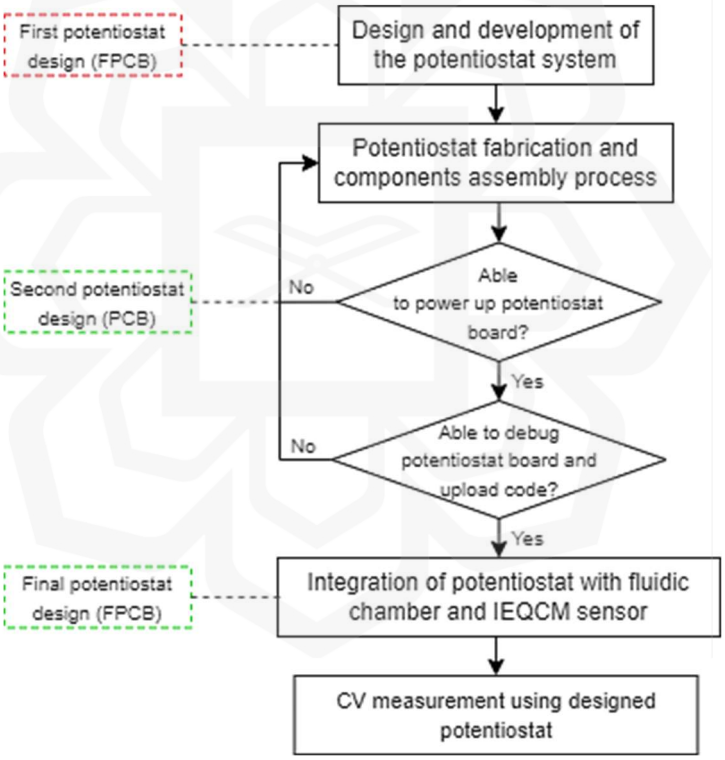

Figure 3.2: Flowchart of the potentiostat design.

The block diagram of the whole potentiostat system is divided into potentiostat and fluidic chamber parts as in Figure 3.3. The potentiostat consists of ATSAMD21 microcontroller and LMP91000 electrochemical sensor chip along with all other required components such as 3.3 V linear voltage regulator IC, micro–B USB, reset

tactile switch and debugger connector header to make up the potentiostat system while the fluidic chamber part comprises the 3D printed fluidic chamber and the IEQCM sensor.

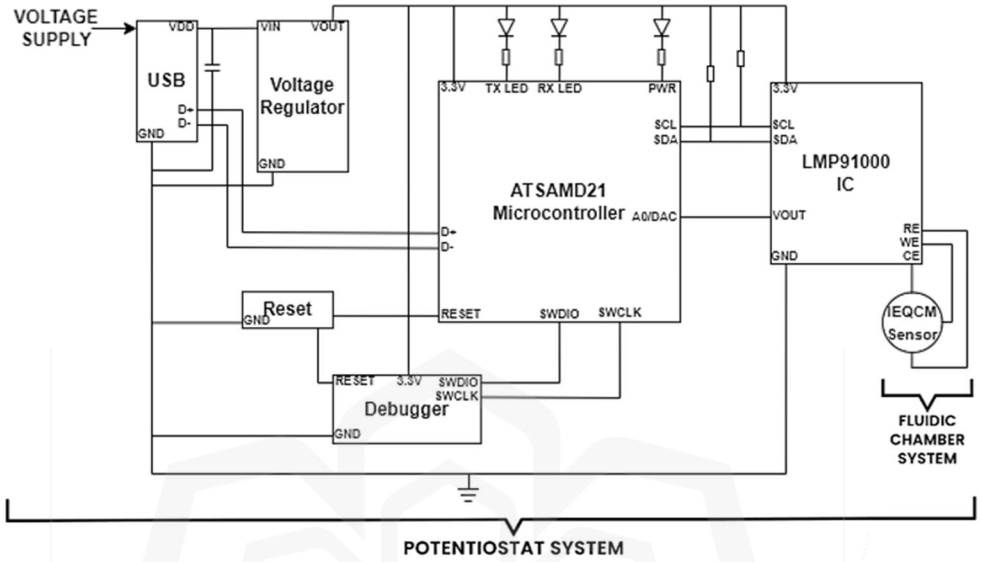

Figure 3.3: Block diagram of the potentiostat system.

3.2.1.2 Main Components Selection

Components selection involves choosing specific electronic components to build a functional potentiostat system. The key components in a potentiostat system include the electrochemical sensor integrated circuit (IC) (LMP91000), which is considered as the heart of this designed potentiostat controlled by a low-power, high-performance microcontroller (ATSAMD21G18A). Appendix A shows the list of specific components used in this potentiostat system.

3.2.1.2.1 Electrochemical Sensor IC (LMP91000)

The electrochemical sensor Integrated Circuit (IC), LMP91000 is a programmable Analog Front-End (AFE) for use in micro-power electrochemical sensing applications (Texas Instruments, 2014). It offers a full signal path solution that creates an output voltage proportionate to the cell current between a sensor and a microcontroller. Instead

of using various discrete solutions, LMP91000 enables its programmability to handle a variety of electrochemical sensors, such as 3-lead toxic gas sensors and 2-lead galvanic cell sensors with a single design. The LMP91000 can accommodate gas sensitivities between 0.5 nA/ppm and 9500 nA/ppm. Additionally, it enables simple conversion of current ranges between 5 µA and 750 µA full scale. The architecture of LMP91000 as shown in Figure 3.3 encompasses an adjustable cell bias and Transimpedance Amplifier (TIA) gain that are programmable through the Inter-Integrated Circuit (I^2C) interface. Sensor diagnostics can also be performed via the I^2C interface. This LMP91000 also entails an embedded temperature sensor that can be measured through the VOUT pin which can then be utilized to validate temperature conditions at the sensor or to offer extra signal correction in µC. The LMP91000 runs across a voltage range of 2.7 V to 5.25 V and is designed for micro-power applications with the overall current draw may be less than 10 µA. Further power savings are attainable by turning off the TIA amplifier and using an internal switch to connect the reference electrode to the working electrode. Appendix B exhibits the pin configuration and functions of LMP91000.

3.2.1.2.2 Microcontroller (ATSAMD21G18)

ATSAMD21G18 is a low-power, high-performance ARM® Cortex®-M0+ Central Processing Unit (CPU) running at operating frequency up to 48 MHz from Microchip Technology (Microchip, 2021). It features 256 KB of in-system self-programmable flash and 32 KB of Static Random-Access Memory (SRAM). It also consists of up to six Serial Communication (SERCOM) interfaces configurable to operate as any combination of Universal Asynchronous Receiver/Transmitter (UART)/ Universal Synchronous/Asynchronous Receiver/Transmitter (USART), Inter-Integrated Circuit (I^2C) and Serial Peripheral Interface (SPI). The peripherals include 32-bit Real Time Counter (RTC) with clock/calendar function and up to five 16-bit Timer/Counters (TC), 20 PWM channels using Timer/Counters (TC) and Timer/Counters for Control (TCC). It also comprises one 12-bit, 350 ksps Analog-to-Digital Converter (ADC) with up to 20 channels and one 10-bit, 350 ksps Digital-to-Analog Converter (DAC). The power supply can operate from 1.62 V up to 3.63 V. The architecture of the ATSAMD21G18 microcontroller is shown in Appendix C.

A comprehensive set of system and programme development tools, including C compilers, macro assemblers, programme debugger/simulators and programmers are available for the SAMD21 microcontrollers. Every gadget has both internal and external oscillators that are precise and low power. The system clock can be sourced from any oscillator. The ability to individually set separate clock domains to operate at various frequencies allows for power savings by allowing each peripheral to operate at its ideal clock frequency, keeping a high CPU frequency but consuming less power. The identifier for each connector is shown in Appendix C for the 48-pin quad-flat no-leads (QFN) package that houses the ATSAMD21G18 microcontroller. The pinouts for the oscillator, serial wire debug interface, SERCOM I^2C pins, and general-purpose input/output (GPIO) clusters are listed in Appendix C. The oscillators are not mapped to the normal port functions and their multiplexing is controlled by registers in the System Controller (SYSCTRL). The operations of the standard port are only mapped to the SWCLK pin. The SWDIO port will be switched to the SWDIO function automatically in response to a debugger cold-plugging or hot-plugging detection.

3.2.1.3 Schematic and Printed Circuit Board (PCB) Design

All schematic and printed circuit board (PCB) designs of the IEQCM biosensor potentiostat system were inspired by KickStat by Hoilett (Hoilett et al., 2020). First, a schematic document was created along with the schematic library for the design. The schematic symbol of the components can be found inside the library of the software itself or it can be downloaded from the free online library. Most of the time, the schematic symbol comes together with the PCB footprint, but it can also be downloaded from SnapEDA or Ultra Librarian online library. Once the schematic design has completed, the PCB document can be automatically created along with its PCB library. From the PCB document, routing needs to be done to get the best PCB design that fits the objective of this project which is small and portable. So, the best routing line should be connected in order to achieve the smallest PCB design possible. The PCB document was then converted to Gerber file for PCB fabrication by the PCB manufacturing companies. Once fabricated, the board will undergo components assembly process before proceeding with the functionality test of the board. If the board is confirmed

working, it will be further integrated with the fluidic chamber for dengue samples testing. Figure 3.4 displays the flowchart of the designed potentiostat system.

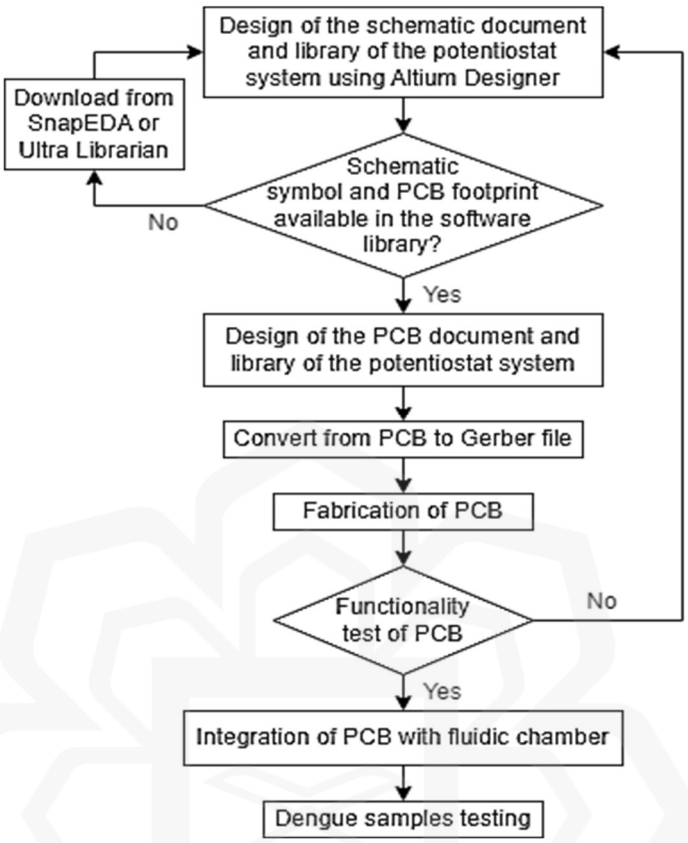

Figure 3.4: Flowchart of the potentiostat design.

3.2.1.3.1 First Potentiostat Design

There are three versions of the designed potentiostat fabricated throughout this research. Figure 3.5 (a, b) shows the first schematic and PCB design of the potentiostat board with the dimensions of 80.0 mm x 92.0 mm. The first PCB design of the potentiostat system was fabricated on a single flexible printed circuit board (FPCB) that was made from polyimide (PI) film. The design was sent to Jabil Circuit, an American manufacturing services company for fabrication. Jabil Circuit was well-known for their specialization in FPCB fabrication as FPCB is the future of the PCB industry. Flex circuits guarantee several advantages over rigid circuits including greater and long-term reliability owing to reduction in size, weight and manufacturing time as well as the elimination of the major source of errors in traditional wire interconnections resulting in less maintenance interventions.

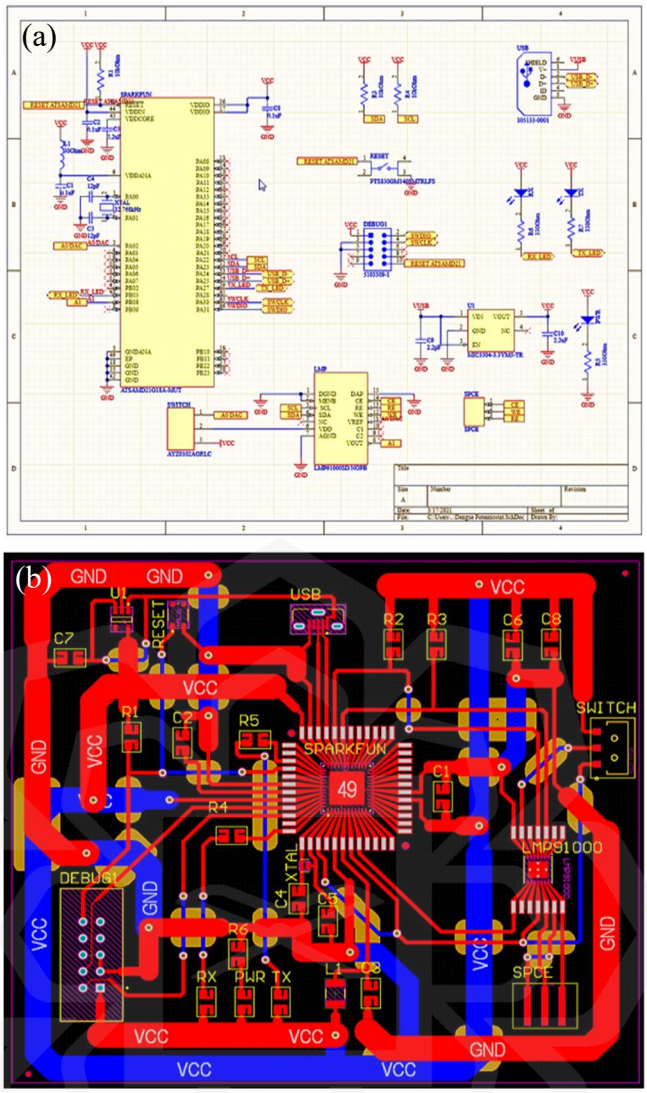

Figure 3.5: (a) Schematic and (b) PCB design of the first potentiostat design.

3.2.1.3.2 Second Potentiostat Design

The development of the second potentiostat design was done to retest the functionality of the new design. The schematic and PCB design of the second potentiostat system with a dimension of 63.0 mm x 68.0 mm is presented in Figure 3.6 (a, b). The second version of the potentiostat system was fabricated on a rigid board that was made from a glass fibre composite with a flame-retardant epoxy resin (FR-4) material. PCBWay was chosen for the fabrication of the second design as it offers top-notch services including fast turnaround time, reliable quality and quick shipment with no limitation to the size, shape or complexity of PCBs that can be designed through a user-friendly

website. Rigid boards are made of solid substrates that provide the board with rigidity and durability. They are also compact, less expensive and easier to troubleshoot compared to flex boards.

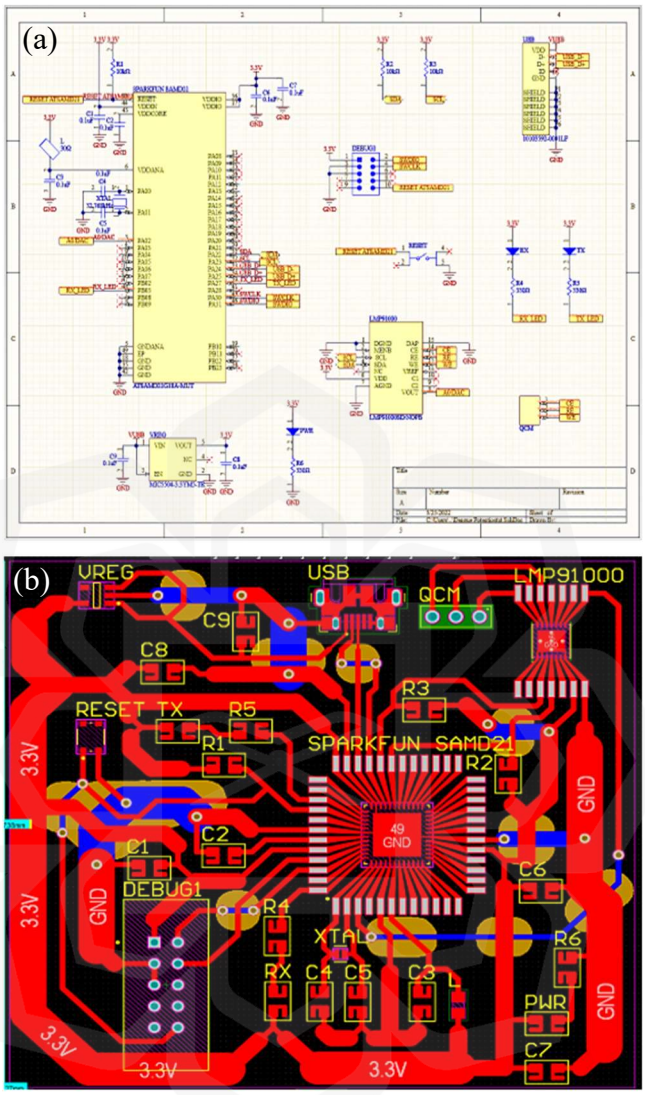

Figure 3.6: (a) Schematic and (b) PCB design of the second potentiostat design.

3.2.1.3.3 Final Potentiostat Design

Final potentiostat design was a copy of the second design with only slight changes to ensure that the final design would perform identically to the fully functioning second design on rigid PCB board when fabricated on FPCB. The final design was fabricated on FPCB by Jabil Circuit which is well-known for their skill in FPCB fabrication. FPCB aligns with the main objective of flexible potentiostat for wearable application. Figure

3.7 (a, b) illustrated the final schematic and PCB design of the potentiostat with the dimensions of 60.0 mm x 65.0 mm. The final design is the smallest design when compared with the other two designs to fit the objective of a miniaturized, wearable and portable potentiostat. Even though FPCB is more expensive than rigid PCB, it conserves more space and weight while saving both labour and material expenses. Table 3.1 displayed the changes made of the components used in all three potentiostat designs.

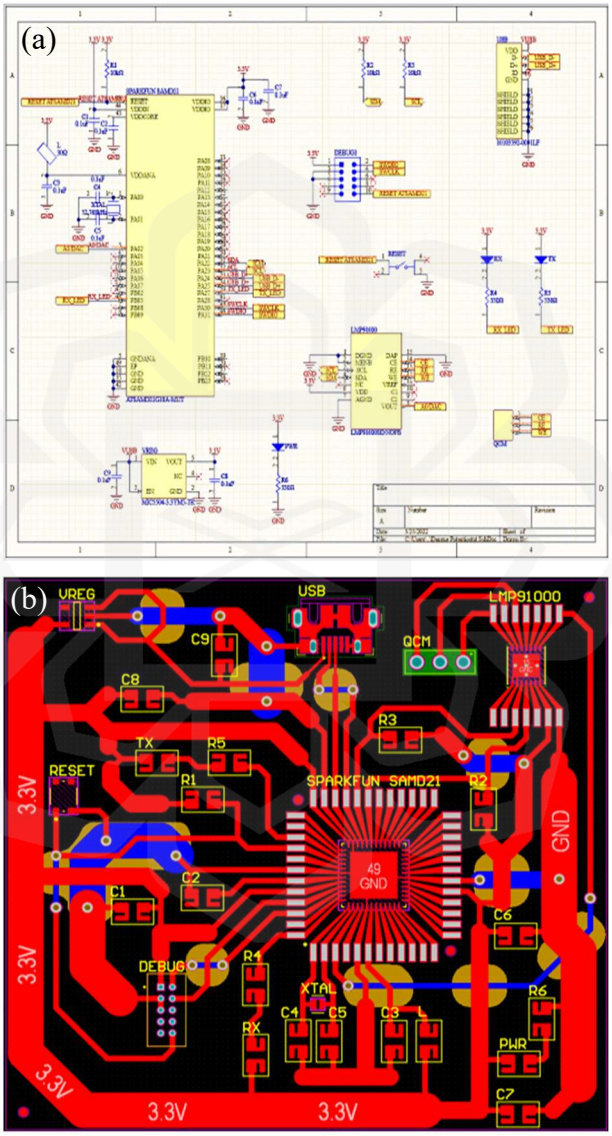

Figure 3.7: (a) Schematic and (b) PCB design of the third potentiostat design.

Table 3.1: Modifications of components in potentiostat designs.

Components	First Potentiostat Design	Second Potentiostat Design	Final Potentiostat Design
Microcontroller	ATSAMD21G18A-MUT	ATSAMD21G18A-MUT	ATSAMD21G18A-MUT
Electrochemical sensor IC	LMP91000SD/NOPB	LMP91000SD/NOPB	LMP91000SD/NOPB
Voltage regulator IC	MIC5504-3.3YM5-TR	MIC5504-3.3YM5-TR	MIC5504-3.3YM5-TR
Micro B USB	10118192-0001LF	10103592-0001LF	10103592-0001LF
Reset tactile switch	PTS830GM140 SMTR LFS	PTS830GM140 SMTR LFS	PTS830GM140 SMTR LFS
Debugger connector header	3020-10-0100-00	3020-10-0100-00	PR20B05VBDN

3.2.2 Software Design

The electrochemical measurement firmware of the potentiostat system was coded in Arduino software. Due to the limitation of the designed potentiostat that utilized LMP91000 chip, the electrochemical measurement that it can support is only Cyclic Voltammetry (CV) and the flowchart for CV measurement is illustrated in Figure 3.8. Only CV measurement was coded and used in this IEQCM biosensor potentiostat system. The CV program starts with supplying DC voltage to the system, changing the voltage of the working electrode of the IEQCM sensor and measuring the resulting current. The resulting output current obtained from Arduino's serial monitor was exported to Excel for further analysis.

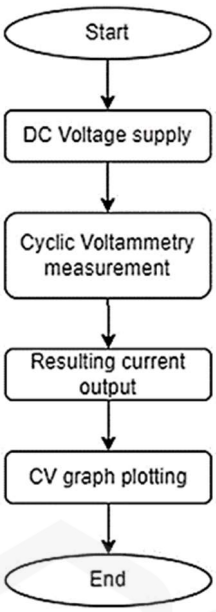

Figure 3.8: Cyclic Voltammetry (CV) measurement flowchart.

The CV program of the potentiostat was coded in Arduino, and the generated output of the code was displayed on the serial monitor interface, as illustrated in Figure 3.9. The data obtained from the CV code was continuously monitored on the serial monitor and collected for further analysis using a tool like Microsoft Excel. By exporting the data, in-depth analysis can be performed and crucial insights can be obtained from the CV plot. The CV graph allowed visualization of the electrochemical behavior, and various parameters, such as peak potential, peak current, and redox potential, could be extracted from the plot to verify the functionality and performance of the Integrated Electrochemical Quartz Crystal Microbalance (IEQCM) sensor integrated with the potentiostat. This critical analysis of the CV measurements played a crucial role in validating the effectiveness of the potentiostat and its potential in biosensing application.

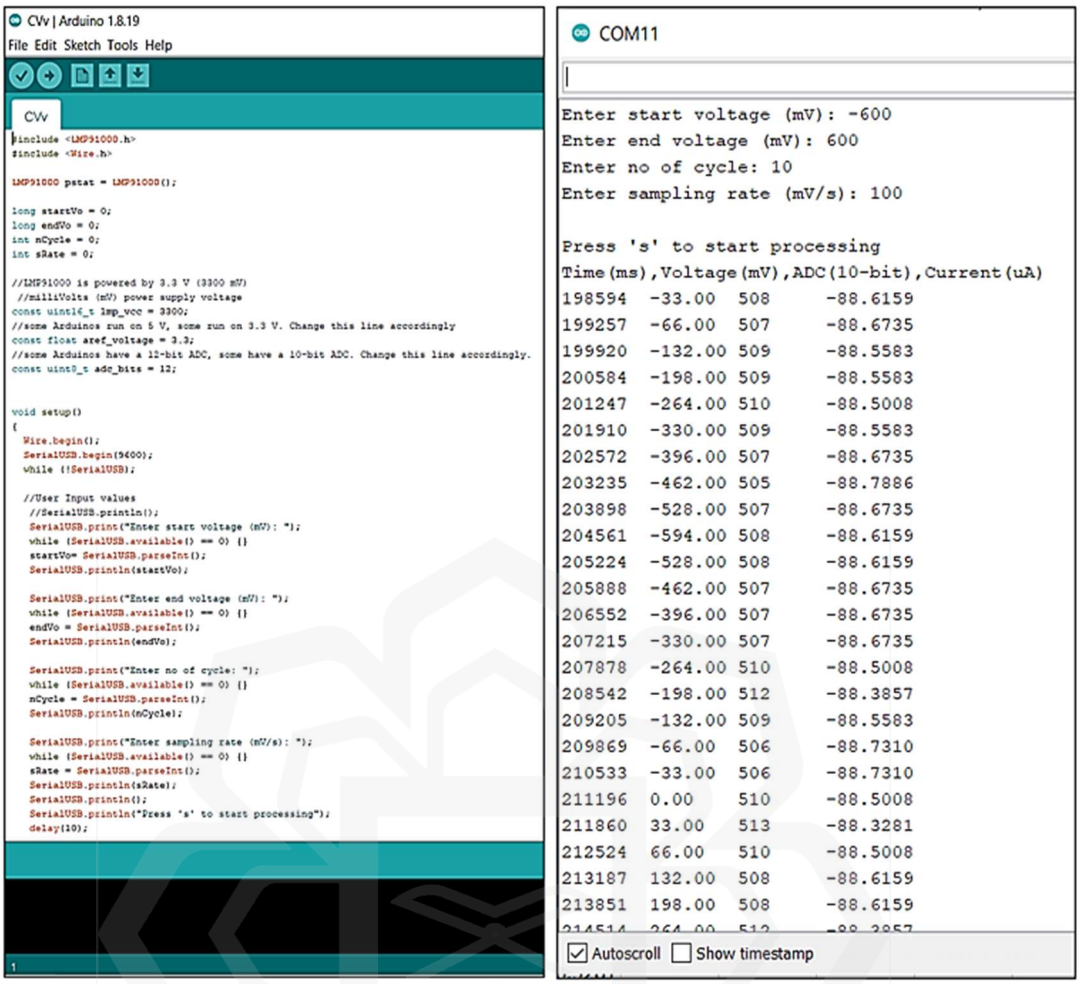

Figure 3.9: CV program and output of the potentiostat system.

3.2.2.1 Software Design Flow

The design methodology of the potentiostat system, which is categorised under ATSAMD21, LMP91000, and IEQCM is shown in Figure 3.10. The registers of the ATSAMD21 and LMP91000 were programmed and configured via System Management Bus (SMBus™) based on the Inter-Integrated Circuit (I²C) bus protocol. The I²C bus and the SMBus™ are popular 2-wire buses that are essentially compatible with each other. In this potentiostat system, both master (ATSAMD21) and slave (LMP9100) are easily interchangeable between both buses with addressable slaves. The registers are controlled by the ATSAMD21 through Arduino Integrated Development Environment (IDE) software and are utilised for functions such as gain, input waveform

generation and mode selection for the electrochemical experiment. The detailed CV code was explained in Appendix D.

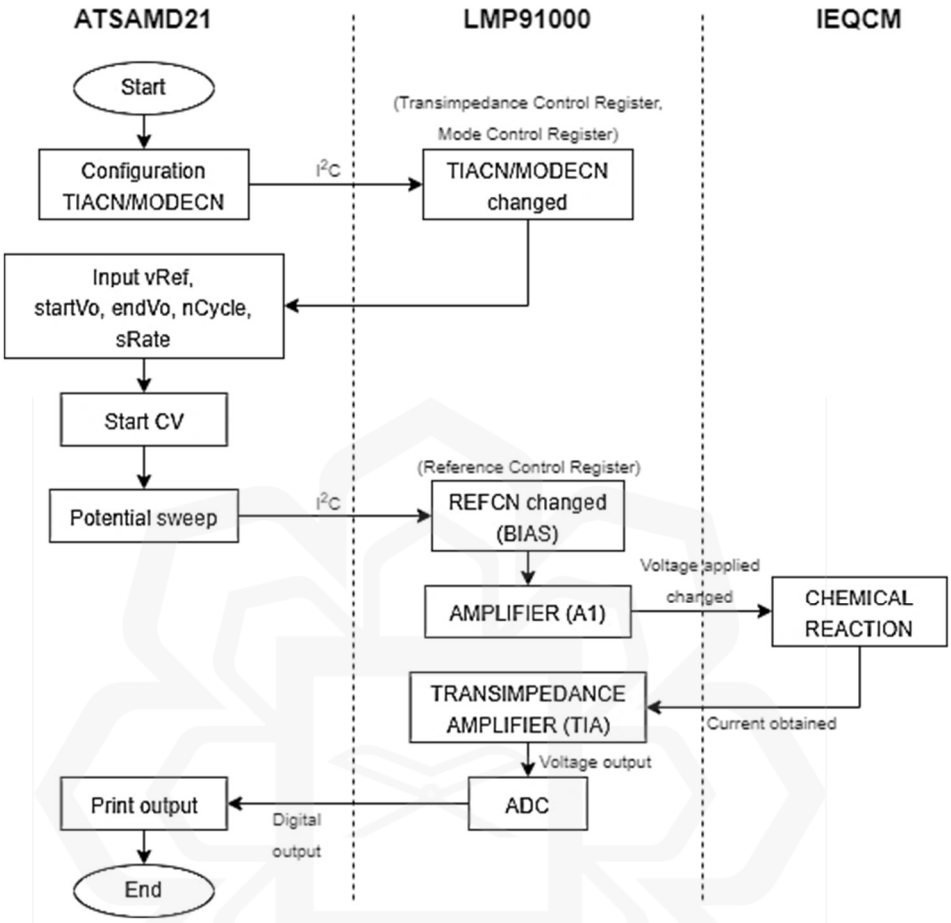

Figure 3.10: The flow chart of the potentiostat system.

3.2.2.1.1 Reference Control Register (REFCN)

The parameters in the Reference Control Register (REFCN) enable the configuration of the internal zero (INT_Z), bias (BIAS) and reference source (REF_SOURCE) which respectively determine the internal zero selection, positive or negative bias as well as the level of bias introduced to the system and voltage source selection respectively as seen in Appendix B. A reference voltage (VREF) attached to the VREF pin serves as the reference when the reference source is external. Rather than using the supply voltage, the internal zero and bias voltage are determined as a percentage of the VREF voltage. Due to the fact that the absolute heights of the peaks of the reduction and oxidation (redox) currents are identical, a reversible electrochemical reaction was

anticipated and the internal zero was set at 50 %. No external supply was required because the internal reference voltage of 3.3 V was used for this application.

The first Amplifier 1 (A1) connects to the RE and CE electrodes and stabilises the redox reaction taking place in these electrodes while the potential sweep is applied. The sweep is performed through the variable bias, which allows the configuration of the voltage, divided into steps ranging from 0 % to 24 % of the VREF. The input potential for cyclic voltammetry will be changed from negative to positive and from positive to negative by varying the percentage reference voltage utilised and the bias sign, the input voltage may be swept from 0 % to 24 % creating a range of -24 % to 24 %. The LMP91000 datasheet specifies using steps of 1 % until 2 % of the VREF is achieved, and then steps of 2 % until 24 % of the VREF, resulting in a total of 14 steps which may vary based on user input. The output current was calculated using the given formula:

$$Iout = \frac{Vout - VRE}{R_{TIA}} \quad \text{(Equation 3.1)}$$

3.2.2.1.2 Transimpedance Control Register (TIACN)

The transimpedance gain (R_{TIA}) and the load resistance (R_{Load}) are programmed using the Transimpedance Control Register (TIACN) as seen in Appendix B. External resistance, 2.75 kΩ, 3.5 kΩ, 7 kΩ, 14 kΩ, 35 kΩ, 120 kΩ and 350 kΩ are possible values for R_{TIA}, whereas the possible values for R_{Load} selection are 10 Ω, 33 Ω, 50 Ω and 100 Ω. The second operational Transimpedance Amplifier (TIA) is responsible for converting the current obtained by the WE into voltage through R_{TIA}. This output signal was amplified and connected directly to a microcontroller analogue pin where it was converted to digital data using the built-in 12-bit Analog-to-Digital Converter (ADC).

3.2.2.1.3 Mode Control Register (MODECN)

The three-electrode system was defined using the Mode Control Register (MODECN) and the parameters listed in Appendix B allow the configuration of the operation mode

of the LMP91000. The output of the temperature sensor is present at the output voltage (VOUT) pin while the LMP91000 is in temperature measurement (TIA ON) mode, whereas the output of the potentiostat circuit is accessible at pin C2.

3.2.3 Fluidic Chamber Design

This research presents the use of a fluidic chamber in a biosensing application for dengue virus detection through chambers in which fluids flow to study the behaviour of the dengue virus. Fluidic systems are non-turbulent, highly ordered fluid flow systems that are progressively being used to control and change cellular microenvironments in controlled biological research effectively. The design of the fluidic chamber has a few versions, the first few designs did not pass the assemble and leakage test. Hence, the final was fabricated with transparent acrylic part for better leakage visualization, Figure 3.11 shows the flowchart of the fluidic chamber design.

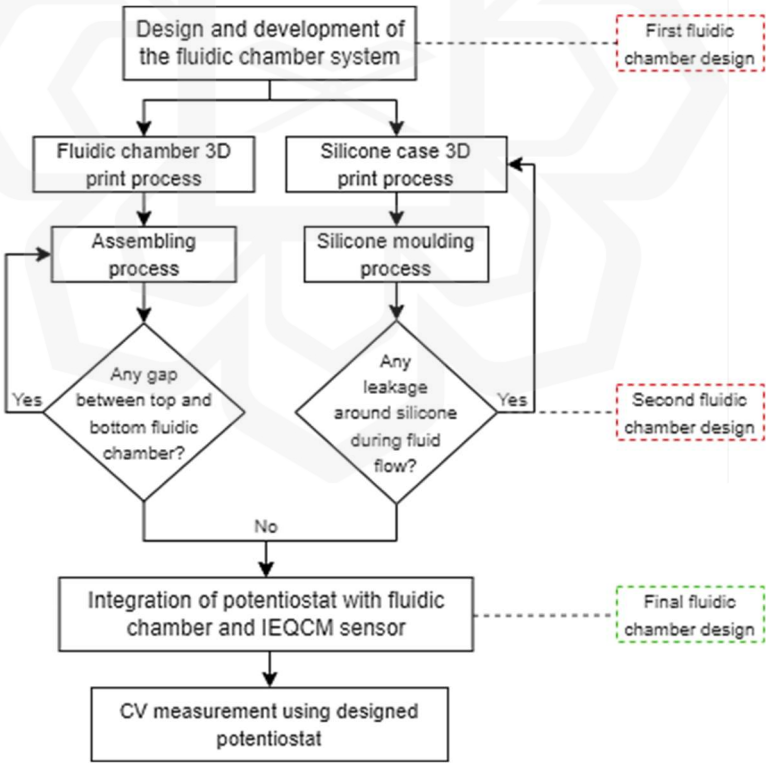

Figure 3.11: Flowchart of the fluidic chamber design.

The IEQCM sensor is very delicate and is required to be placed inside a fluidic chamber to run its data measurements. The fluidic chamber is designed based on the size of IEQCM sensor and the dimensions of fluidic chamber, the 2-dimensional (2-D) design of the fluidic chamber, IEQCM sensor and silicon case are illustrated in Figure 3.12 (a, b). The dimension of the fluidic chamber is 40.0 mm (length) x 40.0 mm (width) x 18.0 mm (height), IEQCM sensor is ⌀13.97 mm (diameter), 6.985 mm (radius) and 0.3 mm (thickness) and silicon case is ⌀15.0 mm (diameter), 4.0 mm (thickness of top case) and 4.5 mm (thickness of bottom case).

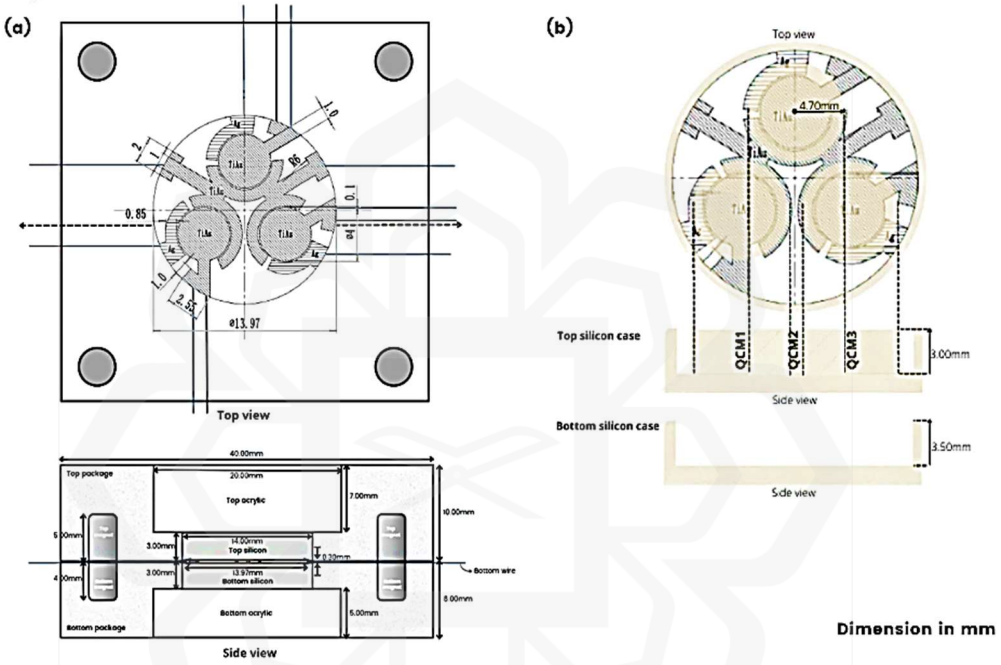

Figure 3.12: (a) Fluidic chamber and IEQCM sensor and (b) silicon case dimension.

SolidWorks software is a solid modelling computer-aided design (CAD) and computer-aided engineering application used to design a 3D CAD model. The fluidic chamber design comprises top and bottom part, top and bottom silicon and IEQCM sensor. All parts were designed using this SolidWorks software before 3D printed it. The top and bottom 3D printed fluidic chamber was used to hold the IEQCM sensor. The silicon layers were moulded from a 3D printed silicon case which is used to allow analyte containment and ensure that the analyte does not leak to the adjacent sensors' chamber. The IEQCM sensor is used for electrochemical measurement. The fluidic chamber has a total of 6 chambers, two chambers for input/output of each sensor. Final version of the fluidic chamber was made with a transparent acrylic window for better

visualization of leakage. Figure 3.13 displays the design of a fluidic chamber using SolidWorks software in top, bottom, assembled and exploded views.

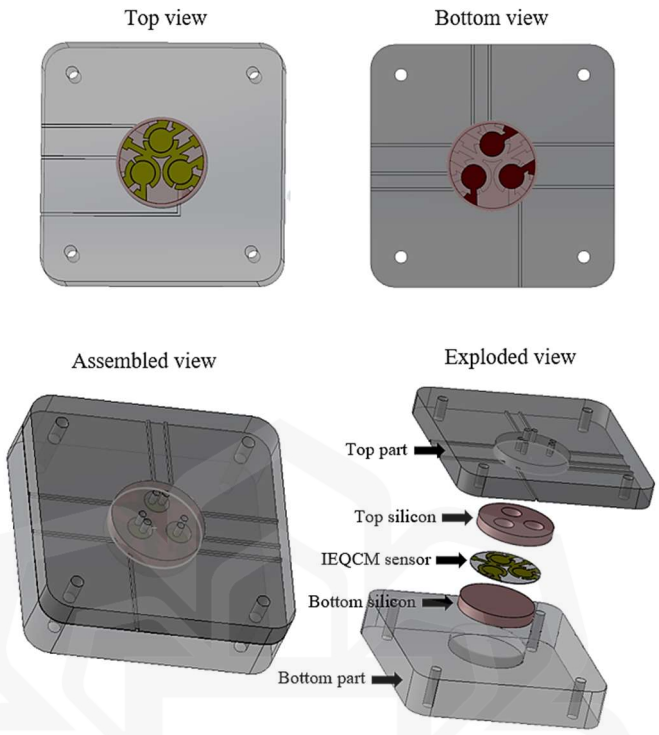

Figure 3.13: Top, bottom, assembled and exploded view of fluidic chamber.

3.3 CHAPTER SUMMARY

This chapter covered the in-depth research design methodology of the potentiostat and fluidic chamber system. It is composed of design specification, main components selection, schematic and PCB design, software design and fluidic chamber design of the potentiostat system. Design specification explained the flow of the potentiostat system and main components selection reviewed the list of components used in the making of the potentiostat system. All of the schematic and PCB design of all of the three versions of the potentiostat was explained thoroughly from the first step until the very last step that was designed using Altium Designer software. The code used to run the CV measurement of the potentiostat was coded in Arduino software. Next, the design of the fluidic chamber was explained, consisting of the top and bottom part of the fluidic chamber, top and bottom of silicon layers and IEQCM sensor, with all being gripped together as a single device.

CHAPTER 4

EXPERIMENTAL WORK

4.1 OVERVIEW OF IEQCM BIOSENSOR POTENTIOSTAT SYSTEM

This chapter presents the overview of the potentiostat integrated with the fluidic chamber using IEQCM biosensor and its outcomes. In this research, all the simulations were done using EmStat Pico board which act as a benchmark for CV and EIS measurement but only CV measurement was coded and implemented in the fabrication of the designed potentiostat board. Since the designed potentiostat board can only support CV program, CV result obtained from this board was compared with the EmStat Pico board to determine whether the designed potentiostat can work as accurately as the commercial potentiostat. Surface bio-functionalization was performed on the surface of the IEQCM sensor for dengue NS1 antibody-antigen binding. EIS measurement was simulated using the EmStat Pico and the modified IEQCM sensor. The overview of the IEQCM biosensor potentiostat and fluidic chamber system for early and variant dengue detection is displayed in Figure 4.1 below.

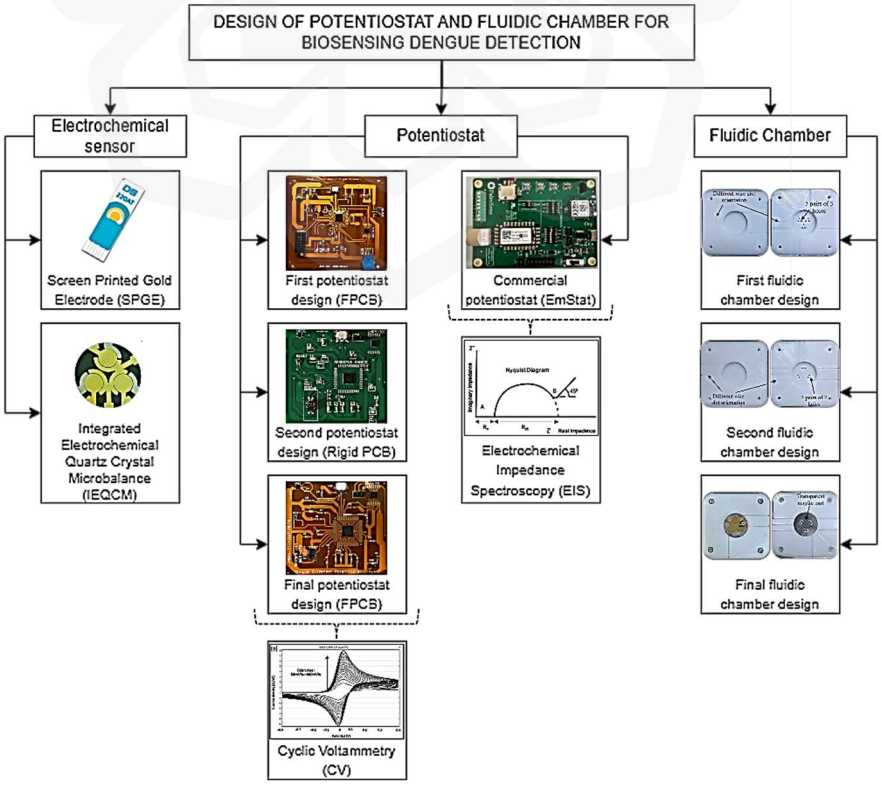

Figure 4.1: Overview of IEQCM biosensor potentiostat system.

4.2 FABRICATION OF DESIGNED POTENTIOSTAT

In this research, three versions of the potentiostat design were sent for fabrication to PCB manufacturing and assembly companies. Three versions were required to correct the errors that were found in the first two boards.

4.2.1 First Potentiostat Design Fabrication

The first design of the potentiostat was fabricated on a flexible polyimide (PI) film substrate with the dimensions of 80.0 mm x 92.0 mm as shown in Figure 4.2 (a, b). It was manufactured by Jabil Circuit, an American manufacturing services company. FPCB represents the future of the PCB industry and Jabil Circuit was renowned for their expertise in FPCB fabrication. Flex circuits have several advantages such as fewer maintenance actions with the elimination of conventional wire connections, higher and longer-term reliability due to reduced size, weight and manufacturing time over rigid circuits.

However, there are a few complications with the internal connection of the first board design causing the board to malfunction. Troubleshooting process was more complicated on a flexible board since not much adjustment can be done as the flexible substrate is more delicate compared to a rigid one. For example, one of the connections was cut straight from the board to fix the short circuit problem but it causes a few components to burn. Once some damage was done on the FPCB, it will remain and cannot be reverted which is different compared to rigid PCB boards that are more durable. There are a few errors that occur within the connection of the first design and Appendix E explained the errors encountered during the troubleshoot phase of the first potentiostat design.

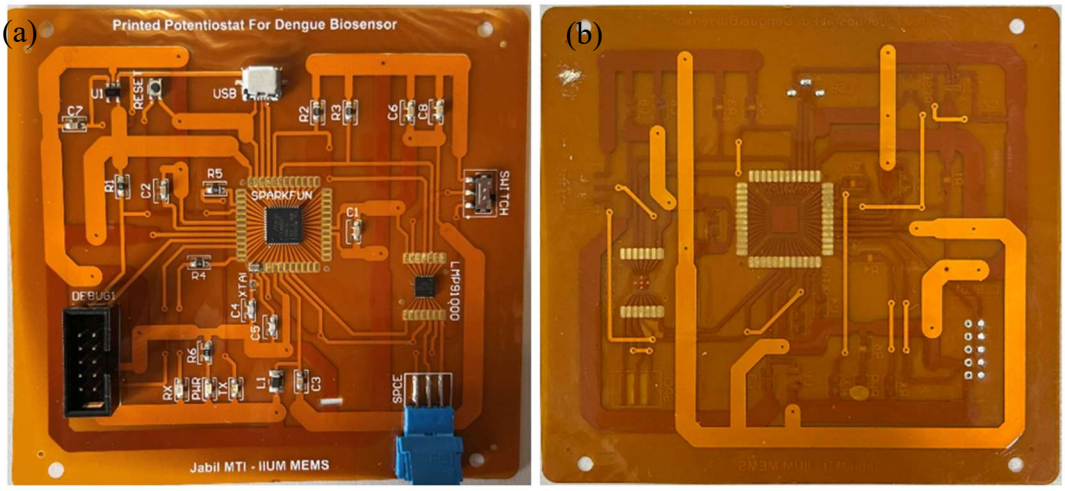

Figure 4.2: (a) Front and (b) back view of the flexible printed circuit board (FPCB) of the first potentiostat.

4.2.2 Second Potentiostat Design Fabrication

The second potentiostat design was created in order to validate the functionality of the new potentiostat design. Many alternatives for board fabrication were discovered throughout this research that can provide fast fabrication and cost-effectiveness. Hence, Figure 4.3 (a, b) displays the second PCB potentiostat board fabricated on a rigid PCB with a dimension of 63.0 mm x 68.0 mm. This board was made from FR-4 material which is a flame-retardant epoxy resin and glass fabric composite and was fabricated by PCBWay, a Chinese-based PCB manufacturing company. PCBWay provides first-rate services such as fast turnaround time, reliable quality and prompt shipment with no restrictions on the size, shape or complexity of boards that can be created via a user-friendly website. Rigid PCBs are built of solid base materials that add rigidity and longevity to the board. When compared to flex boards, they are also more compact, less costly and easier to debug and repair.

The second fabricated potentiostat board managed to be powered up but there were a few issues encountered during the testing phase of the board such as soldering and bootloading issues. Bootloading is one of the required steps for own board fabrication done by burning a custom bootloader to the ATSAMD21G18 microcontroller chip using J-Link debugger purchased from Segger Microcontroller

Systems. The bootloader is a small code that allows the microcontroller to upload firmware, enabling it to be programmed via the Arduino software. Eventually, the board is functioning well after the troubleshooting process and able to run the desired electrochemical measurement. Appendix F showed the problems faced with the second design of the potentiostat.

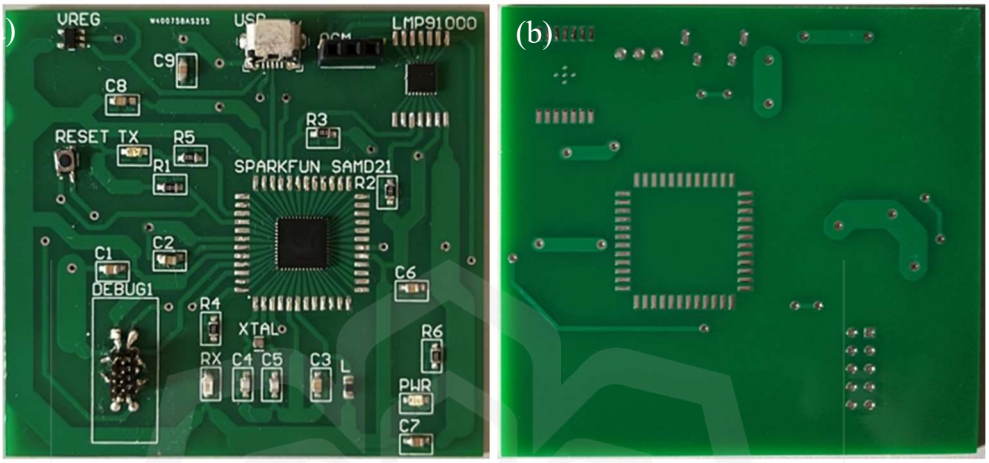

Figure 4.3: (a) Front and (b) back view of the rigid printed circuit board (PCB) of the second potentiostat.

4.2.3 Final Potentiostat Design Fabrication

Final design of the potentiostat with the smallest size of 60.0 mm x 65.0 mm is shown in Figure 4.4. In collaboration with Jabil Circuit, the final design was fabricated on a flexible polyimide (PI) film substrate, aligning with the main objective of flexible potentiostat for wearable application. Flex circuits offer various advantages over rigid circuits, such as reduced size, weight and manufacturing time. This final board is fully functioning just like the second design, with the only change being the substrate type. Made from FPCB, this design is the smallest and flexible iteration while ensuring optimal functionality, making it the most successful design in all of the potentiostat design series. Table 4.1 below described the difference between all potentiostats.

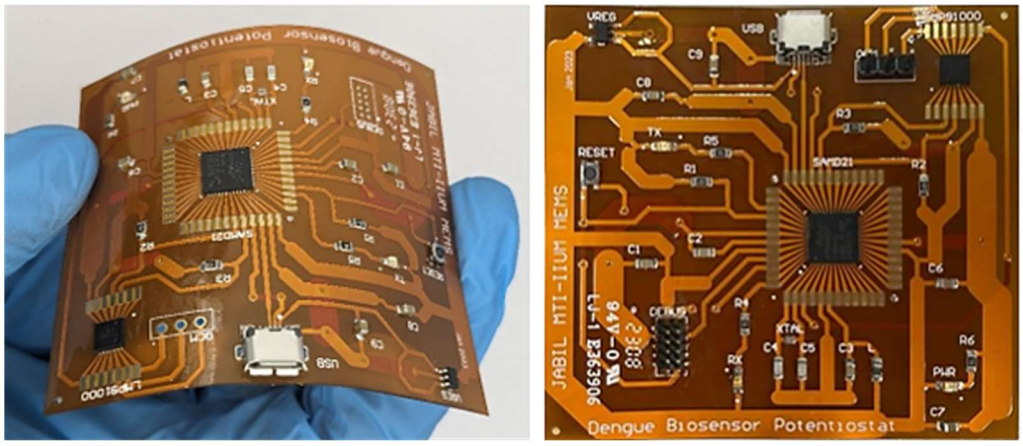

Figure 4.4: Flexible printed circuit board (FPCB) of the final potentiostat.

Table 4.1: Comparison of first and second potentiostat design.

Potentiostat Design	Advantages	Limitations
Flexible PCB (First & final design) 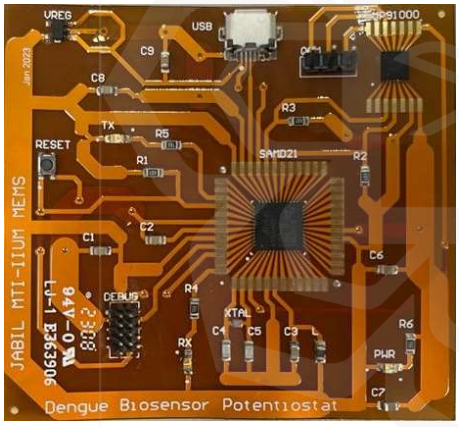	• Fewer maintenance interventions. • Elimination of conventional wire connections. • Higher and longer-term reliability. • Size, weight and manufacturing time reduction.	• Troubleshooting process was more complicated. • Less adjustment can be made as the flexible substrate is more delicate. • More expensive.
Rigid PCB (Second design) 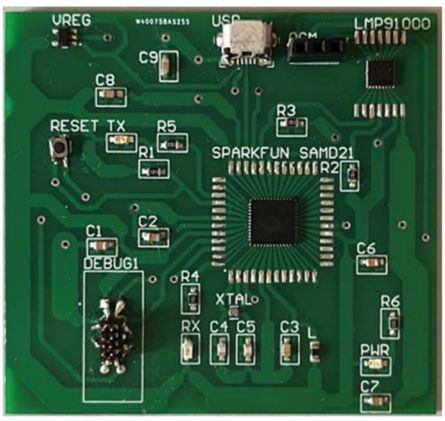	• Built of solid materials that add rigidity and longevity to the board. • More compact. • Cost-effective. • Easier to debug and repair.	• Cannot bend, twist and fold. • Long production time. • Increased circuit size, weight and complexity.

4.3 FABRICATION OF 3D PRINTED FLUIDIC CHAMBER

The 3D printed fluidic chamber was fabricated to hold the IEQCM sensor in place during the electrochemical measurements. It consists of the top and bottom fluidic chamber, top and bottom silicon layer and the IEQCM sensor itself. The fluidic chamber was integrated together with the potentiostats for electrochemical measurements.

4.3.1 Assemble and Leakage Test

The 3D printed fluidic chamber was fabricated as shown in Figures 4.5, 4.6 and 4.7. All of the fluidic chambers were 3D printed using ABS material. This 3D printed fluidic chamber was used to place the IEQCM biosensor for electrochemical measurement. Assemble and leakage test was done to make sure that the solution dropped on the sensor was not spread all over the sensor affecting the measurement. About 0.1 mL of the coloured solution was dropped inside the chamber and observed for 5 minutes. The first and second version did not pass the assembling and leaking test as there is leakage when a coloured solution is dropped inside the chamber due to the gap in between the fluidic chamber as seen in Figure 4.5 and 4.6, but the leakage was not fully visible as the chamber was opaque. The final version was made with a transparent acrylic part for better leakage visualization and the result proved that the coloured solution does not leak to the adjacent sensors' chamber as shown in Figure 4.7.

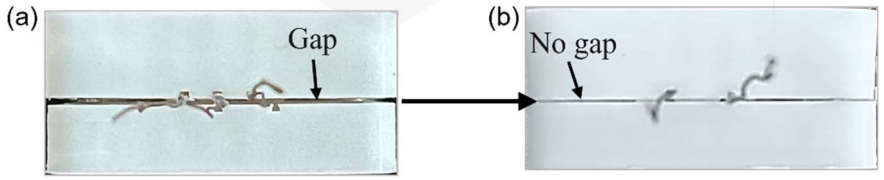

Figure 4.5: (a) First and (b) final version of 3D printed fluidic chamber with no gap issues.

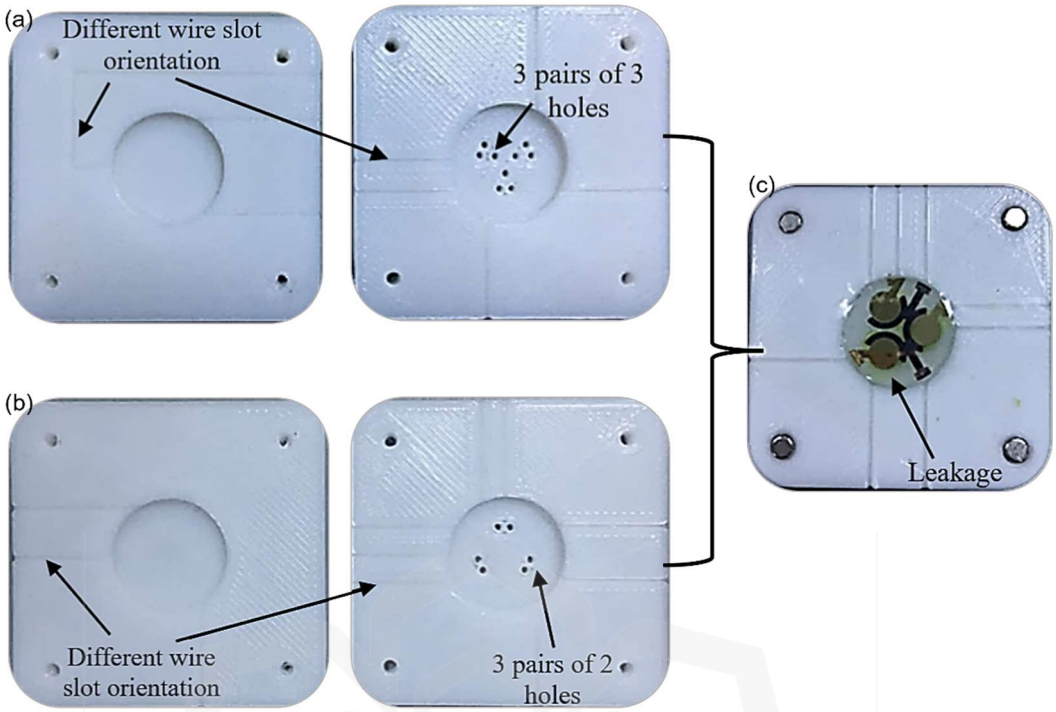

Figure 4.6: (a) First and (b) second version of 3D printed fluidic chamber with (c) leakage test result.

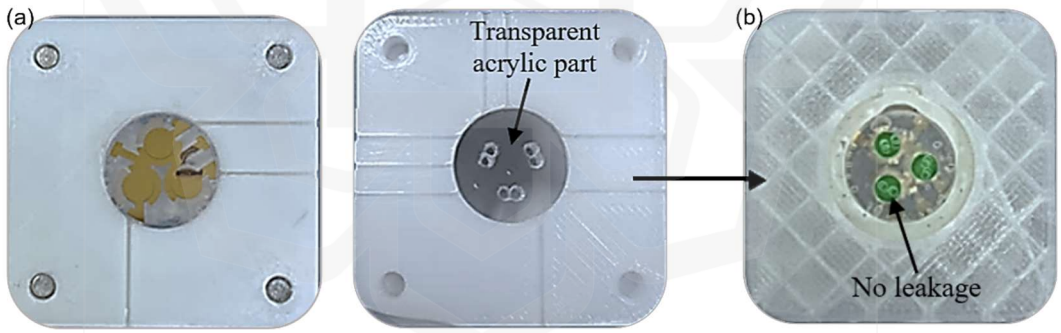

Figure 4.7: (a) Final version of 3D printed fluidic chamber with (b) leakage test result.

4.4 ELECTROCHEMICAL MEASUREMENT

Two types of electrochemical measurement, Cyclic Voltammetry (CV) and Electrochemical Impedance Spectroscopy (EIS) were taken using both the designed potentiostat and the EmStat Pico potentiostat. The 0.5 mM of potassium ferrocyanide solution was dropped onto the IEQCM sensor that was placed inside the fluidic chamber through the holes on its top. Potassium ferrocyanide solution is commonly used as

baseline solutions due to its stable electrochemical behaviour. The fluidic chamber was then connected to the potentiostat for electrochemical measurement. However, the reference electrode on the IEQCM starts to disappear after a few cycles during the measurement. An external reference electrode was opted using a pure silver wire (Ag) with a minimum length of 3 cm. The disposable pure silver wire was immersed in bleach (NaClO) to form silver/silver chloride (Ag/AgCl) for 15 to 30 minutes. Since the IEQCM sensor is reusable, the measurements were conducted multiple times and reliability was confirmed through the acquisition of triplicate measurements (A. A. Zainuddin, 2020; (Wasilewski et al., 2022). The measurement setup of the potentiostat system for electrochemical measurement was displayed in Figure 4.8 below.

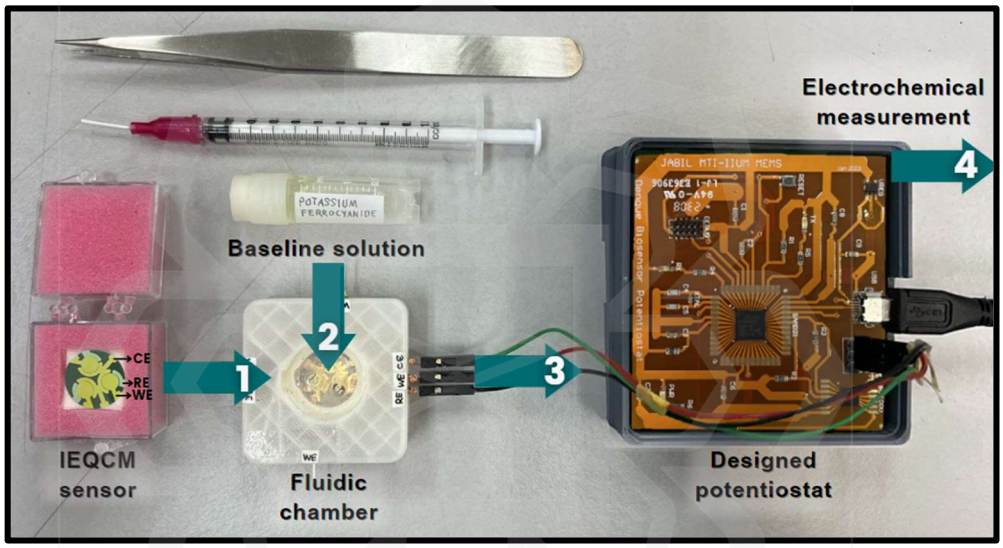

Figure 4.8: Electrochemical measurement setup of the potentiostat and fluidic chamber system.

4.4.1 Cyclic Voltammetry (CV)

Cyclic Voltammetry (CV) is an electrochemical technique for measuring the current response of a redox active solution. It is performed by cycling the potential of a working electrode and measuring the resulting current. CV was first simulated using the EmStat Pico development board, which acted as a benchmark and the data was obtained through the PSTrace software. The actual result of CV measurement was measured using the designed potentiostat and the data was obtained through the Arduino software. Measurements were initially conducted using a dummy cell and Screen-Printed Gold

Electrode (SPGE) before final confirmation with the IEQCM sensor. The IEQCM sensor was made of an array of three QCM on a single quartz substrate. The working and counter electrode of the IEQCM sensor were made from gold because it has better performance and high stability while the reference electrode was made from silver. The measurements were done numerous times and reliability was ensured in triplicate.

4.4.1.1 EmStat Pico (Benchmark)

EmStat Pico is a small, software-enabled potentiostat system on a module that is incorporated with electrochemistry (Stratmann, 2019). This EmStat Pico board acts as a benchmark result for the CV measurement taken using the designed potentiostat to validate the accuracy of the designed potentiostat system. The electrochemical measurement setup using the EmStat Pico development board was portrayed in Figure 4.9 below.

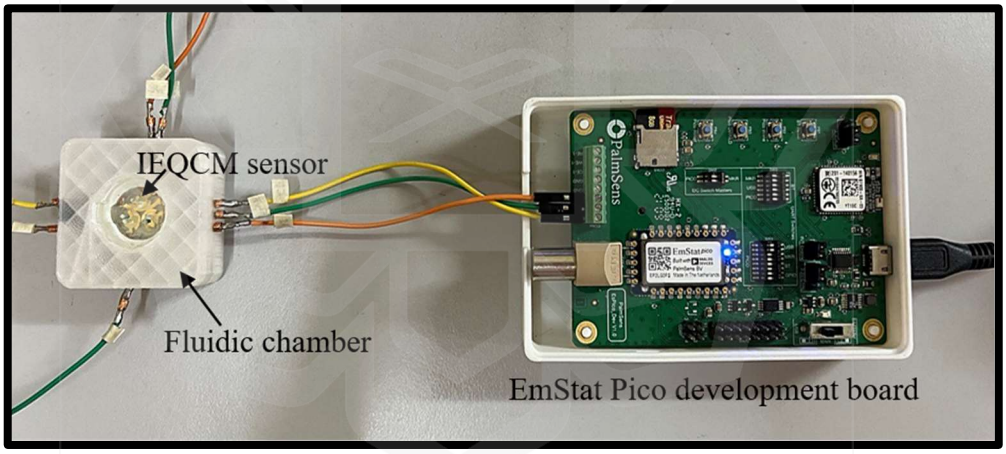

Figure 4.9: Electrochemical measurement setup using EmStat Pico board.

CV measurement was first taken using the EmStat Pico development board along with its provided dummy cell for evaluation purposes. The parameters were set from -400 mV to 700 mV at 1 V/s with current ranging from 100 nA to 1 mA for 15 cycles. Figure 4.10 showed the CV result using the dummy cell with maximum peak potential (E_{pa}): 0.275 V, minimum peak potential (E_{pc}): -0.022 V which gives the peak-to-peak potential (ΔE_p): 0.297 V. The value of ΔE_p was observed, as the smaller the value of ΔE_p, the better and more stable the sensor.

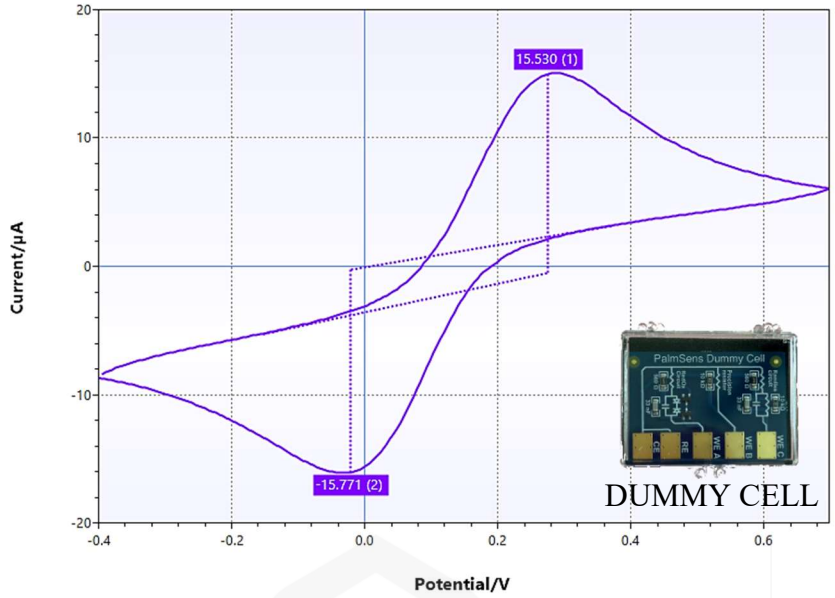

Figure 4.10: CV measurement obtained using a dummy cell.

Next, CV measurement was performed by dropping the baseline solution onto the SPGE sensor. The parameters were set for 15 cycles at 500 mV/s scan rate with voltage sweep around -200 mV to 600 mV and current ranging from 100 nA to 1 mA. The result in Figure 4.11 illustrated the maximum peak potential (E_{pa}): 0.184 V, minimum peak potential (E_{pc}): 0.051 V which gives the peak-to-peak potential (ΔE_p): 0.133 V using the SPGE sensor. A small value of ΔE_p represents a better and more stable sensor since SPGE was made with gold that has high sensitivity and stability.

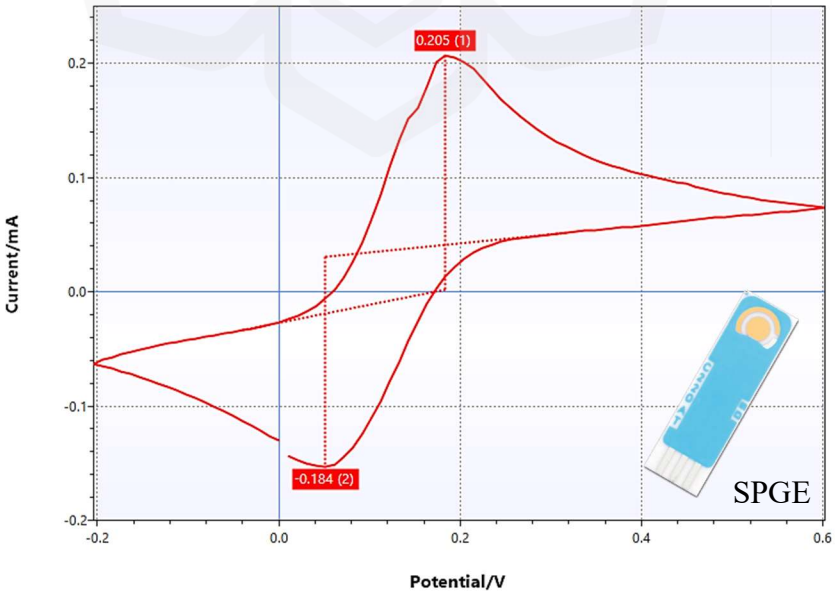

Figure 4.11: CV measurement obtained using SPGE sensor.

Finally, CV measurement was measured using the IEQCM sensor with baseline solution. The same parameters were set at 500 mV/s scan rate with voltage sweep around -200 mV to 600 mV at current ranging from 100 nA to 1 mA for 15 cycles. The result for QCM 1, QCM 2, QCM 3 showed the maximum peak potential (E_{pa}): 0.255 V, 0.255 V, 0.235 V, minimum peak potential (E_{pc}): 0.122 V, 0.122 V, 0.092 V which gives the peak-to-peak potential (ΔE_p): 0.133 V, 0.133 V and 0.143 V respectively were shown in Figure 4.12, 4.13 and 4.14. The small value of ΔE_p obtained with IEQCM was almost similar with SPGE which indicated a highly stable and sensitive sensor since it was made with gold.

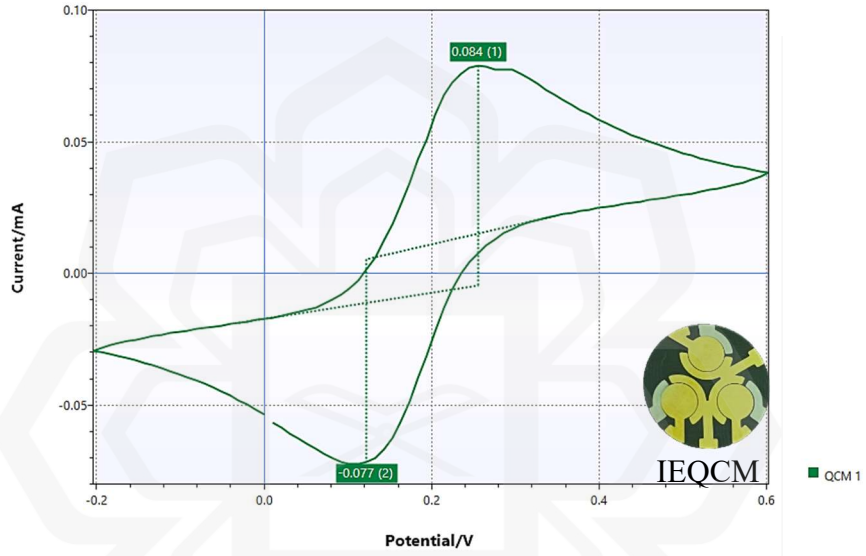

Figure 4.12: CV measurement of QCM 1 from an array of three QCM sensors.

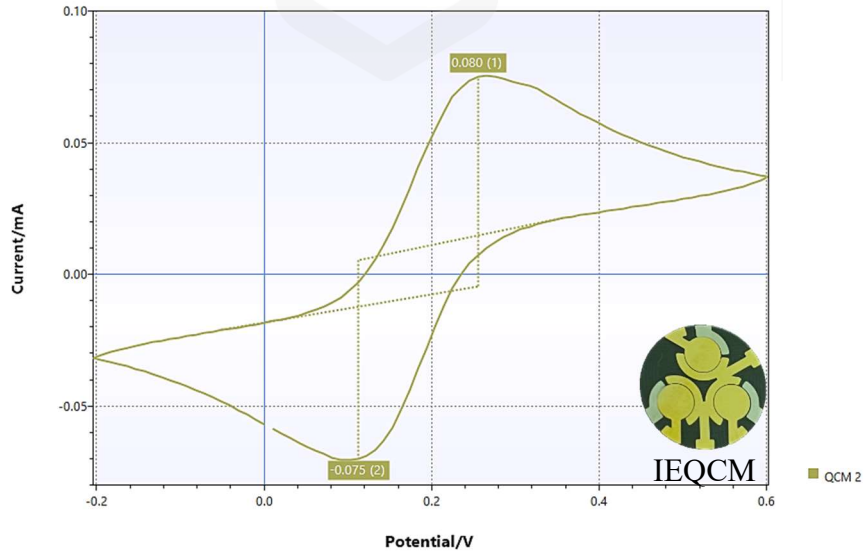

Figure 4.13: CV measurement of QCM 2 from an array of three QCM sensors.

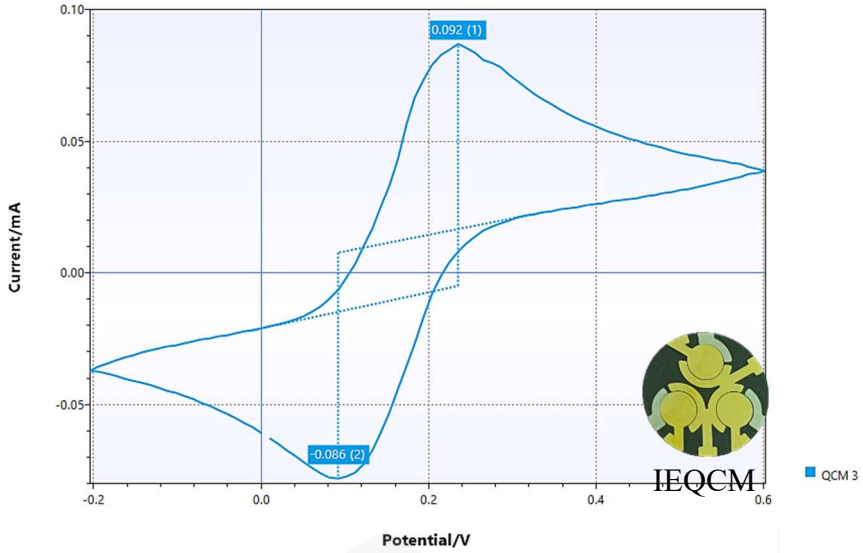

Figure 4.14: CV measurement of QCM 3 from an array of three QCM sensors.

The CV measurement obtained using IEQCM sensor (QCM 1) gives the same value of ΔE_p with the SPGE which is around 0.133 V, indicating that this IEQCM sensor functioning well as the electrodes of both sensors were made with the same gold materials. The working and counter electrode of both SPGE and IEQCM sensor were made from gold while the reference electrode was both made from silver. It is a known fact that gold materials are highly sensitive, conductive and stable. However, IEQCM sensor was specifically designed to have better performance and high stability compared to SPGE.

Electrochemical reversibility of a redox couple is related to the electron transfer rate at the electrode-electrolyte interface. Electrochemical reversibility was determined from the peak-to-peak potential (ΔE_p) separation. ΔE_p was extracted from a CV plot at a fixed scan rate of 500 mV/s. The higher peak current on a CV graph reflects the electrode's ability to transport electrons from the solution to the electrode and vice versa. Types of electrochemical reversibility with ideal values of ΔE_p is shown below:

- Reversible: $\Delta E_p \approx 0.06V$.
- Quasi-reversible: $\Delta E_p > 0.06V$ (with presence of both peaks).
- Irreversible: $\Delta E_p < 0.06V$ (with absence of peak for reverse scan).

Since IEQCM sensor was made of an array of three QCM on a single quartz substrate, Figure 4.15 depicted the CV measurement of all three QCM sensors. From

Figure 4.14, it can be seen that that the IEQCM sensor is accurate as the ΔE_p value of the QCM 1, QCM 2 and QCM 3 sensors is 0.133 V, 0.133 V and 0.143 V respectively which is almost identical but the difference is quite small showing that the IEQCM sensor is stable. This shows that the electrochemical reversibility occurs between IEQCM biosensor and the solution is quasi-reversible as the ΔE_p is more than 0.06 V and both peak is present.

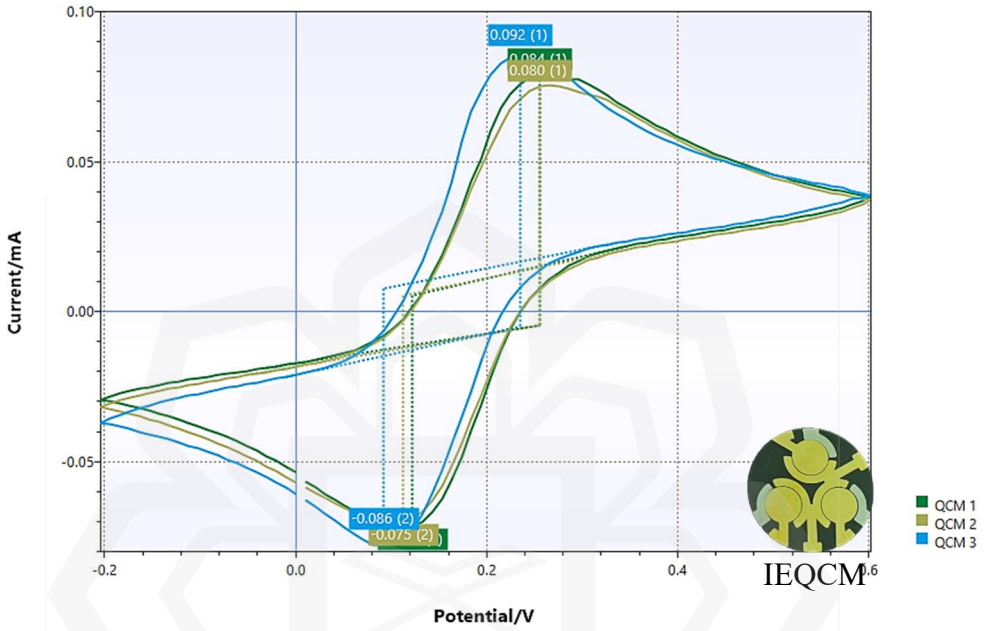

Figure 4.15: CV measurement of an array of three QCM sensors.

Electrokinetic behaviour of electron flow at the electrode-electrolyte interface can be explored in addition to electrochemical reversibility. Figure 4.16 displayed the CV plots at various scan rates ranging from 50 mV/s to 140 mV/s, and Figure 4.17 illustrated the peak current (I_{pa}) against the root-squared scan rate ($v^{1/2}$) to distinguish electrokinetic behaviour of the redox reaction that occurred at the electrode-electrolyte interface. The linear fit on the graph of I_{pa} versus the $v^{1/2}$ primarily represents electron transfer capabilities. The anodic peak was linearly dependent on $v^{1/2}$ with a substantial correlation coefficient ($R^2 \approx 1$), showing that the redox process is diffusion-controlled.

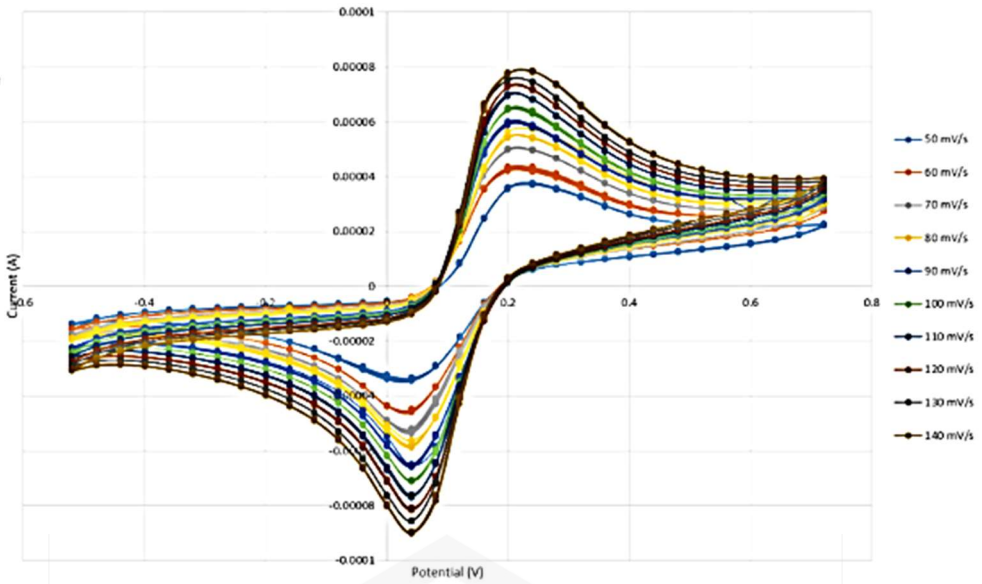

Figure 4.16: CV plot at various scan rates ranging from 50mV/s to 140mV/s.

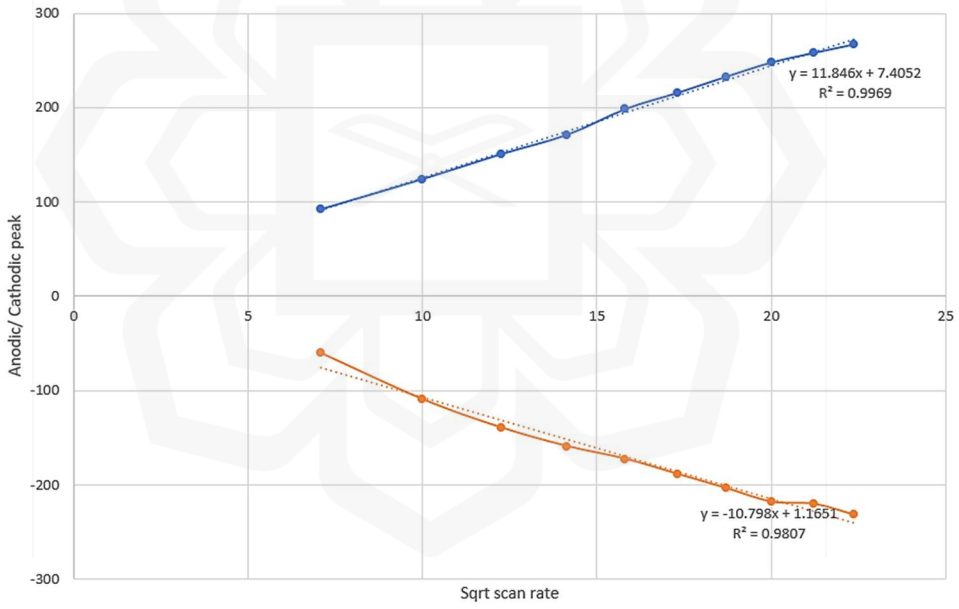

Figure 4.17: Peak current (I_{pa}) against the root-squared scan rate ($v^{1/2}$).

Electrochemical stability of the IEQCM sensor can be studied from Figure 4.18. CV measurement was set for 100 cycles at 500 mV/s to observe the electrochemical stability of the IEQCM sensor. From Figure 4.18, it can be seen that the value of E_p, E_{pa} and E_{pc} values for all cycles show a straight line, considering that the IEQCM sensor is stable as it showed the same value throughout the cycles.

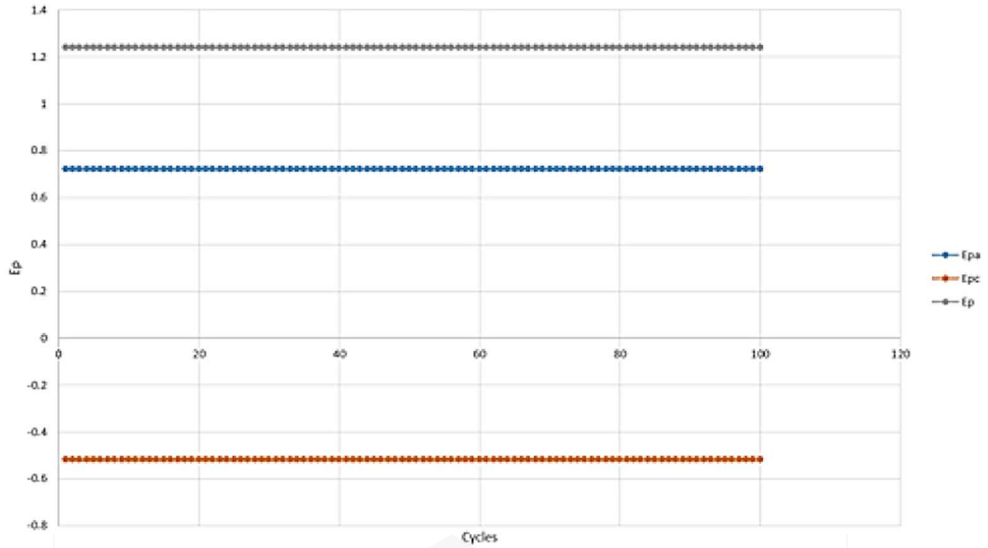

Figure 4.18: Electrochemical stability of IEQCM sensor.

4.4.1.2 Designed Potentiostat (Actual)

Cyclic Voltammetry (CV) measurement was measured using the fabricated potentiostat board and the result obtained from this measurement is the actual result that was compared with the benchmark result using the EmStat Pico board. It was mentioned above that this designed potentiostat only supported CV measurement. Figure 4.19 shows the electrochemical measurement setup using the designed potentiostat board.

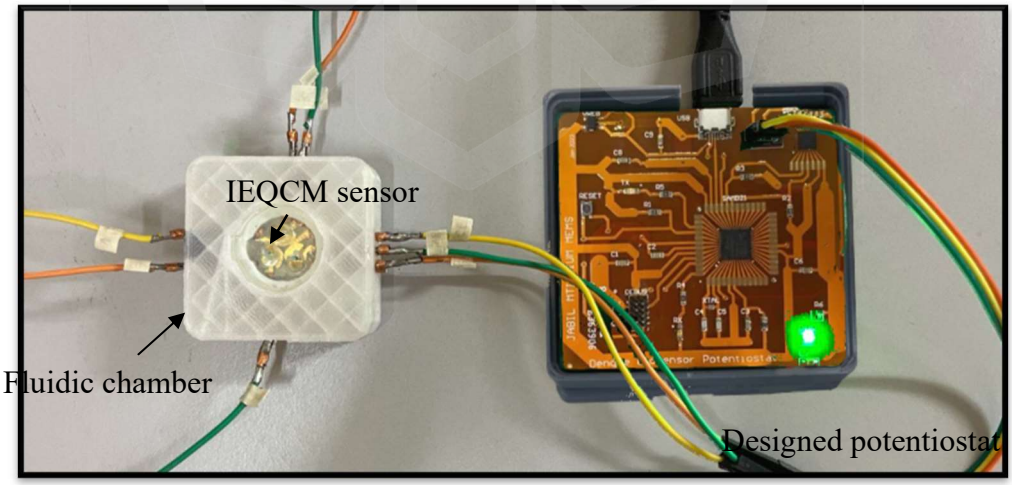

Figure 4.19: Electrochemical measurement setup using designed potentiostat board.

The designed potentiostat board only supported CV measurement instead of both CV and EIS measurements as the commercialized potentiostat, EmStat Pico. The CV measurement programming can be run on Arduino software and the result data can be exported to Microsoft Excel for further analysis. The internal resistance of the LMP91000 is R_{gain} (kΩ) with values of 2.75, 3.5, 7, 14, 35, 120 and 350; R_{load} (Ω) with values of 10, 33, 50 and 100. These values can be adjusted according to the desired value that fits the objectives of the CV measurement. CV measurement was done using the designed potentiostat with different internal resistance, R_{gain} and R_{load}.

The CV with internal resistor values, R_{load} = 50 Ω and R_{gain} = 14 kΩ for 15 cycles at 100 mV/s scan rate with voltage sweep around -400 mV to 600 mV was chosen as the best CV result using the designed potentiostat. 0.5 mM of potassium ferrocyanide solution which is the baseline solution was dropped on the IEQCM sensor surface and the data was collected. The data obtained from the serial monitor of the Arduino software was then exported to Excel and the graph of Voltage (mV) against current (μA) was plotted. From Figure 4.20, the result shows the maximum peak potential (E_{pa}): 0.264 V, minimum peak potential (E_{pc}): 0.132 V which gives the peak-to-peak potential (ΔE_p): 0.132 V for the IEQCM sensor.

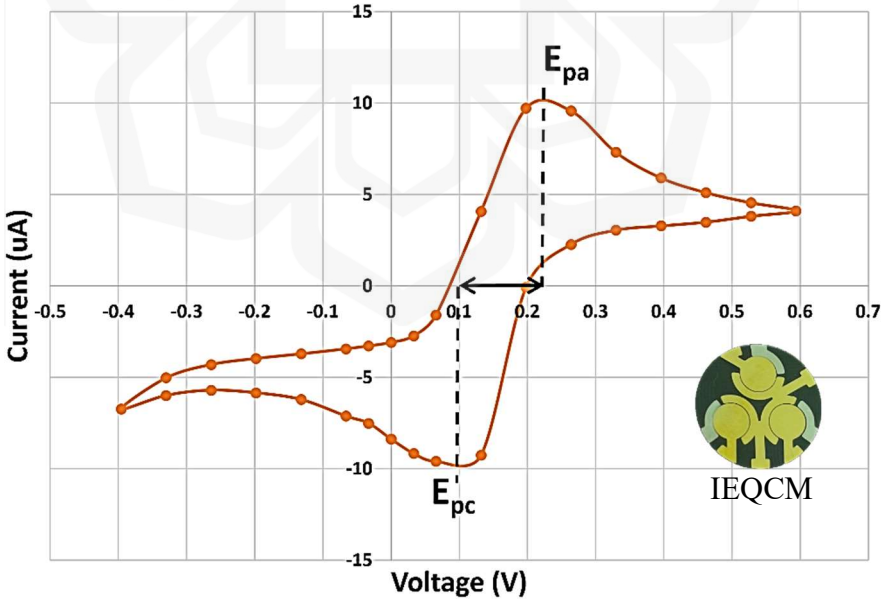

Figure 4.20: Best CV measurement obtained using designed potentiostat.

4.4.1.3 Comparison of EmStat Pico and Designed Potentiostat Board

Figure 4.21 and 4.22 depicted the result of CV measurement obtained using an EmStat Pico development board (benchmark) and the designed potentiostat board (actual) using 0.5 mM of potassium ferrocyanide solution. It is shown that the designed potentiostat is almost accurate as it follows the same pattern as the theoretical result obtained from the EmStat Pico development board. Table 4.2 depicted the comparison of ΔE_p values obtained using EmStat Pico and designed potentiostat. The ΔE_p result using the EmStat Pico and the designed potentiostat is also almost identical with ΔE_p values of 0.133 V and 0.132 V respectively. The difference is about 0.001 V which gives about 99.25 % accuracy, this explains that the performance of the designed potentiostat is almost on par with the ideal EmStat Pico potentiostat board.

Table 4.2: Comparison of peak-to-peak separation voltage (ΔEp) values.

Electrochemical sensor	ΔE_p Value (V)	
	EmStat Pico	Designed Potentiostat
Dummy cell	0.297 V	-
SPGE sensor	0.133 V	-
IEQCM sensor	0.133 V	0.132 V

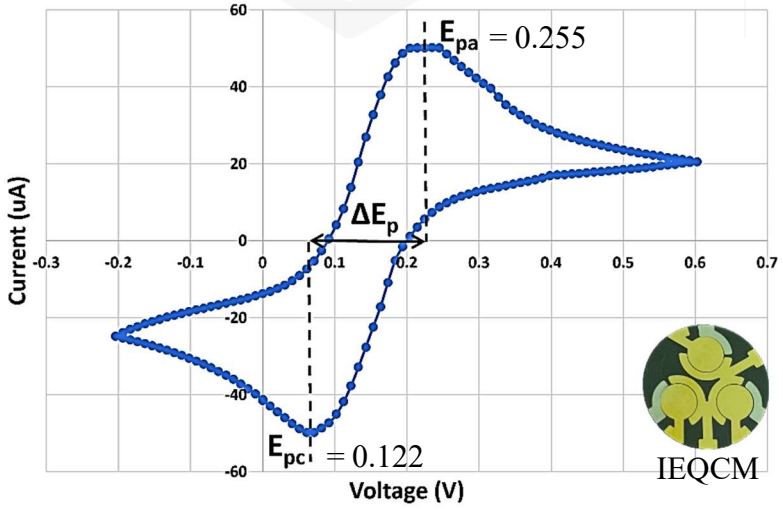

Figure 4.21: CV measurement obtained using EmStat Pico board with $\Delta E_p = 0.133$.

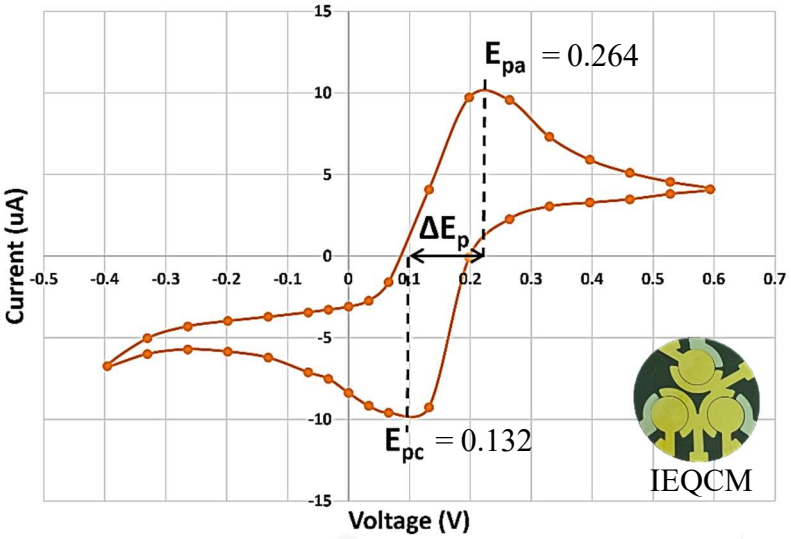

Figure 4.22: CV measurement obtained using designed potentiostat with $\Delta E_p = 0.132$.

4.4.2 Electrochemical Impedance Spectroscopy (EIS)

Electrochemical Impedance Spectroscopy (EIS) is an electrochemical technique used to measure the impedance of a system in dependence of the AC potential frequency. Resulting current was measured by applying a small AC potential to an electrochemical cell. Before performing the EIS measurements, surface bio-functionalization process on the gold surface of the WE of the IEQCM sensor must be conducted. This surface modification and immobilization process was done to ensure a strong attachment of a biorecognition element (NS1 antibody) that binds to the analyte (NS1 antigen) selectively. Preparation of all the chemicals used for surface modification and immobilization on gold surface for NS1 antibody-antigen binding are further explained in APPENDIX G. The EIS result from this NS1 antigen-antibody binding will be compared with previous works.

4.4.2.1 Surface Bio-Functionalization

Surface bio-functionalization is the process of modifying the surface characteristics of the gold IEQCM working electrode using chemicals such as 11-mercaptoundecanoic acid (11-MUA), 6-mercaptohexanol (6-MCH), n-(3-dimethylaminopropyl)-n′-ethylcarbodiimide (EDC), n-hydroxysulfosuccinimide (Sulfo-NHS), ethanolamine (ETA), glycine (Aminoacetic acid), mouse monoclonal [DN3] to dengue virus NS1 glycoprotein with its conjugate recombinant dengue virus 2 NS1 glycoprotein. This surface modification and immobilization was done to strongly bind a biorecognition element (NS1 antibody) to the analyte (NS1 antigen) selectively on the gold surface (A. A. Zainuddin, 2020).

Figure 4.23 shows the surface bio-functionalization process which starts with the pre-cleaning of the bare IEQCM sensor using dilute sulphuric acid. It is followed by the incubation of SAM on the surface of the electrode which was activated by the EDC/sulfo-NHS solution. Next, the dengue NS1 antibody is incubated to allow attachment of NS1 antigen. Ethanolamine and glycine solution were then used to deactivate the unbound active sites of remaining NHS esters and block the remaining free reactive carboxylic groups. After completing the surface bio-functionalization steps on the IEQCM surface, the final step was the NS1 antigen-antibody detection.

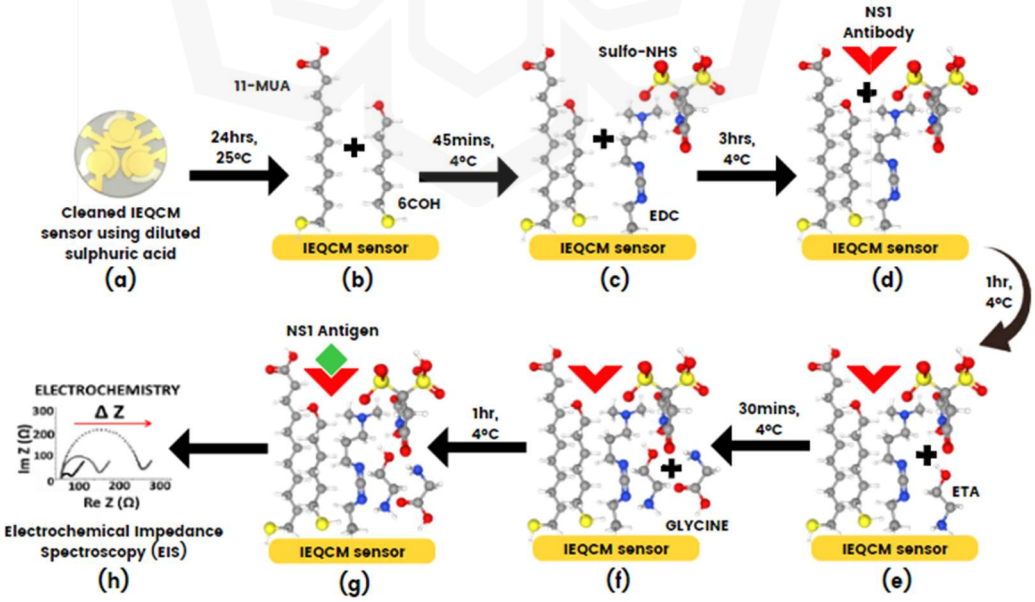

Figure 4.23: Surface bio-functionalization of IEQCM sensor for NS1 antibody-antigen attachment.

4.4.2.1.1 Incubation Process

The first step for surface bio-functionalization process was cleaned the bare IEQCM sensor surface thoroughly using dilute sulphuric acid with cotton bud and placed the clean IEQCM sensor inside the fluidic chamber. Then, the working electrode of the IEQCM sensor was incubated with SAM solution for 24 hours to bind the NS1 antibody to the NS1 antigen (Thébault et al., 2022). Next, activation of the carboxylic acid terminated-group of SAM solution was done by submerging the modified SAM working electrode in EDC/Sulfo-NHS solution for 45 minutes (Lathika et al., 2021). After EDC/Sulfo-NHS incubation, the modified electrode was incubated with anti-NS1 antibody for 3 hours (Lathika et al., 2021). Before the incubation of different NS1 antigen concentrations, the modified SAM-EDC/Sulfo-NHS-NS1Antibody electrode was immersed in ETA and glycine solution for 1 hour and 30 minutes respectively (Raymundo-Pereira et al., 2021; Mendonça et al., 2021). Finally, the modified SAM-EDC/Sulfo-NHS-NS1Antibody-ETA-Glycine electrode was incubated with six different concentrations of NS1 antigen which are 10, 50, 100, 500, 1000 and 2000 ng/mL (A. A. Zainuddin et al., 2019). All of the surface modification process done on the working electrode of IEQCM sensor was incubated at 4 °C and rinsed with PBS solution after the completion of each step. EIS measurement was taken at the end of every surface bio-functionalization process using a baseline solution to study the behaviour of the electron transfer after every layer of surface modification.

4.4.2.1.2 Surface Bio-Functionalization Verification

After the completion of the surface bio-functionalization process on the IEQCM sensor, this IEQCM sensor was integrated with commercial potentiostat, EmStat Pico and fluidic chamber for EIS measurement. EIS measurement validation of the surface bio-functionalization and dengue NS1 antigen-antibody detection was done based on previous works. The first EIS measurement was tested with the provided dummy cell for evaluation purposes. The parameters were set at 10 mV and the frequency was swept from 10 Hz to 10 kHz with current ranging from 1 µA to 1 mA. Figure 4.24 portrayed the EIS result using the dummy cell. The solution resistance (R_s), charge-transfer

resistance (R_{ct}) and double-layer capacitance (C_{dl}) values that followed the Randle's equivalent circuit which are 560.50 Ω, 9977.00 Ω and 32.99 nF showed a very low percentage error which are 0.146 %, 0.156 % and 0.14 5% respectively with a very low x^2 value.

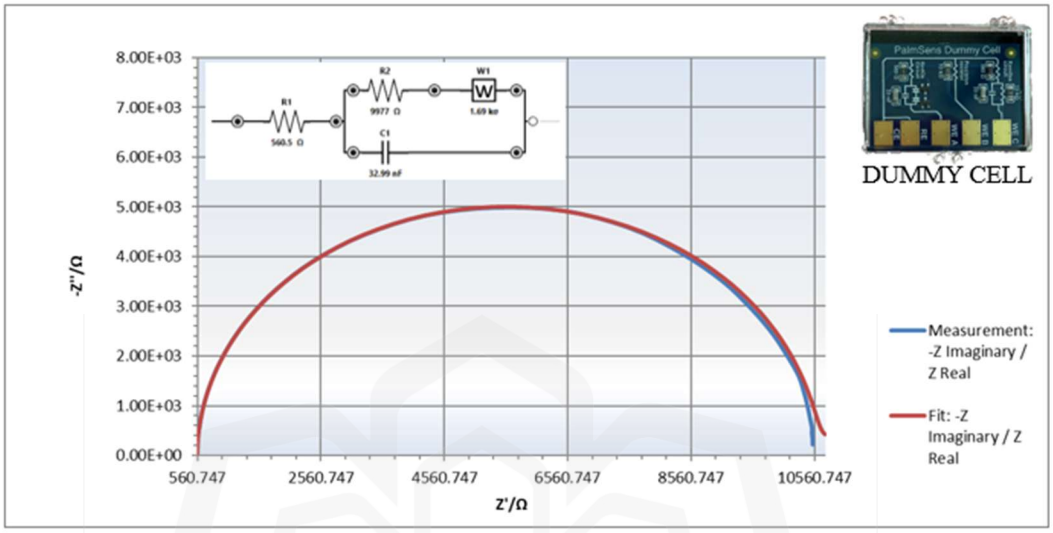

Element	Fitted Value	Min Value	Max Value	Unit	Error%
R_s	560.5	1.00E-6	1.00E+12	Ω	0.146
R_{ct}	9977	1.00E-6	1.00E+12	Ω	0.156
W	1690	1.00E-6	1.00E+12	σ	9.917
C_{dl}	3.299E-8	1.00E-12	1.00E-3	F	0.145
Chi-Squared:	2.33E-5	Iterations:	7		

Figure 4.24: Surface bio-functionalization of IEQCM sensor for NS1 antibody-antigen attachment.

Next, EIS measurement was measured by dropping 0.5 mM of potassium ferrocyanide solution onto the surface of the Screen-Printed Gold Electrode (SPGE) sensor. The parameters were set at 10 mV AC potential with current ranging from 1 µA to 10 mA and swept the frequency from 1 Hz to 10 kHz. Figure 4.25 showed the EIS result using the SPGE sensor. The x^2 value of the EIS circuit fitting graph is close to zero which is 0.0171 indicating a good fitting graph. The R_s, R_{ct} and C_{dl} values followed the Randle's equivalent circuit which are 29.32 Ω, 920.50 Ω and 1.79 µF respectively. R_s, R_{ct} and C_{dl} values also showed quite a low percentage error for the curve fitting measurement which are 4.799 %, 3.927 % and 3.536 % respectively.

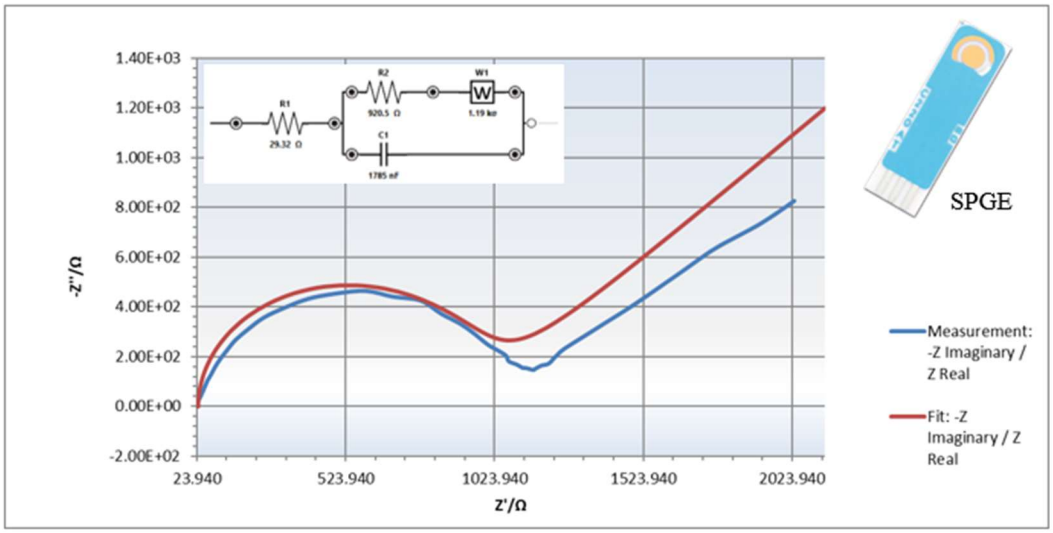

Element	Fitted Value	Min Value	Max Value	Unit	Error%
R_s	29.32	1.00E-6	1.00E+12	Ω	4.799
R_{ct}	920.5	1.00E-6	1.00E+12	Ω	3.927
W	1190	1.00E-6	1.00E+12	σ	9.880
C_{dl}	1.785E-6	1.00E-12	1.00E-3	F	3.536
Chi-Squared:	0.0171	Iterations:	67		

Figure 4.25: EIS measurement and Randle's equivalent circuit (circuit fitting) obtained using SPGE sensor.

Finally, EIS measurement was done using IEQCM sensor using the same baseline solution. The frequency of this measurement swept from 1 Hz to 100 kHz with current ranging from 1 µA to 10 mA at 10 mV AC potential. The x^2 value of the EIS circuit fitting graph shown in Figure 4.26 using IEQCM sensor is 0.0090 which is much closer to zero that represents a good fitting graph. Further analysis was done on the Nyquist plot by curve fitting the data obtained during the EIS measurement. The R_s, R_{ct} and C_{dl} values followed the Randle's equivalent circuit which are 28.52 Ω, 298.90 Ω and 2.30 µF with lower percentage error for the curve fitting measurement which are 2.867 %, 3.422 % and 2.955 % respectively. The EIS measurement done using IEQCM sensor indicates the best measurement due to the lower percentage error when compared with SPGE. This explained that IEQCM is more accurate and sensitive compared to SPGE.

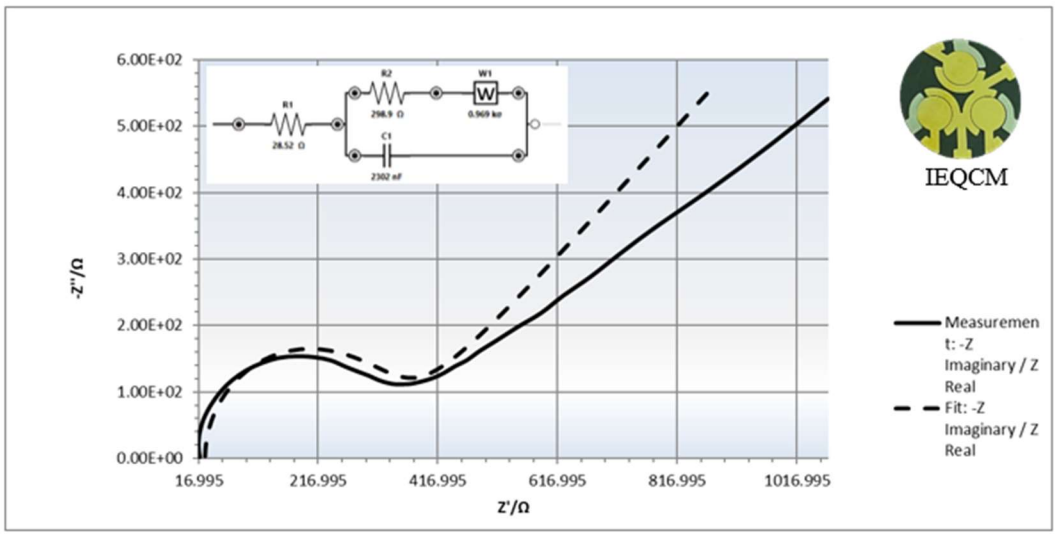

Element	Fitted Value	Min Value	Max Value	Unit	Error%
R_s	28.52	1.00E-6	1.00E+12	Ω	2.867
R_{ct}	298.9	1.00E-6	1.00E+12	Ω	3.422
W	968.7	1.00E-6	1.00E+12	σ	5.355
C_{dl}	2.302E-6	1.00E-12	1.00E-3	F	2.955
Chi-Squared:	0.0090	Iterations:	3		

Figure 4.26: EIS measurement and Randle's equivalent circuit (circuit fitting) obtained using IEQCM sensor.

Another EIS measurement was performed using the IEQCM sensor without the surface bio-functionalization process with a few analytes such as the baseline solution, sample with uninfected dengue virus, sample with DENV-1 and DENV-2. In Figure 4.27 (a, b), the Nyquist and Bode plot of the EIS measurement was presented using the above-mentioned analytes. This measurement was done to observe if there is any difference between each analyte. From the figure, it is shown that different analytes give different EIS measurement values. This indicates that the IEQCM sensor has high sensitivity and specificity as it can differentiate different dengue viruses which are DENV1 and DENV2 from the EIS measurement. This fits the aim of this research to have a potentiostat with high sensitivity and specificity. However, the real EIS measurement that needs to be tested with the dengue samples, needs to undergo the surface bio-functionalization process to ensure the NS1 antibody-antigen attachment of the dengue virus.

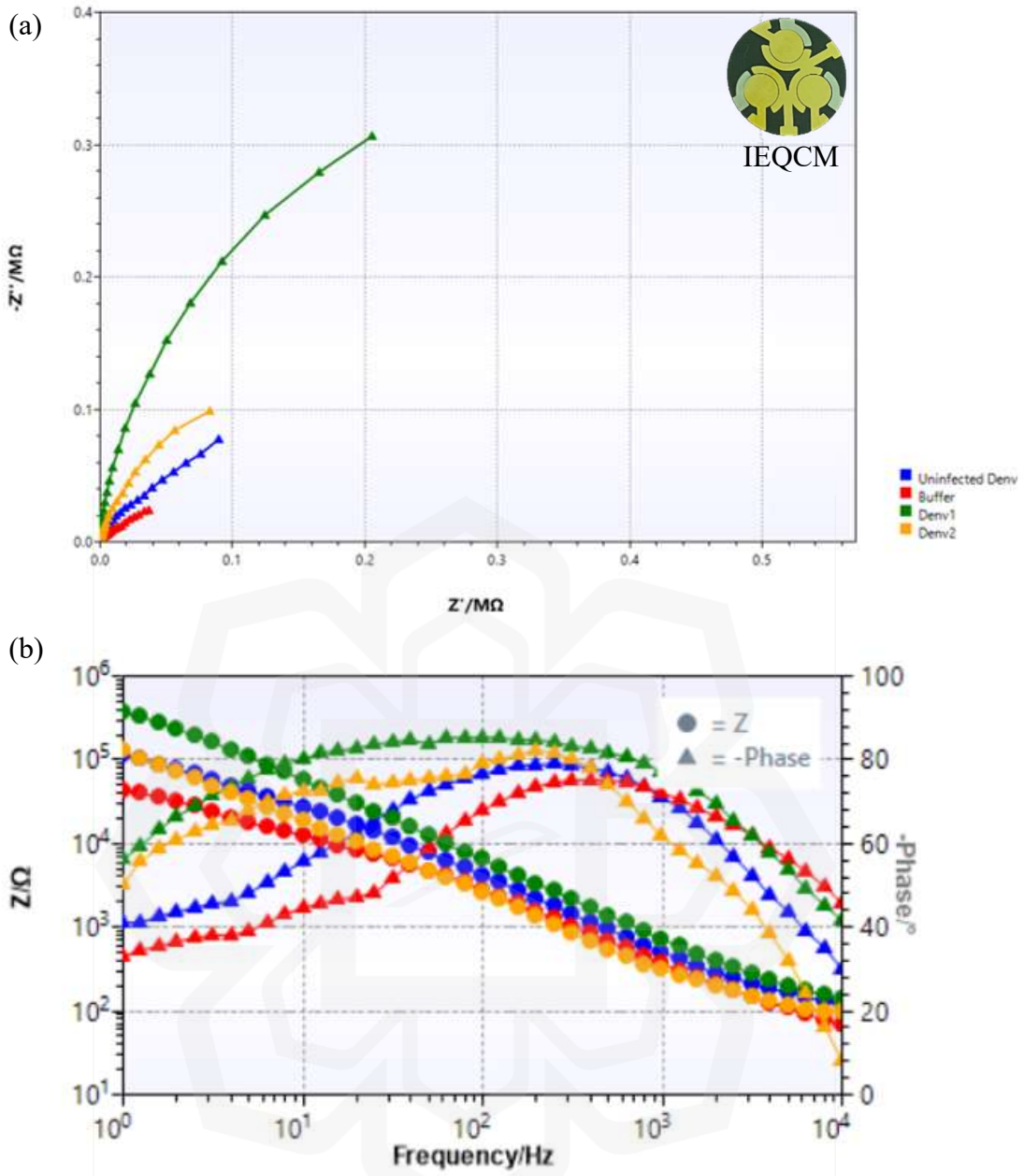

Figure 4.27: (a) Nyquist and (b) bode plot of different analyte samples.

The surface bio-functionalization results for step (a, b, c, d, e, f) are shown in Figure 4.28, 4.29, 4.30, 4.31, 4.32 and 4.33 respectively. A small fluctuation which is about ± 30 Ω in the solution resistance (R_s), was expected due to the inconsistent temperature and uneven distance between electrodes. From the results, the bare IEQCM exhibited a low resistance, suggesting a fast electron transfer of the redox probe to the electrode surface. After the bare IEQCM was immersed in the mix solution of 11-MUA and 6-MCH, a SAM layer was formed on the electrode surface that would inhibit the

electron transfer due to the high resistance of the SAM layer. Thus, an increase of the charge transfer resistance (R_{ct}) of the redox process was expected after the SAM layer formation. A further increase in R_{ct} will appear after the next subsequent step of the surface modification using EDC/sulfo-NHS, NS1 antibody, ethanolamine and glycine. The percentage error values of R_{ct} obtained for each subsequent step were <5 % indicating a good fitting curve of EIS measurement. The double layer capacitance (C_{dl}) is the electrical double layer that appears at the interface between the NS1-modified electrode and solution. The Warburg diffusion element, W is an equivalent electrical circuit component that models the diffusion process but is negligible in this system due to it not significantly contributing to the overall impedance.

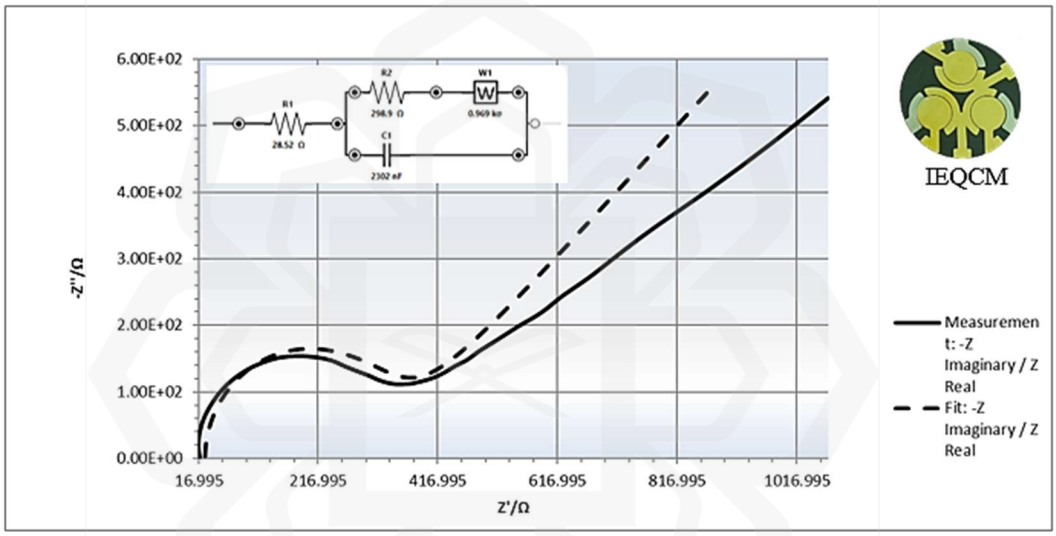

Element	Fitted Value	Min Value	Max Value	Unit	Error%
R_s	28.52	1.00E-6	1.00E+12	Ω	2.867
R_{ct}	298.9	1.00E-6	1.00E+12	Ω	3.422
W	968.7	1.00E-6	1.00E+12	σ	5.355
C_{dl}	2.302E-6	1.00E-12	1.00E-3	F	2.955
Chi-Squared:	0.0090	Iterations:	3		

Figure 4.28: EIS curve fitting graph of a bare IEQCM (Step (a)) with R_s = 28.52 Ω, R_{ct} = 298.90 Ω and C_{dl} = 2.302×10−6 F, percentage error of <5 %.

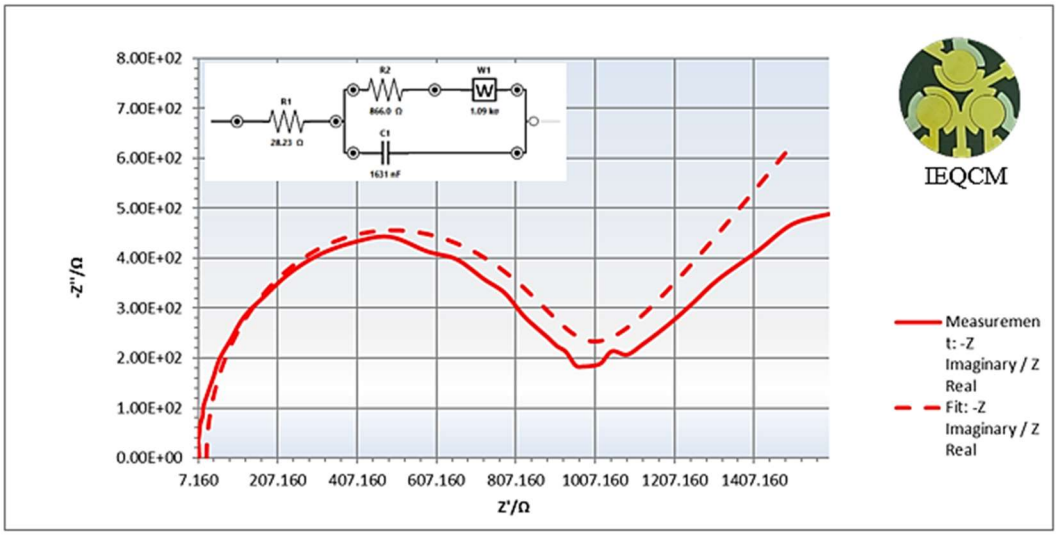

Element	Fitted Value	Min Value	Max Value	Unit	Error%
R_s	28.23	1.00E-6	1.00E+12	Ω	2.086
R_{ct}	866.0	1.00E-6	1.00E+12	Ω	3.371
W	1090	1.00E-6	1.00E+12	σ	9.971
C_{dl}	1.631E-6	1.00E-12	1.00E-3	F	2.574
Chi-Squared:	0.0118	Iterations:	4		

Figure 4.29: EIS curve fitting graph of a modified SAM IEQCM (Step (b)) with R_s = 28.23 Ω, R_{ct} = 866.00 Ω and C_{dl} = 1.631×10−6 F, percentage error of <5 %.

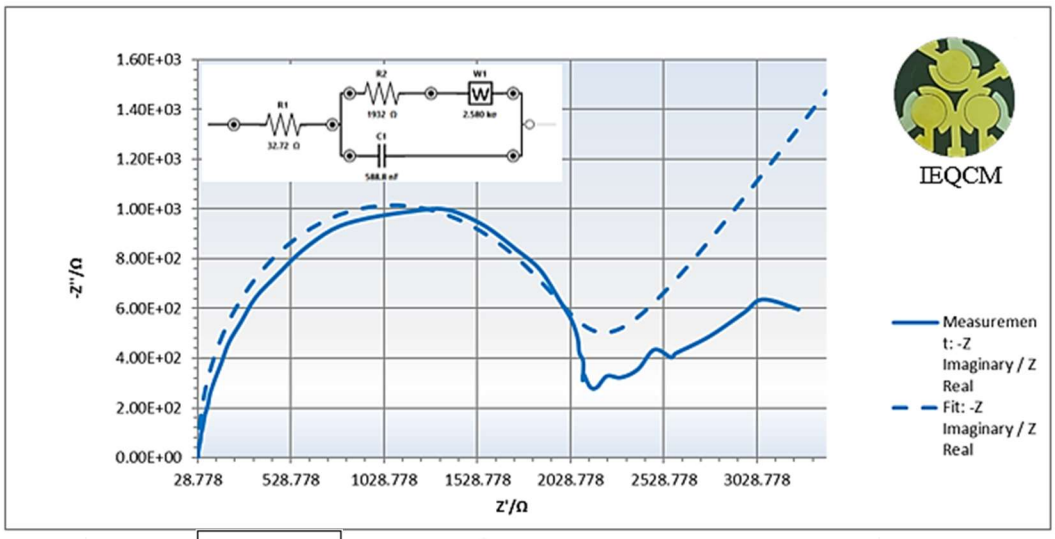

Elem	tted Value	Min Value	Max Value	Unit	Error%
R 1	.72	1.00E-6	1.00E+12	Ω	4.504
R 2	1932	1.00E-6	1.00E+12	Ω	3.298
W 1	2580	1.00E-6	1.00E+12	σ	9.128
C 1	5.888E-7	1.00E-12	1.00E-3	F	2.840
Chi-Squared:	0.0132	Iterations:	5		

R_s

R_{ct}

W

C_{dl}

Figure 4.30: EIS curve fitting graph of a modified SAM-EDC/Sulfo-NHS IEQCM (Step (c)) with R_s = 32.72 Ω, R_{ct} = 1932.00 Ω and C_{dl} = 5.888×10−7 F, percentage error of <5 %.

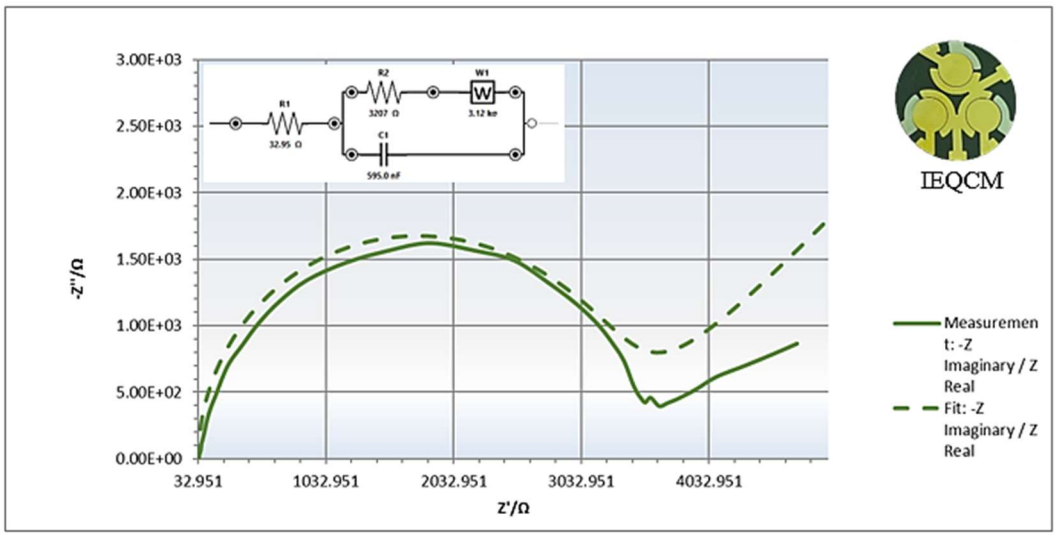

Element	Fitted Value	Min Value	Max Value	Unit	Error%
R_s	32.95	1.00E-6	1.00E+12	Ω	4.892
R_{ct}	3207	1.00E-6	1.00E+12	Ω	3.114
W	3120	1.00E-6	1.00E+12	σ	9.987
C_{dl}	5.950E-7	1.00E-12	1.00E-3	F	2.529
Chi-Squared:	0.0115	Iterations:	4		

Figure 4.31: EIS curve fitting graph of a modified SAM-EDC/Sulfo-NHS-NS1Antibody IEQCM (Step (d)) with R_s = 32.95 Ω, R_{ct} = 3207.00 Ω and C_{dl} = 5.950×10−7 F, percentage error of <5 %.

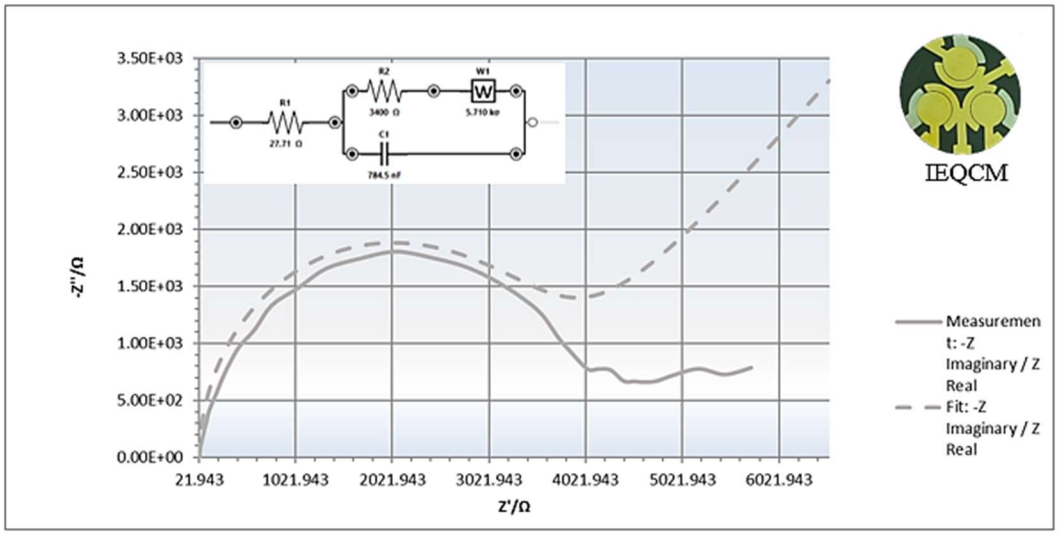

Element	Fitted Value	Min Value	Max Value	Unit	Error%
R_s	27.71	1.00E-6	1.00E+12	Ω	6.839
R_{ct}	3400	1.00E-6	1.00E+12	Ω	4.643
W	5710	1.00E-6	1.00E+12	σ	9.984
C_{dl}	7.845E-7	1.00E-12	1.00E-3	F	3.022
Chi-Squared:	0.0181	Iterations:	13		

Figure 4.32: EIS curve fitting graph of a modified SAM-EDC/Sulfo-NHS-NS1Antibody-ETA IEQCM (Step (e)) with R_s = 27.71 Ω, R_{ct} = 3400.00 Ω and C_{dl} = 7.845×10−7 F, percentage error of <5 %.

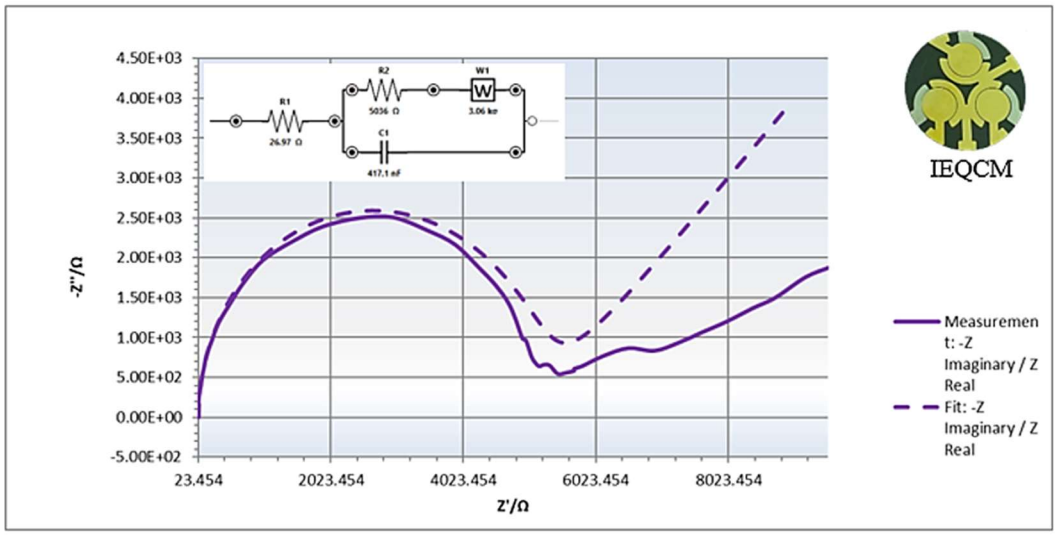

Element	Fitted Value	Min Value	Max Value	Unit	Error%
R_s	26.97	1.00E-6	1.00E+12	Ω	5.117
R_{ct}	4119	1.00E-6	1.00E+12	Ω	2.605
W	3060	1.00E-6	1.00E+12	σ	9.979
C_{dl}	4.171E-7	1.00E-12	1.00E-3	F	2.387
Chi-Squared:	0.0123	Iterations:	3		

Figure 4.33: EIS curve fitting graph of a modified SAM-EDC/Sulfo-NHS-NS1Antibody-ETA-Glycine IEQCM (Step (f)) with R_s = 26.97 Ω, R_{ct} = 4119.00 Ω and C_{dl} = 4.171×10−7 F, percentage error of <5 %.

This research was done based on previous work that utilized the similar IEQCM sensor, the result of surface bio-functionalization was compared with the benchmark result (A. A. Zainuddin, 2020). It can be seen from the results in Figure 4.34 and 4.35 that the final result of the EIS measurement follows a similar pattern to the benchmark with the increment of the R_{ct} values for each subsequent surface modification step. R_{ct} values are observed to study the behaviour of the electron transfer at the electrode-electrolyte interface of this system. This concluded that the IEQCM sensor used in this research was highly accurate and sensitive with percentage error below 5 %.

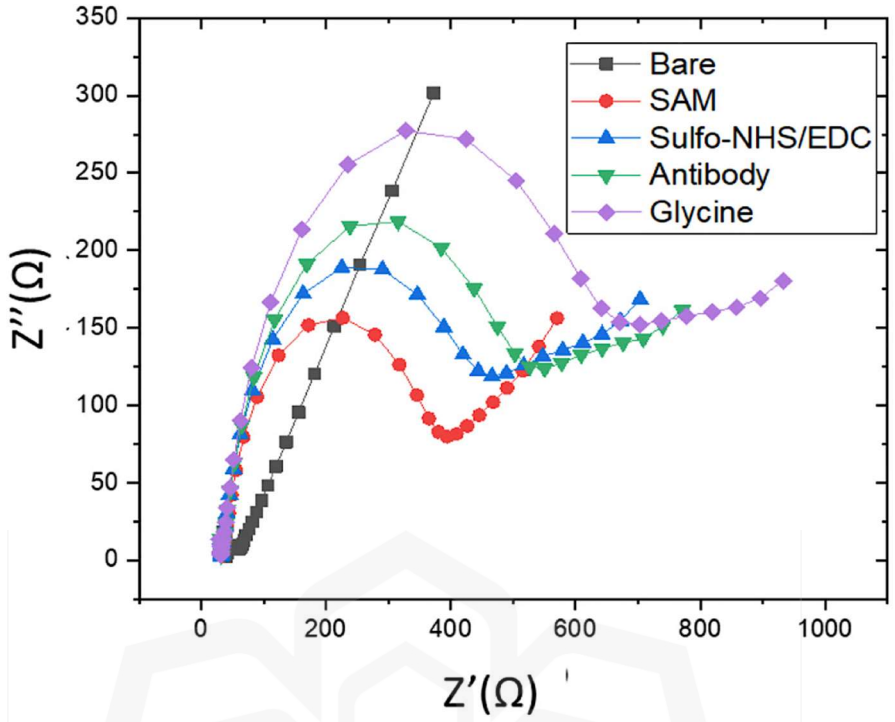

Figure 4.34: Benchmark EIS result of surface bio-functionalization (A. A. Zainuddin, 2020).

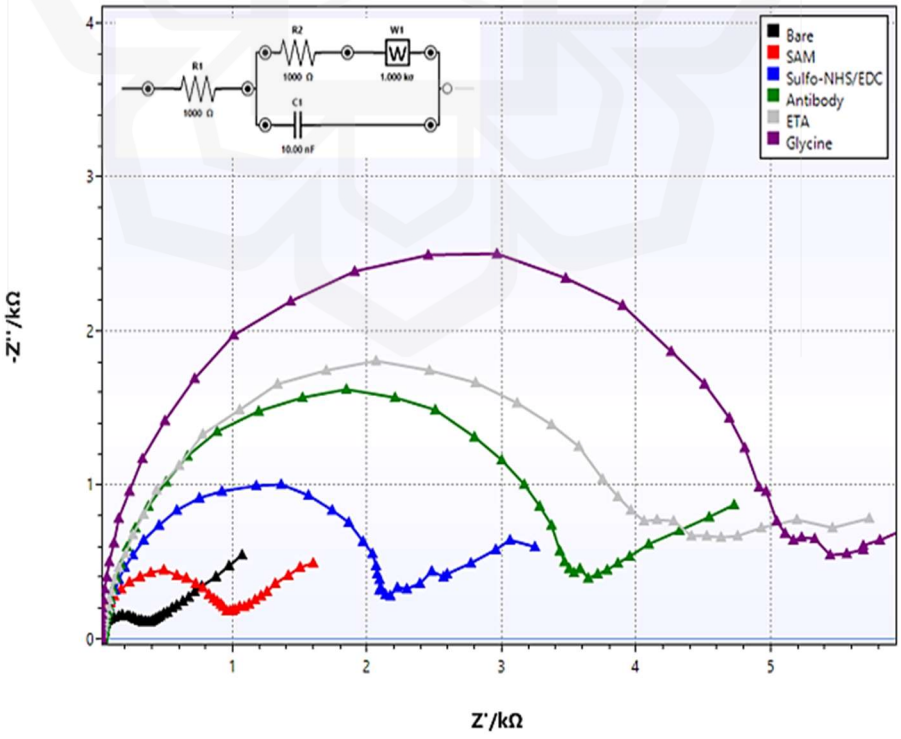

Figure 4.35: Final EIS result of surface bio-functionalization using EmStat Pico.

4.4.2.2 Dengue NS1 Antibody-Antigen Detection

The final EIS measurement results of NS1 antigen attachment to the antibody after the surface bio-functionalization process. Six different concentrations of the NS1 antigen which are 10, 50, 100, 500, 1000 and 2000 ng/mL were prepared to detect the lowest concentration of NS1 antigen that the antibody can capture. The EIS measurement was recorded in the presence of the redox probe via the EmStat Pico potentiostat to monitor changes in charge-transfer resistance associated with target binding. Figure 4.36 showed the triplicate result of blank electrode, the result obtained from the modified SAM-EDC/Sulfo-NHS-NS1Antibody-ETA-Glycine on the IEQCM after the surface modification and immobilization process. The triplicate EIS measurement results of NS1 antigen with different concentrations and its circuit fitting were depicted in Figure 4.37, 4.38, 4.39, 4.40, 4.41 and 4.42 respectively. The electron transfer properties of the redox active solution after the surface bio-functionalization of the electrode can be observed from the charge transfer resistance, R_{ct} obtained from the NS1 antigen detection.

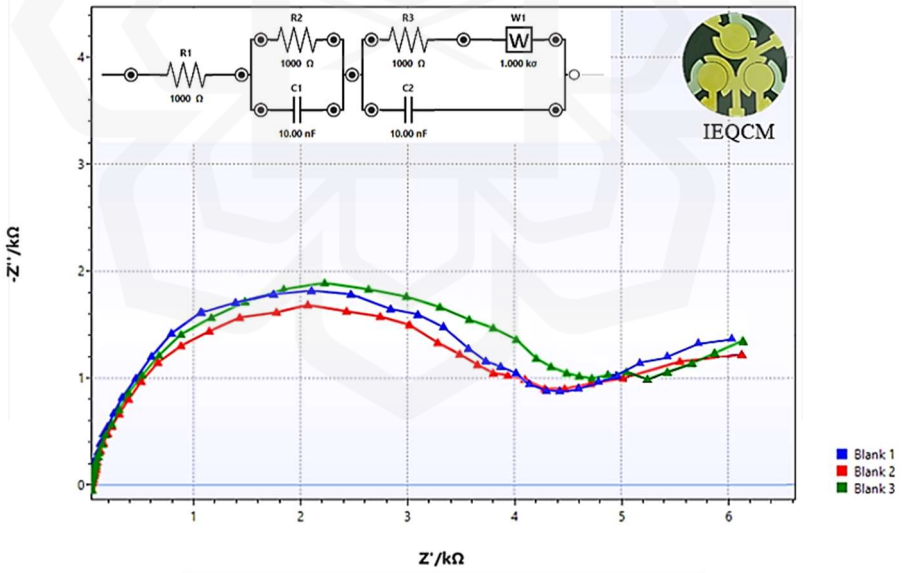

Element	Fitted Value	Unit	Error%
R_{ct} (1)	4203	Ω	2.605
R_{ct} (2)	4119	Ω	2.906
R_{ct} (3)	4517	Ω	2.535
Average R_{ct}	4279.666667		

Figure 4.36: EIS triplicate results of blank electrode with R_{ct} (1) = 4203.00 Ω, R_{ct} (2) = 4119.00 Ω, R_{ct} (3) = 4517.00 Ω, average R_{ct} = 4279.67 Ω, percentage error of <5 %.

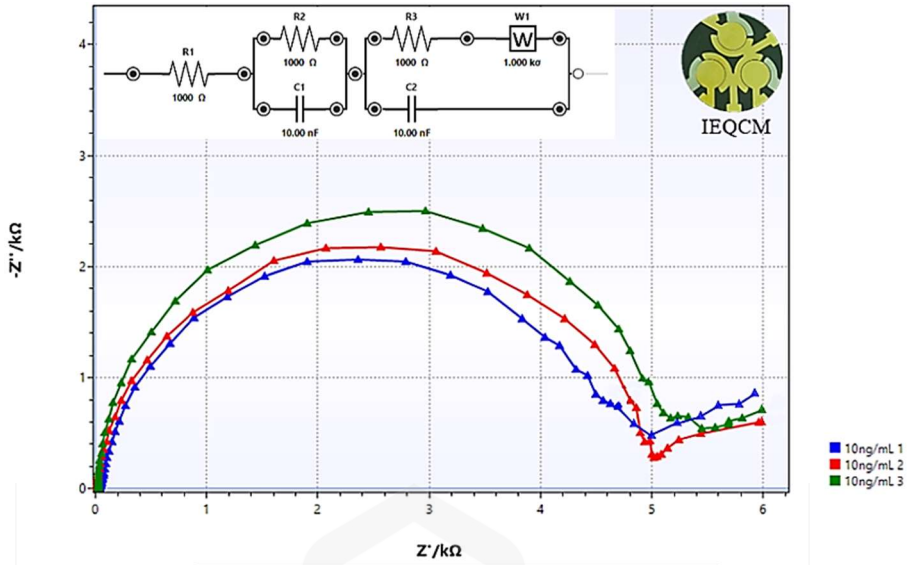

Element	Fitted Value	Unit	Error%
R_{ct} (1)	4123	Ω	1.612
R_{ct} (2)	4538	Ω	3.286
R_{ct} (3)	4744	Ω	2.568
Average R_{ct}	4468.333333		

Figure 4.37: EIS triplicate results of electrode incubated with 10 ng/mL NS1 antigen concentration with R_{ct} (1) = 4123.00 Ω, R_{ct} (2) = 4538.00 Ω, R_{ct} (3) = 4744.00 Ω and average R_{ct} = 4468.33 Ω, percentage error of <5 %.

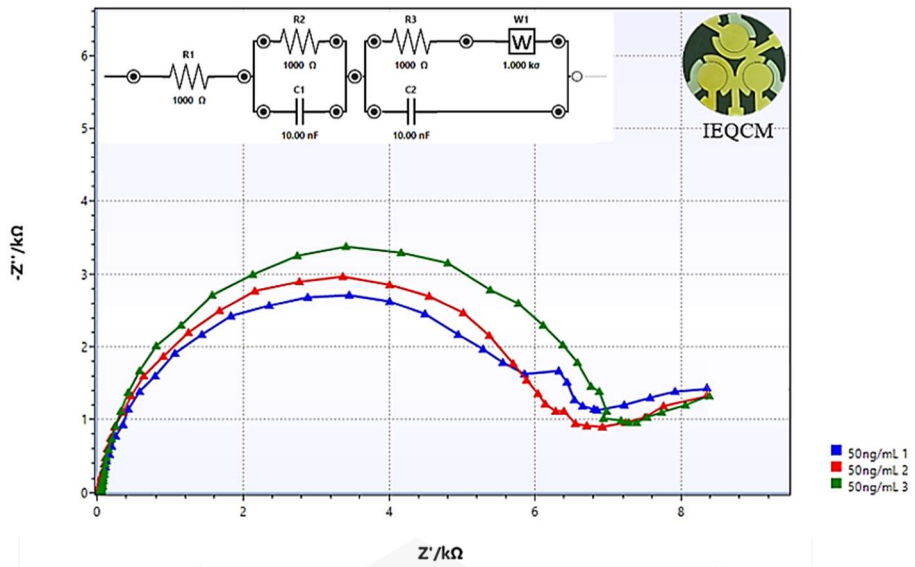

Element	Fitted Value	Unit	Error%
R_{ct} (1)	7971	Ω	2.726
R_{ct} (2)	7959	Ω	3.033
R_{ct} (3)	7996	Ω	4.279
Average R_{ct}	7975.333333		

Figure 4.38: EIS triplicate results of electrode incubated with 50 ng/mL NS1 antigen concentration with R_{ct} (1) = 7971.00 Ω, R_{ct} (2) = 7959.00 Ω, R_{ct} (3) = 7996.00 Ω and average R_{ct} = 7975.33 Ω, percentage error of <5 %.

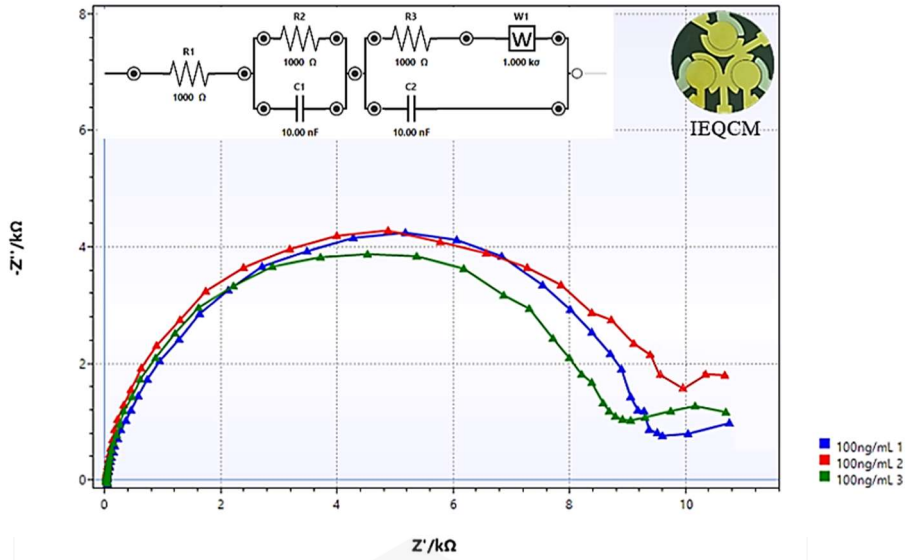

Element	Fitted Value	Unit	Error%
R_{ct} (1)	10789	Ω	2.476
R_{ct} (2)	11698	Ω	3.387
R_{ct} (3)	10406	Ω	1.743
Average R_{ct}	10964.33333		

Figure 4.39: EIS triplicate results of electrode incubated with 100 ng/mL NS1 antigen concentration with R_{ct} (1) = 10789.00 Ω, R_{ct} (2) = 11698.00 Ω, R_{ct} (3) = 10406.00 Ω and average R_{ct} = 10964.33.33 Ω, percentage error of <5 %.

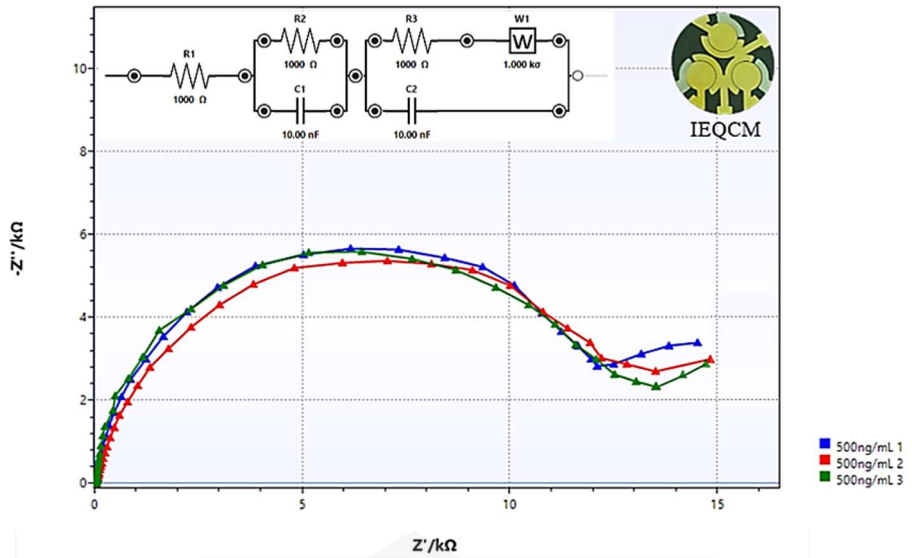

Element	Fitted Value	Unit	Error%
R_{ct} (1)	15897	Ω	2.840
R_{ct} (2)	15976	Ω	4.200
R_{ct} (3)	15954	Ω	2.697
Average R_{ct}	15942.33333		

Figure 4.40: EIS triplicate results of electrode incubated with 500 ng/mL NS1 antigen concentration with R_{ct} (1) = 15897.00 Ω, R_{ct} (2) = 15976.00 Ω, R_{ct} (3) = 15954.00 Ω and average R_{ct} = 15942.33 Ω, percentage error of <5 %.

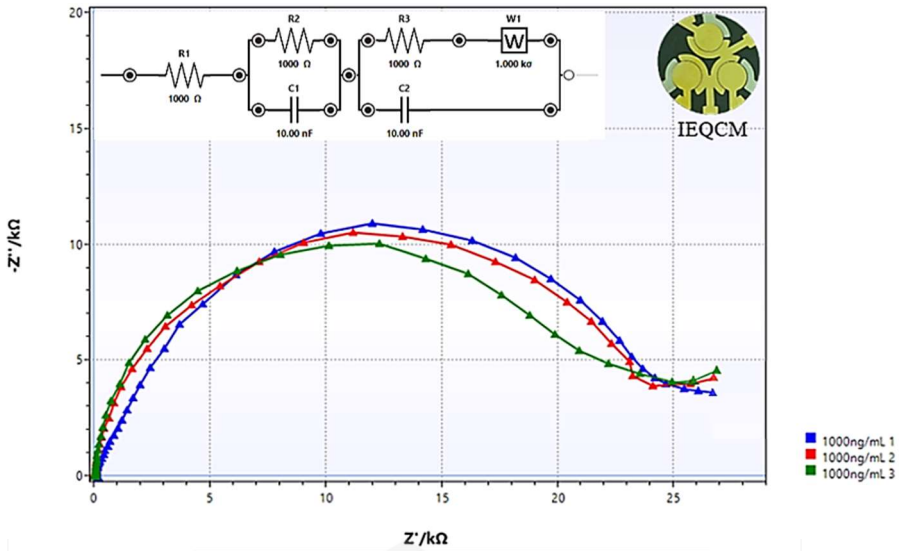

Element	Fitted Value	Unit	Error%
R_{ct} (1)	21885	Ω	2.256
R_{ct} (2)	21870	Ω	3.726
R_{ct} (3)	21986	Ω	3.861
Average R_{ct}	21913.66667		

Figure 4.41: EIS triplicate results of electrode incubated with 1000 ng/mL NS1 antigen concentration with R_{ct} (1) = 21885.00 Ω, R_{ct} (2) = 21870.00 Ω, R_{ct} (3) = 21986.00 Ω and average R_{ct} = 21913.67 Ω, percentage error of <5 %.

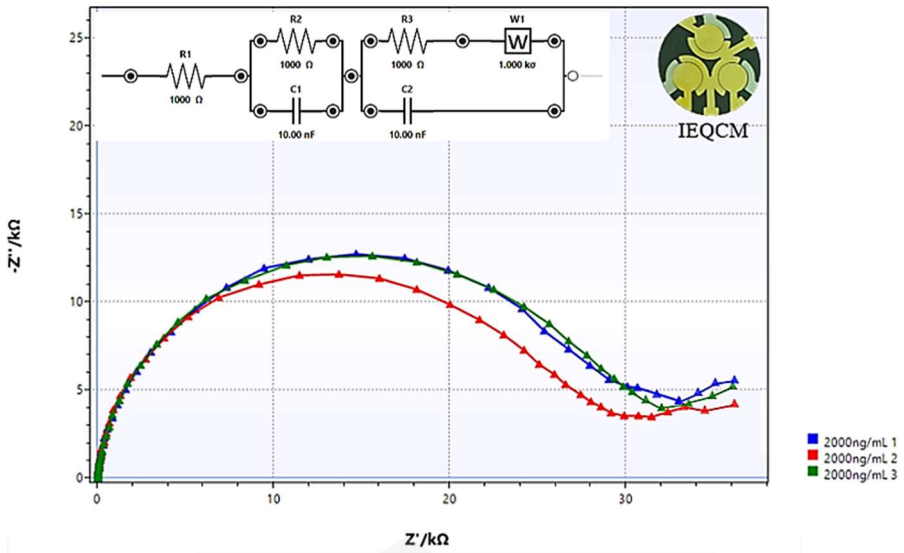

Element	Fitted Value	Unit	Error%
R_{ct} (1)	27115	Ω	4.425
R_{ct} (2)	26075	Ω	2.043
R_{ct} (3)	28036	Ω	2.847
Average R_{ct}	27075.33333		

Figure 4.42: EIS triplicate results of electrode incubated with 2000 ng/mL NS1 antigen concentration with R_{ct} (1) = 27115.00 Ω, R_{ct} (2) = 26075.00 Ω, R_{ct} (3) = 28036.00 Ω and average R_{ct} = 27075.33 Ω, percentage error of <5 %.

This research was done based on previous work that utilized the similar IEQCM sensor, the result of this NS1 antigen detection was compared with the benchmark result (A. A. Zainuddin, 2020). It can be seen from the results in Figure 4.43 and 4.44 that the final result of the EIS measurement follows a similar pattern to the benchmark with the increment of the R_{ct} values for each subsequent concentration of the NS1 antigen. R_{ct} values are observed to study the attachment of the NS1 antigen prior to the NS1 antibody that was incubated during the surface bio-functionalization process. The higher the concentration of the NS1 antigen, the higher the R_{ct} value obtained from the redox active solution. This concluded that the IEQCM sensor used in this research was highly accurate and sensitive with percentage error approximately around 5 %.

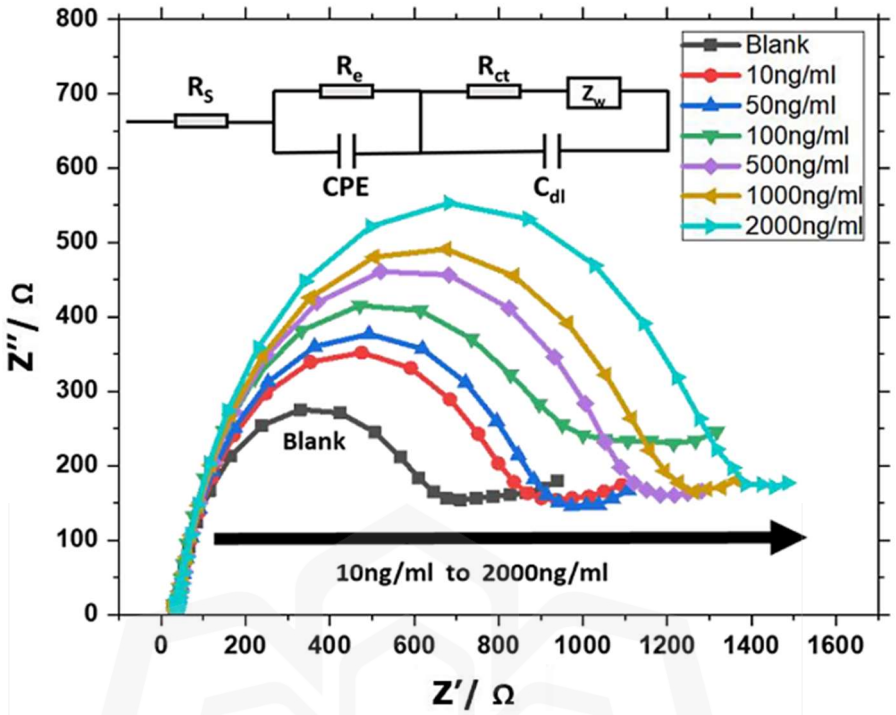

Figure 4.43: EIS benchmark result of different NS1 antigen concentration detection (A. A. Zainuddin, 2020).

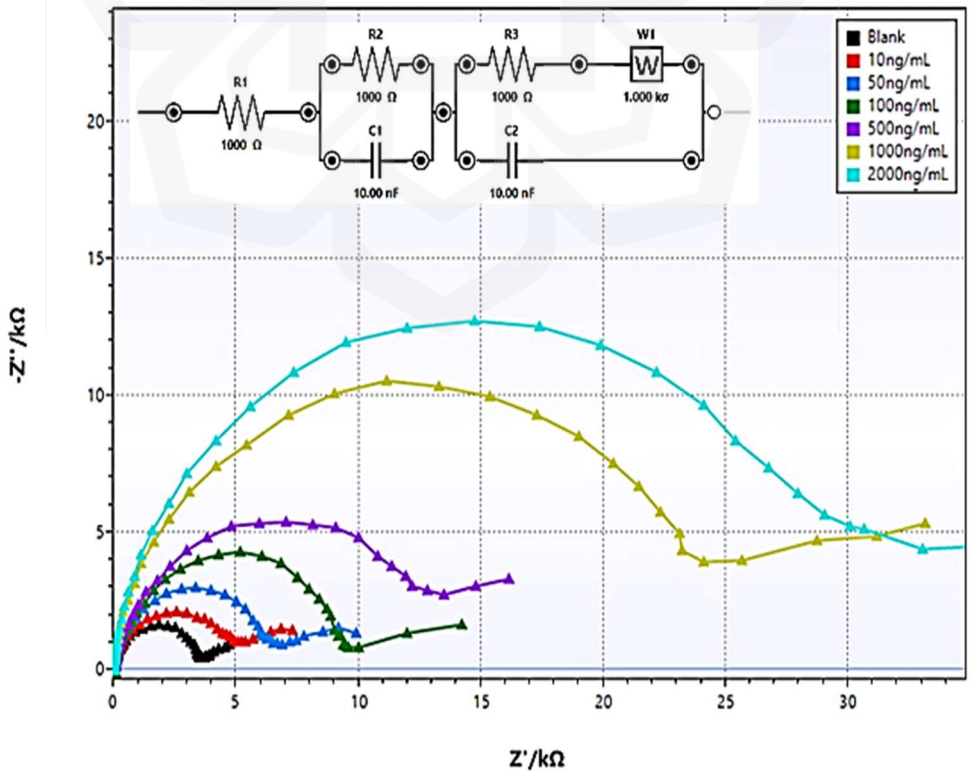

Figure 4.44: Final EIS result of different NS1 antigen concentration detection.

Triplicate result of each concentration is required to determine the lowest limit of detection (LoD) as well as the smallest limit of quantification (LoQ) obtained by the IEQCM sensor as depicted in Table 4.3. The average of R_{ct} (%) was calculated using:

$$R_{ct}\ (\%) = 100 \times (R_{ct\ sample} - R_{ct\ blank}) / R_{ct\ blank} \qquad \text{(Equation 4.1)}$$

The standard error of intercept, standard deviation of intercept, LoD and LoQ values was also depicted in Table 4.3. ELISA is one of the gold standards for dengue NS1 detection with minimum detection levels of 3.906 ng/mL (Lai et al., 2019). An alternative technology to conventional method, with LoD of 50.00 ng/mL uses electrolateral flow immunosensor (ELLI) stabilized electroactive immunonanoparticles that bind to the target biomarker on biofunctionalized screen-printed gold electrodes (SPGE) (Sinawang et al., 2018). Recent development of a multiplex electrochemical device with four independent working electrodes to distinguish between Zika and Dengue using NS1 as biomarkers, gave LoD about 1.17 ng/mL (Sampaio et al., 2022).

Table 4.3: Triplicate result of different NS1 antigen concentration with its standard error of intercept, standard deviation of intercept, LoD and LoQ values.

NS1 concentration (ng/mL)	R_{ct} (1) (Ω)	R_{ct} (2) (Ω)	R_{ct} (3) (Ω)	Average R_{ct} (Ω)	Average of R_{ct} (%)
Blank	4203	4119	4517	4279.67	0
10	4123	4538	4744	4468.33	4.41
50	7971	7959	7996	7975.33	86.36
100	10789	11698	10406	10964.33	156.20
500	15897	15976	15954	15942.33	272.51
1000	21885	21870	21986	21913.67	412.05
2000	27115	26075	28036	27075.33	532.65
Standard Error of intercept	39.35				
Standard Deviation of intercept	68.15				
Limit of Detection (LoD)	2.31 ng/mL				
Limit of Quantitation (LoQ)	6.99 ng/mL				

The LoD and LoQ result of different NS1 antigen concentrations was compared with the benchmark result that utilized IEQCM, as seen from Figure 4.45 and 4.46 (A. A. Zainuddin, 2020). The lowest NS1 antigen concentrations that can be detected are LoD = 2.31 ng/mL and LoD = 4.7 ng/mL for both final and benchmark results respectively. While the smallest NS1 antigen concentrations that can be detected with acceptable repeatability and accuracy are LoQ = 6.99 ng/mL and LoQ = 17.7 ng/mL and for both final and benchmark results respectively. Table 4.4 displayed the comparison of dengue NS1 detection with previous research that used conventional and electrochemical methods. The LoD and LoQ values obtained using the IEQCM sensor and potentiostat exhibit lowest values when compared to the benchmark result, even if the y-intercept in a logarithmic curve is negative, provided that the curve fits the data well. This is inherent in logarithmic functions, when the logarithmic function approaches negative infinity as x approaches zero causing the curve to start from a negative y value. This proved that the IEQCM sensor used in this research is more sensitive compared to most previous works.

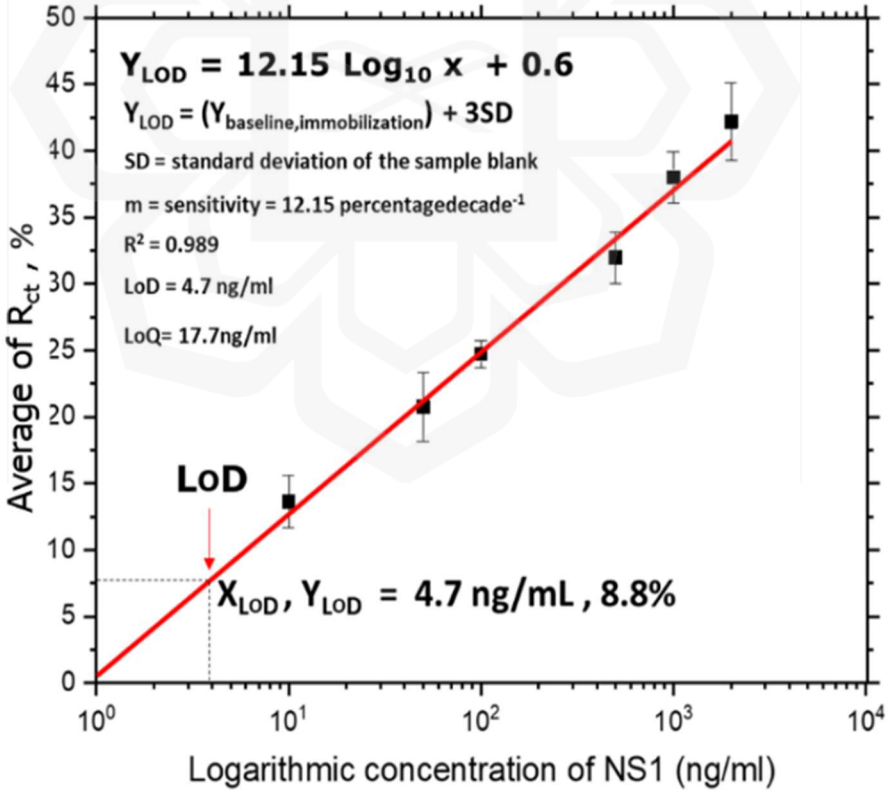

Figure 4.45: Benchmark result of Limit of Detection (LoD) and Limit of Quantitation (LoQ) (A. A. Zainuddin, 2020).

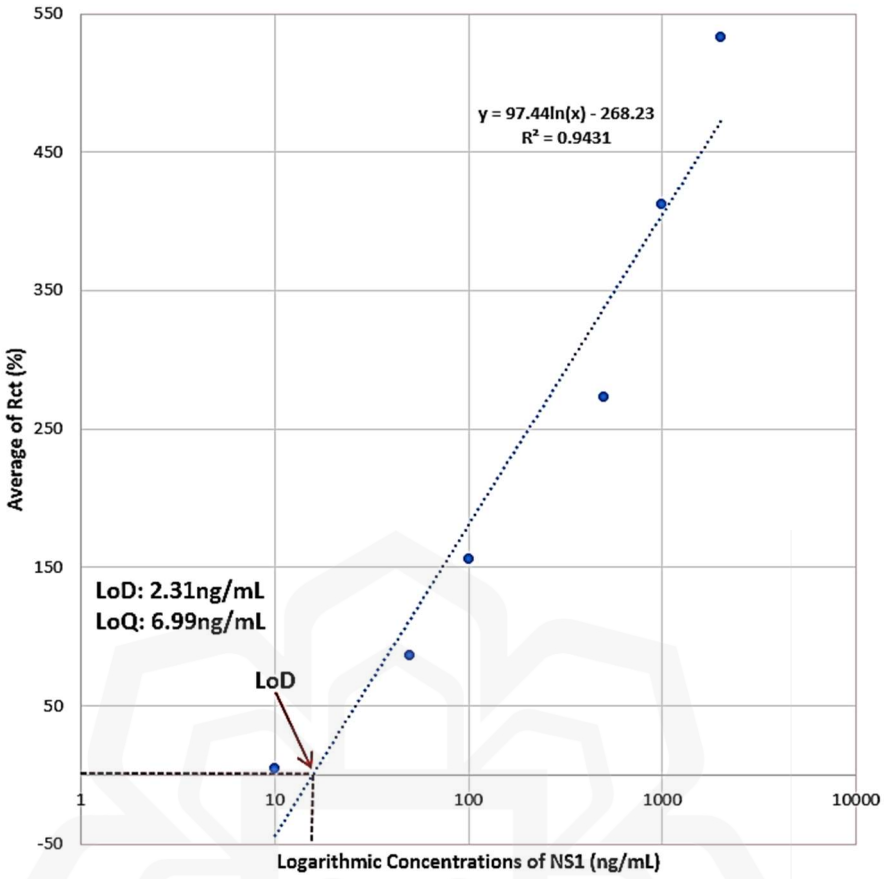

Figure 4.46: Final result of Limit of Detection (LoD) and Limit of Quantitation (LoQ) using the IEQCM sensor.

Table 4.4: Comparison of dengue NS1 detection with previous research that used conventional and electrochemical method.

Method	Target	Limit of Detection (LoD)
Enzyme-linked immunosorbent assay (ELISA) (Lai et al., 2019).	Dengue NS1	3.906 ng/mL
Electrolateral flow immunosensor (ELLI) (Sinawang et al., 2018).	Dengue NS1	50.00 ng/mL
Multiplex electrochemical device (Sampaio et al., 2022).	Dengue NS1	1.17 ng/mL

Integrated, Electrochemical and Mass Three-sensor Array Quartz Crystal Microbalance (IEQCM) (A. Zainuddin et al., 2022).	Dengue NS1	4.7 ng/mL
Integrated Electrochemical Quartz Crystal Microbalance (IEQCM) (This research).	Dengue NS1	2.31 ng/mL

4.5 CHAPTER SUMMARY

This chapter summarizes the final results of the electrochemical measurement that was obtained using the EmStat Pico development board and as well as the designed potentiostat board. The EmStat board was used as a benchmark for the electrochemical measurement, specifically CV and EIS. The ΔE_p value from the CV plot acquired from the designed potentiostat board was almost identical with the one obtained from EmStat board with only 0.001 V difference which gives about 99.25 % accuracy. This indicated that the performance of the designed potentiostat is almost on par with the commercial EmStat potentiostat. The percentage error of R_{ct} values obtained from EIS measurement using IEQCM sensor taken during the surface bio-functionalization process and the NS1 antigen detection is approximately less than 5 %. The final result of the LoD and LoQ of the EIS measurement is LoD = 2.31 ng/mL and LoQ = 6.99 ng/mL for a range of 10, 50, 100, 500, 1000, 2000 ng/mL NS1 antigen concentration showed that the IEQCM have high sensitivity and specificity compared to previous research.

CHAPTER 5

CONCLUSION AND RECOMMENDATION

5.1 CONCLUSION

The Integrated Electrochemical Quartz Crystal Microbalance (IEQCM) sensor in the proposed potentiostat and fluidic chamber system brings together biotechnology, semiconductor and electronics on a single chip enabling rapid and efficient dengue detection. The electrochemical measurement capabilities, particularly Cyclic Voltammetry (CV) is the primary focus of this research. This research has successfully achieved all its objectives, encompassing the design and development of the potentiostat system, fluidic chamber and IEQCM sensor as well as the validation of the final NS1 antigen detection result against benchmark data from previous works. The designed potentiostat, fluidic chamber and IEQCM sensor developed in this study have demonstrated sensitivity and accuracy rate of ~99.25 %. This indicates that the performance of the designed potentiostat is comparable to that of commercially available potentiostat boards.

The IEQCM sensor and commercial potentiostat used in this research have achieved impressive results in detecting NS1 antigen concentrations with the lowest limit of detection (LoD), were found to be 2.31 ng/mL. Additionally, the smallest detectable concentrations with acceptable repeatability and accuracy, known as the limit of quantification (LoQ) was 6.99ng/mL. Remarkably, the LoD and LoQ values obtained with the IEQCM sensor were significantly lower than those of the benchmark result. This demonstrates the superior sensitivity of the IEQCM sensor used in this research, showcasing its ability to detect very low concentrations and operate within a wider dynamic range for disease sensing compared to previous works. This innovative approach paves the way for future advancements in biosensing technologies, with the potential to revolutionize disease diagnostics and contribute significantly to public health, medical research and beyond.

5.2 RECOMMENDATION

Despite achieving good results with high accuracy using the designed potentiostat, fluidic chamber, and IEQCM sensor, there are still some gaps in this research. The inclusion of Electrochemical Impedance Spectroscopy (EIS) measurement capabilities in the potentiostat would require a more complex design circuit, leading to higher fabrication costs. This is the reason why commercialized potentiostats with EIS capabilities are often expensive due to the complexity of the EIS program. For future dengue diagnostic methods, a small, portable and affordable potentiostat with both Cyclic Voltammetry (CV) and EIS measurements capabilities is highly desirable. Additionally, having a potentiostat system that can utilize all three arrays of the IEQCM sensor in a single measurement would be advantageous, as it would enhance efficiency and reduce the need for multiple measurements. The ongoing evolution of technology paves the way for a highly accurate and sensitive potentiostat device that is not only affordable but also easily accessible to public or healthcare facilities. This advancement would undoubtedly play a crucial role in early dengue detection and overall disease management.

RESEARCH PUBLICATION

Azmi, N. H., Nordin, A. N., Cheung, M. W., Rahim, R. A., Ramli, N., Zainuddin, A. A., Samsudin, Z., Suhaimi, M. I., Ming, L. L., & Hao, F. T. L. (2022). I-Denv™: Intelligent, Accurate Detection of Early Dengue and Dengue Variants. *International Conference and Exposition on Inventions by Institutions of Higher Learning 2022 (PECIPTA 2022). –Poster (Gold Award)*

Azmi, N. H., Nordin, A. N., Suhaimi, M. I., Ming, L. L., Rahim, R. A., Riza, M. S., & Samsudin, Z. (2023). Portable Data Acquisition and Fluidic System for Electrochemical Sensors. *IEEE International Instrumentation and Measurement Technology Conference 2023 (I2MTC). –Published*

Malla, P., Faizan, M., Liu, C. H., Azmi, N. H., & Nordin, A. N. (2023). Ultrasensitive Electrochemiluminescence Biosensor for Simultaneous Detection of Dual micro-RNAs. *International Conference on Green Electrochemical Technologies (ICGET-Tw). –Submitted*

Soon, C. F., Yee, S. K., Nordin, A. N., Rahim, R. A., Ma, N. L., Abd Hamed, I. S. L., Tee, K. S., Azmi, N. H., Sunar, N. M., & Heng, C. (2024). Advancements in biodegradable printed circuit boards: Review of material properties, applications and challenges. *Sustainable Development. –Published*

Azmi, N. H., Nordin, A. N., Suhaimi, M. I., Ming, L. L., Rahim, R. A., Samsudin, Z., & Md Ralib @ Md Raghib, A. A. (2024). Flexible Potentiostat Readout Circuit for Electrochemical Sensors. *Indonesian Journal of Electrical Engineering and Informatics (IJEEI). –Published*

REFERENCES

Abdullah, S., Tonello, S., Borghetti, M., Sardini, E., & Serpelloni, M. (2019). Potentiostats for protein biosensing: Design considerations and analysis on measurement characteristics. *Journal of Sensors*, *2019*.

Adams, S. D., Doeven, E. H., Quayle, K., & Kouzani, A. Z. (2019). MiniStat: Development and Evaluation of a Mini-Potentiostat for Electrochemical Measurements. *IEEE Access*, *7*, 31903–31912.

Alao, O. (2018). (PDF) Online condition monitoring of Lithium-ion and Lead acid batteries for renewable energy applications. https://www.researchgate.net/publication/333403369_Online_condition_monitoring_of_Lithium_ion_and_Lead_acid_batteries_for_renewable_energy_applications.

Anasir, M. I., Ramanathan, B., & Poh, C. L. (2020). Structure-based design of antivirals against envelope glycoprotein of dengue virus. In *Viruses* (Vol. 12, Issue 4). MDPI AG.

Anusha, J. R., Kim, B. C., Yu, K. H., & Raj, C. J. (2019). Electrochemical biosensing of mosquito-borne viral disease, dengue: A review. *Biosensors and Bioelectronics*, *142*.

Barton, J., García, M. B. G., Santos, D. H., Fanjul-Bolado, P., Ribotti, A., McCaul, M., Diamond, D., & Magni, P. (2016). Screen-printed electrodes for environmental monitoring of heavy metal ions: a review. *Microchimica Acta*, *183*(2), 503–517.

Benoudjit, A. (2021). A Stable Solid Contact Transducer and Ionophore-Free All-Solid-State Ammonium Ion-Selective Electrode for Mobile Sensor Application In Aqueous Media.

Bezuidenhout, P., Smith, S., Land, K., & Joubert, T.-H. (2017). A Low-Cost Potentiostat for Point-of-Need Diagnostics.

Bhalla, N., Jolly, P., Formisano, N., & Estrela, P. (2016). Introduction to biosensors. *Essays in Biochemistry*, *60*(1), 1.

Bobb-Semple, D., Nardi, K. L., Draeger, N., Hausmann, D. M., & Bent, S. F. (2019). Area-Selective Atomic Layer Deposition Assisted by Self-Assembled Monolayers: A Comparison of Cu, Co, W, and Ru. *Chemistry of Materials*, *31*(5), 1635–1645.

Bollella, P., & Gorton, L. (2018). Enzyme based amperometric biosensors. *Current Opinion in Electrochemistry*, *10*, 157–173.

Cagnani, G. R., da Costa Oliveira, T., Mattioli, I. A., Sedenho, G. C., Castro, K. P. R., & Crespilho, F. N. (2022). From research to market: correlation between publications, patent filings, and investments in development and production of technological innovations in biosensors. In *Analytical and Bioanalytical Chemistry*. Springer Science and Business Media Deutschland GmbH.

Chadha, U., Bhardwaj, P., Agarwal, R., Rawat, P., Agarwal, R., Gupta, I., Panjwani, M., Singh, S., Ahuja, C., Selvaraj, S. K., Banavoth, M., Sonar, P., Badoni, B., & Chakravorty, A. (2022). Recent progress and growth in biosensors technology: A critical review. *Journal of Industrial and Engineering Chemistry*, *109*, 21–51.

Codeço, C. T., Villela, D. A. M., & Coelho, F. C. (2018). Estimating the effective reproduction number of dengue considering temperature-dependent generation intervals. *Epidemics*, *25*, 101–111.

Cook, A. M., Faustini, S. E., Williams, L. J., Cunningham, A. F., Drayson, M. T., Shields, A. M., Kay, D., Taylor, L., Plant, T., Huissoon, A., Wallis, G., Beck, S., Jossi, S. E., Perez-Toledo, M., Newby, M. L., Allen, J. D., Crispin, M., Harding, S., & Richter, A. G. (2021). Validation of a combined ELISA to detect IgG, IgA and IgM antibody responses to SARS-CoV-2 in mild or moderate non-hospitalised patients. *Journal of Immunological Methods*, *494*, 113046.

Cook, J. (2020). SIMstat: Hardware Design Considerations for Implementing a Low-Cost, Portable Potentiostat.

Damiati, S., & Schuster, B. (2020). Electrochemical biosensors based on S-layer proteins. *Sensors (Switzerland)*, *20*(6).

Ding, J., & Qin, W. (2020). Recent advances in potentiometric biosensors. *TrAC Trends in Analytical Chemistry*, *124*, 115803.

Doğan, M., Çelikkol, A., Yilmaz, B., & Erdem, I. (2022). [Investigation of Factors Affecting Viral Clearance Time by Real-Time Polymerase Chain Reaction Method in Nasopharyngeal Swab Samples of COVID-19 Patients]. *Mikrobiyoloji Bulteni*, *56*(3), 545–552.

Drobysh, M., Liustrovaite, V., Baradoke, A., Rucinskiene, A., Ramanaviciene, A., Ratautaite, V., Viter, R., Chen, C. F., Plikusiene, I., Samukaite-bubniene, U., Slibinskas, R., Ciplys, E., Simanavicius, M., Zvirbliene, A., Kucinskaite-kodze, I., & Ramanavicius, A. (2022). Electrochemical Determination of Interaction

between SARS-CoV-2 Spike Protein and Specific Antibodies. *International Journal of Molecular Sciences 2022, Vol. 23, Page 6768*, *23*(12), 6768.

DropSens. (n.d.-a). *Screen-Printed Carbon Electrode (SPCE)*. www.dropsens.com

DropSens. (n.d.-b). *Screen-Printed Gold Electrodes (SPGE)*. www.dropsens.com

Eivazzadeh-Keihan, R., Pashazadeh-Panahi, P., Mahmoudi, T., Chenab, K. K., Baradaran, B., Hashemzaei, M., Radinekiyan, F., Mokhtarzadeh, A., & Maleki, A. (2019). Dengue virus: a review on advances in detection and trends – from conventional methods to novel biosensors. *Microchimica Acta*, *186*(6).

Ekici, R., Bozdoğan, B., & Denkbaş, E. B. (2022). Development of Electrochemical Biosensor Platforms for Determination of Environmental Viral Structures. *Applied Sciences (Switzerland)*, *12*(24).

Environmental Expert. (n.d.). *Metrohm Autolab - PGSTAT302N AUT302N.S - Electrochemistry - ...* Retrieved Janua

ry 5, 2024, from https://www.environmental-expert.com/products/metrohm-autolab-model-pgstat302n-aut302ns-high-end-high-current-potentiostat-galvanostats-627120

Erba Mannheim. (2018). Significance of Serological Markers in the Diagnosis of Dengue: Erba Mannheim. https://www.erbamannheim.com/article/scientific-updates/158

Escobedo, P., Manjakkal, L., Ntagios, M., & Dahiya, R. (2020). Flexible Potentiostat Readout Circuit Patch for Electrochemical and Biosensor Applications. *FLEPS 2020 - IEEE International Conference on Flexible and Printable Sensors and Systems*, 20–23.

Hegde, S. S., & Bhat, B. R. (2022). Dengue detection: Advances and challenges in diagnostic technology. *Biosensors and Bioelectronics: X*, *10*, 100100.

Hoilett, O. S., Walker, J. F., Balash, B. M., Jaras, N. J., Boppana, S., & Linnes, J. C. (2020). Kickstat: A coin-sized potentiostat for high-resolution electrochemical analysis. *Sensors (Switzerland)*, *20*(8).

Izuan Abdul Rashid, J., & Azah Yusof, N. (2018). Laboratory Diagnosis and Potential Application of Nucleic Acid Biosensor Approach for Early Detection of Dengue Virus Infections. *Biosciences, Biotechnology Research Asia*, *15*(2), 245–255.

Jampasa, S., Lae-ngee, P., Patarakul, K., Ngamrojanavanich, N., Chailapakul, O., & Rodthongkum, N. (2019). Electrochemical immunosensor based on gold-labeled

monoclonal anti-LipL32 for leptospirosis diagnosis. *Biosensors and Bioelectronics*, *142*.

Jenkins, D. M., Lee, B. E., Jun, S., Reyes-De-Corcuera, J., & McLamore, E. S. (2019). ABE-Stat, a Fully Open-Source and Versatile Wireless Potentiostat Project Including Electrochemical Impedance Spectroscopy. *Journal of The Electrochemical Society*, *166*(9), B3056–B3065.

Khristunova, E., Dorozhko, E., Korotkova, E., Kratochvil, B., Vyskocil, V., & Barek, J. (2020). Label-free electrochemical biosensors for the determination of flaviviruses: Dengue, Zika, and Japanese encephalitis. In *Sensors (Switzerland)* (Vol. 20, Issue 16, pp. 1–24). MDPI AG.

Kilic, T., Valinhas, A. T. D. S., Wall, I., Renaud, P., & Carrara, S. (2018). Label-free detection of hypoxia-induced extracellular vesicle secretion from MCF-7 cells. *Scientific Reports*, *8*(1).

Kim, J., Campbell, A. S., de Ávila, B. E. F., & Wang, J. (2019). Wearable biosensors for healthcare monitoring. *Nature Biotechnology 2019 37:4*, *37*(4), 389–406.

Lai, S. C., Huang, Y. Y., Shu, P. Y., Chang, S. F., Hsieh, P. S., Wey, J. J., Tsai, M. H., Ben, R. J., Hsu, Y. M., Fang, Y. C., Hsiao, M. L., & Lin, C. C. (2019). Development of an enzyme-linked immunosorbent assay for rapid detection of dengue virus (DENV) NS1 and differentiation of DENV serotypes during early infection. *Journal of Clinical Microbiology*, *57*(7), 221–240.

Lasia, A. (1999). Electrochemical Impedance Spectroscopy and its Applications. *32*, 143–248.

Lathika, S., Raj, A., & Sen, A. K. (2021). LSPR based on-chip detection of dengue NS1 antigen in whole blood. *RSC Advances*, *11*(53), 33770–33780.

Laurent Bleu Medical Clinic. (2021). COVID-19 Screening - Laurent Bleu Medical Clinic.

Li, G., Fei, J., Xu, Y., Sun, B., & Li, J. (2019). Tuning Thiol-Based Self-Assembled Monolayer Chemistry on a Gold Surface towards the Synthesis of Biochemical Fuel. *Angewandte Chemie - International Edition*, *58*(4), 1110–1114.

Liu, Z., Ramakrishna, S., & Liu, X. (2020). Electrospinning and emerging healthcare and medicine possibilities. *APL Bioengineering*, *4*(3).

Loo, J. F. C., Ho, A. H. P., & Mak, W. C. (2023). Printed microfluidic biosensors and their biomedical applications. *Microfluidic Biosensors*, 1–40.

Lovera, D., Martínez-Cuellar, C., Galeano, F., Amarilla, S., Vazquez, C., & Arbo, A. (2019). Clinical manifestations of primary and secondary dengue in Paraguay and its relation to virus serotype. *Journal of Infection in Developing Countries*, *13*(12), 1127–1134.

Magar, H. S., Hassan, R. Y. A., & Mulchandani, A. (2021). Electrochemical impedance spectroscopy (Eis): Principles, construction, and biosensing applications. In *Sensors* (Vol. 21, Issue 19). MDPI.

Mendonça, P. D., Santos, L. K. B., Foguel, M. V, Rodrigues, M. A. B., Cordeiro, M. T., Luís, &, Gonçalves, M., Marques, E. T. A., & Dutra, R. F. (2021). NS1 glycoprotein detection in serum and urine as an electrochemical screening immunosensor for dengue and Zika virus.

Microchip. (2021). SAM D21/DA1 Family Low-Power, 32-bit Cortex-M0+ MCU with Advanced Analog and PWM Features.

Muller, D. A., Depelsenaire, A. C. I., & Young, P. R. (2017). Clinical and Laboratory Diagnosis of Dengue Virus Infection. *The Journal of Infectious Diseases*, *215*(suppl_2), S89–S95.

Mustafa, M. S., Rasotgi, V., Jain, S., & Gupta, V. (2015). Discovery of fifth serotype of dengue virus (DENV-5): A new public health dilemma in dengue control. *Medical Journal, Armed Forces India*, *71*(1), 67.

Muzammil, I., Aqib, A. I., Tanveer, Q., Muzmmal, S., Naseer, M. A., & Tahir, M. (2021). COVID-19 diagnosis-myths and protocols. In *Data Science for COVID-19: Volume 2: Societal and Medical Perspectives* (pp. 335–353). Elsevier.

Nanaware, N., Banerjee, A., Bagchi, S. M., Bagchi, P., & Mukherjee, A. (2021). Dengue virus infection: A tale of viral exploitations and host responses. In *Viruses* (Vol. 13, Issue 10). MDPI.

Narayan, T., Kumar, S., Kumar, S., Augustine, S., Yadav, B. K., & Malhotra, B. D. (2019). Protein functionalised self-assembled monolayer based biosensor for colon cancer detection. *Talanta*, *201*, 465–473.

Nielsen, A. v., Beauchamp, M. J., Nordin, G. P., & Woolley, A. T. (2020). 3D Printed Microfluidics.

Oliveira, N. M., Vilabril, S., Oliveira, M. B., Reis, R. L., & Mano, J. F. (2019). Recent advances on open fluidic systems for biomedical applications: A review. *Materials Science and Engineering: C*, *97*, 851–863.

Omar, N. A. S., Fen, Y. W., Abdullah, J., Mustapha Kamil, Y., Daniyal, W. M. E. M. M., Sadrolhosseini, A. R., & Mahdi, M. A. (2020). Sensitive Detection of Dengue Virus Type 2 E-Proteins Signals Using Self-Assembled Monolayers/Reduced Graphene Oxide-PAMAM Dendrimer Thin Film-SPR Optical Sensor. *Scientific Reports*, *10*(1).

Parkash, O., Abdullah, M. A., Yean, C. Y., Sekaran, S. D., & Shueb, R. H. (2021). Development and evaluation of an electrochemical biosensor for detection of dengue-specific igm antibody in serum samples. *Diagnostics*, *11*(1).

Piironen, K., Haapala, M., Talman, V., Järvinen, P., & Sikanen, T. (2020). Lab on a Chip Cell adhesion and proliferation on common 3D printing materials used in stereolithography of microfluidic devices. *20*, 2372.

Pokharna, P. P., Ghantasala, M. K., & Rozhkova, E. A. (2021). 3D printed polylactic acid and acrylonitrile butadiene styrene fluidic structures for biological applications: Tailoring bio-material interface via surface modification. *Materials Today Communications*, *27*, 102348.

Preuß, J. A., Reich, P., Bahner, N., & Bahnemann, J. (2020). Impedimetric Aptamer-Based Biosensors: Applications. *Advances in Biochemical Engineering/Biotechnology*, *174*, 43–91.

Qualitas Health Malaysia. (2023). COVID-19 PCR & RT-Antigen Tests - Qualitas Health Malaysia. https://qualitashealth.com.my/covid-19-test-rtk-pcr-qualitas-clinics/

Quick Lab. (2024). Dengue IgM ELISA KIT - Detect Acute Dengue Infection. https://quicklab.in/product/dengue-igm-elisa-kit/?wcpbc-manual-country=IN

Raafat, N., Blacksell, S. D., & Maude, R. J. (2019). A review of dengue diagnostics and implications for surveillance and control. *Transactions of the Royal Society of Tropical Medicine and Hygiene*, *113*(11), 653–660.

Raymundo-Pereira, P. A., De Oliveira Pedro, R., Carr, O., Melendez, M. E., Gobbi, A. L., Helena De Oliveira Piazzetta, M., Carvalho, A. L., Reis, R. M., Miranda, P. B., & Oliveira, O. N. (2021). Influence of the Molecular Orientation and Ionization of Self-Assembled Monolayers in Biosensors: Application to Genosensors of Prostate Cancer Antigen 3. *Journal of Physical Chemistry C*, *125*(1), 498–506.

Ryan, S. J., Carlson, C. J., Mordecai, E. A., & Johnson, L. R. (2019). Global expansion and redistribution of Aedes-borne virus transmission risk with climate change. *PLOS Neglected Tropical Diseases*, *13*(3), e0007213.

Sabir, M. J., Al-Saud, N. B. S., & Hassan, S. M. (2021). Dengue and human health: A global scenario of its occurrence, diagnosis and therapeutics. *Saudi Journal of Biological Sciences*, *28*(9), 5074–5080.

Sakellari, G. I., Hondow, N., & Gardiner, P. H. E. (2020). Factors Influencing the Surface Functionalization of Citrate Stabilized Gold Nanoparticles with Cysteamine, 3-Mercaptopropionic Acid or l-Selenocystine for Sensor Applications. *Chemosensors*, *8*(3).

Sampaio, I., Quatroni, F. D., Yamauti Costa, J. N., & Zucolotto, V. (2022). Electrochemical detection of Zika and Dengue infections using a single chip. *Biosensors and Bioelectronics*, *216*.

Sinawang, P. D., Fajs, L., Elouarzaki, K., Nugraha, J., & Marks, R. S. (2018). TEMPO-based immuno-lateral flow quantitative detection of dengue NS1 protein. *Sensors and Actuators, B: Chemical*, *259*, 354–363.

Sinawang, P. D., Rai, V., Ionescu, R. E., & Marks, R. S. (2016). Electrochemical lateral flow immunosensor for detection and quantification of dengue NS1 protein. *Biosensors and Bioelectronics*, *77*, 400–408.

Singh, M., Kaur, N., & Comini, E. (2020). The role of self-assembled monolayers in electronic devices. *Journal of Materials Chemistry C*, *8*(12), 3938–3955.

Singhal, C., Shukla, S. K., Jain, A., Pundir, C., Khanuja, M., Narang, J., & Shetti, N. P. (2020). Electrochemical Multiplexed Paper Nanosensor for Specific Dengue Serotype Detection Predicting Pervasiveness of DHF/DSS. *ACS Biomaterials Science and Engineering*, *6*(10), 5886–5894.

Soldatkina, O. v., Soldatkin, O. O., Velychko, T. P., Prilipko, V. O., Kuibida, M. A., & Dzyadevych, S. v. (2018). Conductometric biosensor for arginine determination in pharmaceutics. *Bioelectrochemistry (Amsterdam, Netherlands)*, *124*, 40–46.

Stanković, V., Đurđić, S., Ognjanović, M., Antić, B., Kalcher, K., Mutić, J., & Stanković, D. M. (2020). Anti-human albumin monoclonal antibody immobilized on EDC-NHS functionalized carboxylic graphene/AuNPs composite as promising electrochemical HSA immunosensor. *Journal of Electroanalytical Chemistry*, *860*.

Stiba, K. (2015). Reliably recognizing dengue at any time - *EUROIMMUNBlog*. https://www.euroimmunblog.com/recognizing-dengue/

Stratmann, L. (2019). EMStat Pico: An Electrochemical System on Module for Integration of Standard Analysis Methods with a Minimum of Development Effort.

Texas Instruments. (2014). LMP91000 Sensor AFE System: Configurable AFE Potentiostat for Low-Power Chemical- Sensing Applications. www.ti.com

Thébault, P., Ammoun, M., Boudjemaa, R., Ouvrard, A., Steenkeste, K., Bourguignon, B., & Fontaine-Aupart, M.-P. (2022). Surface functionalization strategy to enhance the antibacterial effect of nisin Z peptide. https://www.elsevier.com/open-access/userlicense/1.0/

Thomas, S. J., & Yoon, I.-K. (2019). Human Vaccines & Immunotherapeutics *ISSN: (Print) (Online) Journal homepage: https://www.tandfonline.com/loi/khvi20 A review of Dengvaxia®: development to deployment*.

Tricase, A., Imbriano, A., MacChia, E., Picca, R. A., Blasi, D., Torsi, L., & Bollella, P. (2022). Electrochemical Investigation of Self-Assembling Monolayers toward Ultrasensitive Sensing. *FLEPS 2022 - IEEE International Conference on Flexible and Printable Sensors and Systems, Proceedings*.

Tsai, J. J., Liu, W. L., Lin, P. C., Huang, B. Y., Tsai, C. Y., Chou, P. H., Lee, F. C., Ping, C. F., Lee, P. Y. A., Liu, L. T., & Chen, C. H. (2019). An RT-PCR panel for rapid serotyping of dengue virus serotypes 1 to 4 in human serum and mosquito on a field-deployable PCR system. *PLOS ONE*, *14*(3), e0214328.

Tsai, T. C., Liu, C. W., Wu, Y. C., Ondevilla, N. A. P., Osawa, M., & Chang, H. C. (2019). In situ study of EDC/NHS immobilization on gold surface based on attenuated total reflection surface-enhanced infrared absorption spectroscopy (ATR-SEIRAS). *Colloids and Surfaces B: Biointerfaces*, *175*, 300–305.

University of Antwerp. (n.d.). Metrohm Autolab PGSTAT 302N with ECD and FRA module | *A-Sense Lab | University of Antwerp*. Retrieved January 17, 2023, from https://www.uantwerpen.be/en/research-groups/a-sense-lab/service-equipment/equipment/electrochemistry/metrohm-autolab-pgst/

Urbano-Gámez, J. D., Valdés-Sánchez, L., Aracil, C., de la Cerda, B., Perdigones, F., Reyes, Á. P., Díaz-Corrales, F. J., López, I. R., & Quero, J. M. (2021). Biocompatibility Study of a Commercial Printed Circuit Board for Biomedical Applications: Lab-on-PCB for Organotypic Retina Cultures. *Micromachines 2021, Vol. 12, Page 1469*, *12*(12), 1469.

Wang, W. H., Urbina, A. N., Chang, M. R., Assavalapsakul, W., Lu, P. L., Chen, Y. H., & Wang, S. F. (2020). Dengue hemorrhagic fever – A systemic literature review of current perspectives on pathogenesis, prevention and control. *Journal of Microbiology, Immunology and Infection*, *53*(6), 963–978.

Wasilewski, T., Szulczyński, B., Dobrzyniewski, D., Jakubaszek, W., Gębicki, J., & Kamysz, W. (2022). Development and Assessment of Regeneration Methods for Peptide-Based QCM Biosensors in VOCs Analysis Applications. *Biosensors 2022, Vol. 12, Page 309*, *12*(5), 309.

Wongkaew, N., Simsek, M., Griesche, C., & Baeumner, A. J. (2019). Functional Nanomaterials and Nanostructures Enhancing Electrochemical Biosensors and Lab-on-a-Chip Performances: Recent Progress, Applications, and Future Perspective. *Chemical Reviews*, *119*(1), 120–194.

World Health Organization (WHO). (2022). Update on the Dengue situation in the Western Pacific Region Northern Hemisphere.

Yan, G., Lee, C. K., Lam, L. T. M., Yan, B., Chua, Y. X., Lim, A. Y. N., Phang, K. F., Kew, G. Sen, Teng, H., Ngai, C. H., Lin, L., Foo, R. M., Pada, S., Ng, L. C., & Tambyah, P. A. (2020). Covert COVID-19 and false-positive dengue serology in Singapore. *The Lancet Infectious Diseases*, *20*(5), 536.

Yang, C. H., Chen, C. A., & Chen, C. F. (2018). Surface-modified cellulose paper and its application in infectious disease diagnosis. *Sensors and Actuators, B: Chemical*, *265*, 506–513.

Yao, J., Yin, H., Wu, Z., -, al, Hou, Z., Ning, Z. H., Huang, J. Q., Guo, S. X., & Wang, L. H. (2020). A Portable Potentiostat for Three-Electrode Electrochemical Sensor. *Journal of Physics: Conference Series PAPER • OPEN ACCESS Journal of Physics: Conference Series*, *1550*, 42049.

Zainuddin, A. A. (2020). Integrated electrochemical and mass biosensor for early dengue detection. http://studentrepo.iium.edu.my/handle/123456789/10088

Zainuddin, A. A., Nordin, A. N., Asri, M. A. M., Rahim, R. A., Guines, C., Chatras, M., Pothier, A., & Mak, W. C. (2019). Development of integrated electrochemical-quartz crystal microbalance biosensor arrays: Towards ultrasensitive, multiplexed and rapid point-of-care dengue detection. *BIODEVICES 2019 - 12th International Conference on Biomedical Electronics and Devices, Proceedings; Part of 12th International Joint Conference on Biomedical Engineering Systems and Technologies, BIOSTEC 2019*, 220–227.

Zainuddin, A., Asri, M., Guines, C., Zabedi, M., Htay, K., Rahim, A., Chatras, M., Pothier, A., Mak, W., & Nordin, A. (2022). Prototyping and Early Validation of an Integrated, Electrochemical and Mass Three-sensor Array for Dengue Detection. 204–211.

APPENDICES

APPENDIX A: THE POTENTIOSTAT SYSTEM.

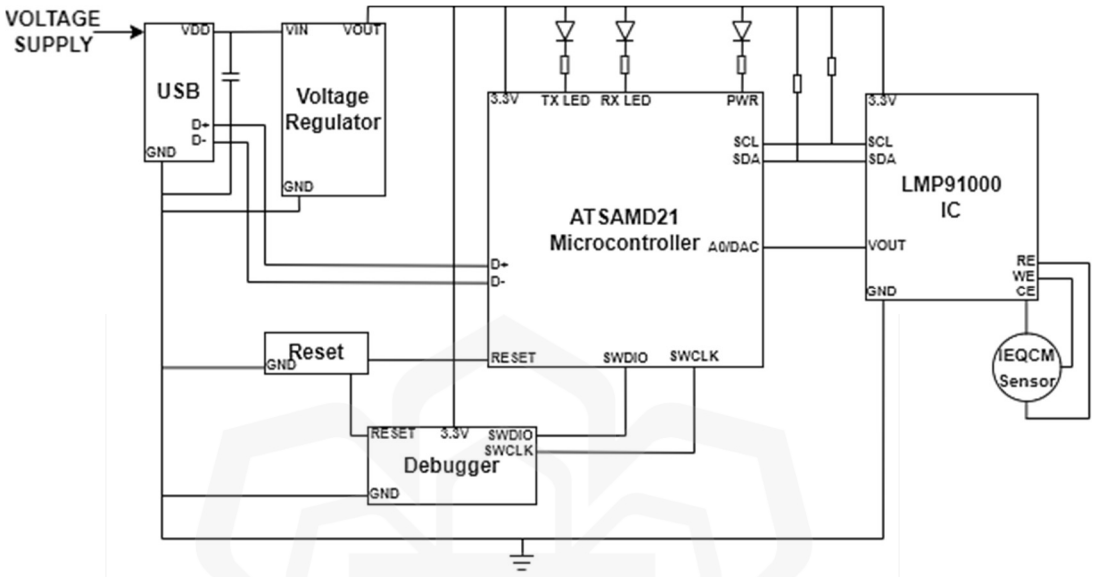

Block diagram of the potentiostat system.

List of components used in the potentiostat system.

No.	Components	Manufacturer	Manufacturer Part No.
1.	Microcontroller, ARM® Cortex®-M0+, SAM D21G, Functional Safety (FuSa), 32-Bit Single-Core, 48MHz, 256KB (256K x 8), FLASH, 48-QFN (7x7).	Microchip Technology	ATSAMD21 G18A-MUT
2.	Electrochemical Sensor IC, 1 Channel Analog Front End (AFE), 8 Bit, 14-WSON (4x4).	Texas Instruments	LMP91000S D/NOPB
3.	10kΩ Resistor, ±5%, 0.125W, 1/8W Chip Resistor, 0805, Thick Film.	Stackpole Electronics	RMCF0805J T10K0
4.	330Ω Resistor, ±5%, 0.125W, 1/8W Chip Resistor, 0805, Thick Film.	Stackpole Electronics	RMCF0805J T330R

5.	0.1µF Capacitor, ±10%, 10V Ceramic Capacitor, X5R, 0805.	KYOCERA AVX	0805ZD104KAT2A
6.	2.2µF Capacitor, ±10%, 10V Ceramic Capacitor, X5R, 0805.	KYOCERA AVX	0805ZD225KAT2A
7.	12pF Capacitor, ±5%, 50V Ceramic Capacitor, C0G, NP0, 0805.	KYOCERA AVX	08055A120JAT2A
8.	Ferrite Bead, 220Ω @ 100MHz, 1 Power, Signal Line Ferrite Bead, 0805, 2A, 50mΩ.	Laird-Signal Integrity Products	MI0805M221R-10
9.	PWR LED, Green, 520nm, 3.2V, 0805.	Inolux	IN-S85ATG
10.	RX LED, Red, 630nm, 2V, 0805.	Rohm Semiconductor	SML-M13VTT86
11.	TX LED, Yellow, 590nm, 2V, 0805.	Kingbright	APT2012SYCK
12.	3.3V Linear Voltage Regulator IC, Positive, Fixed, 300mA.	Microchip Technology	MIC5504-3.3YM5-TR
13.	32.768kHz Crystal, ±20ppm, 12.5pF, 90kΩ, 2-SMD, No Lead.	ECS Inc	ECS-.327-12.5-1210-TR
14.	QCM Connector Header Through Hole 3 position 0.100" (2.54mm).	Würth Elektronik	61300311121
15.	Micro B USB 2.0, Receptacle, 5 Position, Surface Mount, Right Angle, Through Hole.	Amphenol ICC (FCI)	10103592-0001LF
16.	DEBUG Connector Header Through Hole 10 position 0.050" (1.27mm).	METZ CONNECT USA	PR20B05VBDN
17.	RESET Tactile Switch, SPST-NO, Top Actuated, Surface Mount.	C&K	PTS830GM140 SMTR LFS

APPENDIX B: LMP91000 ELECTROCHEMICAL IC.

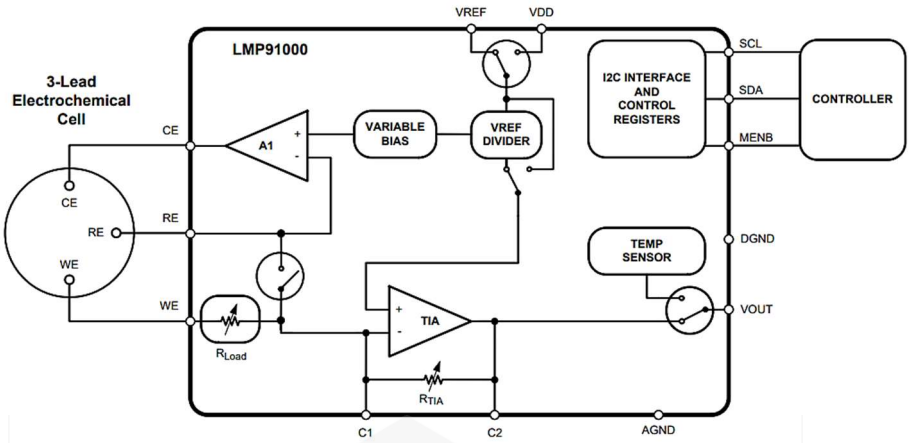

The architecture of LMP91000 (Texas Instruments, 2014).

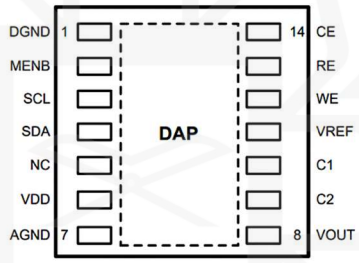

The 14-pin configuration of LMP91000 (Texas Instruments, 2014).

Pin functions of LMP91000 (Texas Instruments, 2014).

PIN		I/O	DESCRIPTION
NAME	NO.		
DGND	1	G	Connect to ground
MENB	2	I	Module Enable, Active-Low
SCL	3	I	Clock signal for I^2C compatible interface
SDA	4	I/O	Data for I^2C compatible interface
NC	5	N/A	Not Internally Connected
VDD	6	P	Supply Voltage
AGND	7	G	Ground
VOUT	8	O	Analog Output
C2	9	N/A	External filter connector (Filter between C1 and C2)
C1	10	N/A	External filter connector (Filter between C1 and C2)
VREF	11	I	Voltage Reference input
WE	12	I	Working Electrode. Output to drive the Working Electrode of the chemical sensor
RE	13	I	Reference Electrode. Input to drive Counter Electrode of the chemical sensor
CE	14	I	Counter Electrode. Output to drive Counter Electrode of the chemical sensor
DAP	—	N/C	Connect to AGND

Parameters in the Reference Control Register (REFCN) (Texas Instruments, 2014).

Bit	Name	Function
7	REF_SOURCE	Reference voltage source selection **0 Internal (default)** 1 external
[6:5]	INT_Z	Internal zero selection (Percentage of the source reference) 00 20% **01 50% (default)** 10 67% 11 Internal zero circuitry bypassed (only in O_2 ground referred measurement)
4	BIAS_SIGN	Selection of the Bias polarity **0 Negative ($V_{WE} - V_{RE}$)<0V (default)** 1 Positive ($V_{WE} - V_{RE}$)>0V
[3:0]	BIAS	BIAS selection (Percentage of the source reference) **0000 0% (default)** 0001 1% 0010 2% 0011 4% 0100 6% 0101 8% 0110 10% 0111 12% 1000 14% 1001 16% 1010 18% 1011 20% 1100 22% 1101 24%

Parameters in the Transimpedance Control Register (TIACN) (Texas Instruments, 2014).

Bit	Name	Function
[7:5]	RESERVED	RESERVED
[4:2]	TIA_GAIN	TIA feedback resistance selection **000 External resistance (default)** 001 2.75kΩ 010 3.5kΩ 011 7kΩ 100 14kΩ 101 35kΩ 110 120kΩ 111 350kΩ
[1:0]	RLOAD	R_{Load} selection 00 10Ω 01 33Ω 10 50Ω **11 100Ω (default)**

Parameters in the Mode Control Register (MODECN) (Texas Instruments, 2014).

Bit	Name	Function
7	FET_SHORT	Shorting FET feature **0 Disabled (default)** 1 Enabled
[6:3]	RESERVED	
[2:0]	OP_MODE	Mode of Operation selection **000 Deep Sleep (default)** 001 2-lead ground referred galvanic cell 010 Standby 011 3-lead amperometric cell 110 Temperature measurement (TIA OFF) 111 Temperature measurement (TIA ON)

APPENDIX C: ATSAMD21G18A MICROCONTROLLER.

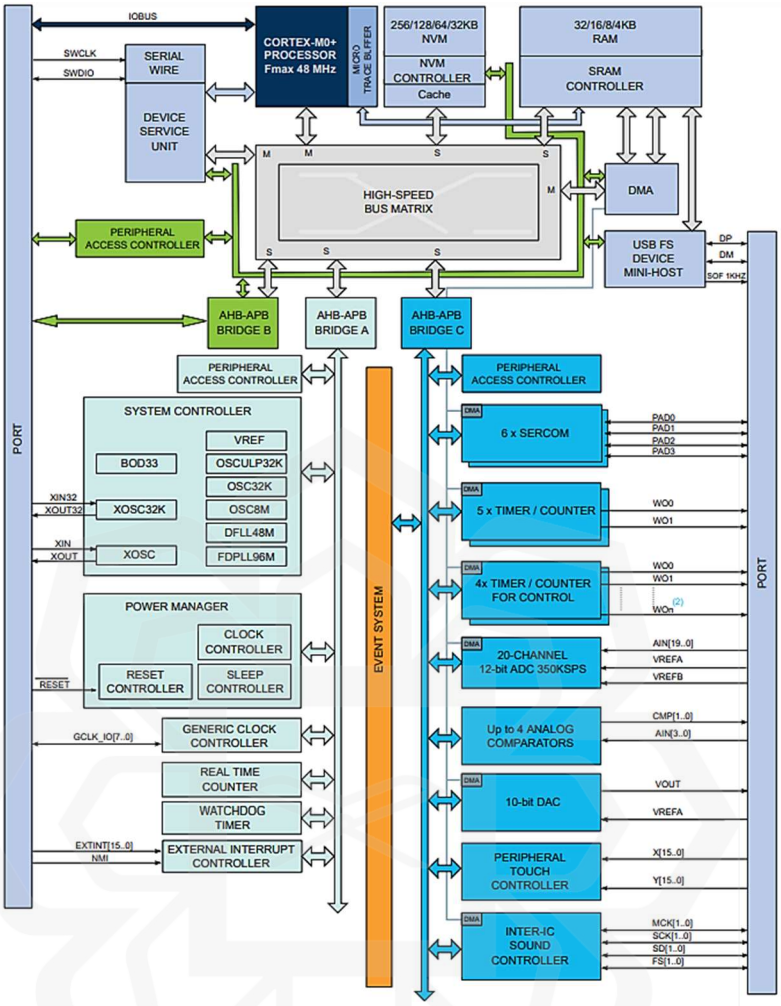

The architecture of SAMD21 (Microchip, 2021).

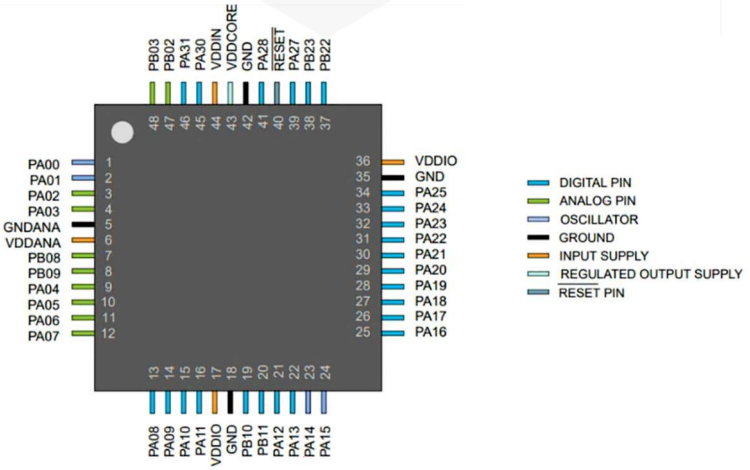

The 48-pin configuration of SAMD21 QFN package (Microchip, 2021).

Oscillator pinouts (Microchip, 2021).

Oscillator	Supply	Signal	I/O Pin
XOSC	VDDIO	XIN	PA14
		XOUT	PA15
XOSC32K	VDDANA	XIN32	PA00
		XOUT32	PA01

Serial wire debug interface (Microchip, 2021).

Signal	Supply	I/O Pin
SWCLK	VDDIO	PA30
SWDIO	VDDIO	PA31

SERCOM I^2C pins (Microchip, 2021).

Device	Pins Supporting I^2C mode
48 pins	PA08, PA09, PA12, PA13, PA16, PA17, PA22, PA23

GPIO clusters (Microchip, 2021).

PACKAGE	CLUSTER	GPIO															SUPPLIES PINS CONNECTED TO THE CLUSTER
48pins	1	PA31	PA30														VDDIN pin44/GND pin42
	2	PA28	PA27	PB23	PB22												VDDIN pin44/GND pin42 and VDDIO pin36/GND pin35
	3	PA25	PA24	PA23	PA22	PA21	PA20	PA19	PA18	PA17	PA16	PA15	PA14	PA13	PA12	PB11	PB10	VDDIO pin36/GND pin35 and VDDIO pin17/GND pin18
	4	PA11	PA10	PA09	PA08												VDDIO pin17/GND pin18
	5	PA07	PA06	PA05	PA04	PB09	PB08										VDDANA pin6/GNDANA pin5
	6	PA03	PA02	PA01	PA00	PB03	PB02	PB05	PB04	PB01	PB00						VDDANA pin6/GNDANA pin5

APPENDIX D: ARDUINO CV CODE DESCRIPTION

Arduino CV code description.

Description	Code
These libraries allow I^2C communication with LMP91000.	#include <LMP91000.h> #include <Wire.h>

Declare all the variables and initialize them with 0 for start voltage, end voltage, number of cycles and scan rate.	long startVo = 0;
	long endVo = 0;
	int nCycle = 0;
	int sRate = 0;

Set the voltage to power up both ATSAMD21 and LMP91000.	const uint16_t lmp_vcc = 3300; const float aref_voltage = 3.3;

Adjust the LMP91000 settings through TIACN for R_{TIA} and R_{Load} value and MODECN to disable FET feature.	pstat.disableFET();
	pstat.setGain(4);
	pstat.setRLoad(2);
	pstat.setIntRefSource();
	pstat.setIntZ(1);
	pstat.setThreeLead();

Math formula for voltage bias increment.	int16_t incrV = abs((endVo-startVo)/(lmp_vcc*0.04));

Sweep the voltage on negative values by varying the voltage bias.	pstat.setNegBias();
	for (int i = 1; i <= incrV+1; i++)
	{
	pstat.setBias(i);
	delay(settling_time);
	uint16_t adcVal = analogRead(A0);
	Serial.print(millis());
	Serial.print("\t");
	Serial.print(-1*TIA_BIAS[i]*lmp_vcc);
	Serial.print("\t");
	Serial.print(adcVal);
	Serial.print("\t");

	Serial.print(pstat.getCurrent(adcVal, aref_voltage, adc_bits)*1000000,4);
	Serial.println();
	}
	for (int i = incrV; i >= 0; i--)
	{
	pstat.setBias(i);
	delay(settling_time);
	uint16_t adcVal = analogRead(A0);
	Serial.print(millis());
	Serial.print("\t");
	Serial.print(-1*TIA_BIAS[i]*lmp_vcc);
	Serial.print("\t");
	Serial.print(adcVal);
	Serial.print("\t");
	Serial.print(pstat.getCurrent(adcVal, aref_voltage, adc_bits)*1000000,4);
	Serial.println();
	}

Sweep the voltage on positive values by varying the voltage bias.	pstat.setPosBias();
	for (int i = 1; i <= incrV+1 ; i++)
	{
	pstat.setBias(i);
	delay(settling_time);
	uint16_t adcVal = analogRead(A0);
	Serial.print(millis());
	Serial.print("\t");
	Serial.print(TIA_BIAS[i]*lmp_vcc);
	Serial.print("\t");
	Serial.print(adcVal);
	Serial.print("\t");
	Serial.print(pstat.getCurrent(adcVal, aref_voltage, adc_bits)*1000000,4);

```
      Serial.println();
    }
    for (int i = incrV; i >= 0; i--)
    {
      pstat.setBias(i);
      delay(settling_time);
      uint16_t adcVal = analogRead(A0);
Serial.print(millis());
      Serial.print("\t");
      Serial.print(TIA_BIAS[i]*lmp_vcc);
      Serial.print("\t");
      Serial.print(adcVal);
      Serial.print("\t");
      Serial.print(pstat.getCurrent(adcVal,
aref_voltage, adc_bits)*1000000,4);
      Serial.println();
    }
```

APPENDIX E: ISSUES IN THE FIRST POTENTIOSTAT DESIGN.

Errors found on the first potentiostat design.

No.	Components	Error Description
1.	SAMD21 Microcontroller 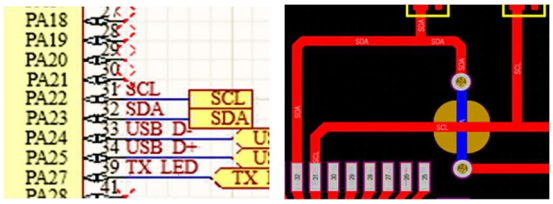	The SCL and SDA pin from pin 31 and 32 of SAMD21 microcontroller is inverted and need to be flipped. Pin 31 and 32 should be connected to SDA and SCL respectively.
2.	SAMD21 Microcontroller 	GND pin 35 should be connected together with EP pin 49.
3.	LMP91000 electrochemical chip 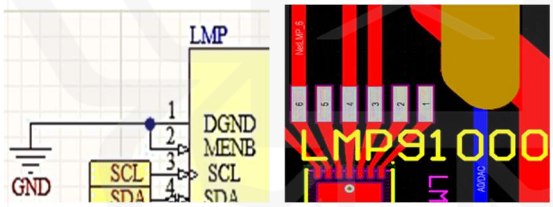	DGND and MENB pins on schematic design are connected to ground but on the PCB design, the connection is missing, there is no route that is connected to ground.
4.	LMP91000 electrochemical chip 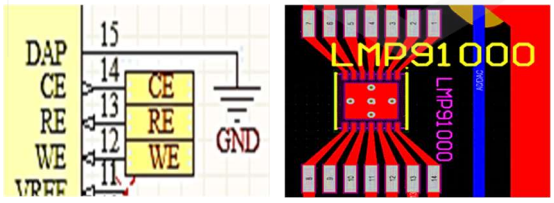	DAP pin in schematic design is connected to ground but on the PCB design, the DAP pin, which is the middle pad, is not connected to ground.
5.	LMP91000 electrochemical chip 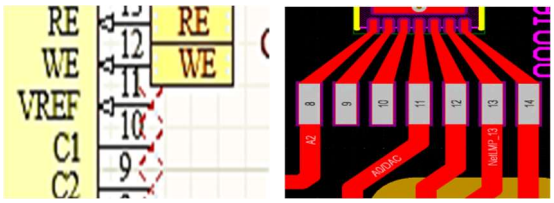	VREF pin in schematic design is not connected, but in PCB design the VREF pin 11 is connected to pin A0/DAC.

6.	DEBUG1 Connector 	Pin 6 of DEBUG in schematic design is not connected. In PCB design, pin 6 is also not connected though it seems like there is routing line. The connection between pin 5 and 3 was deleted to show the difference between the routing line and the component line. So, there is no problem with this part.
7.	Micro USB 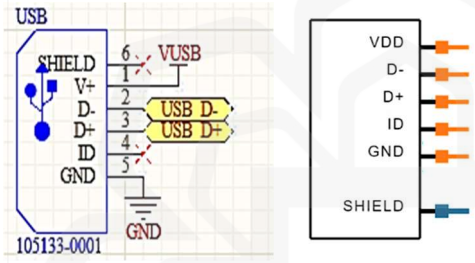 Incorrect (left) and correct (right) schematic symbol 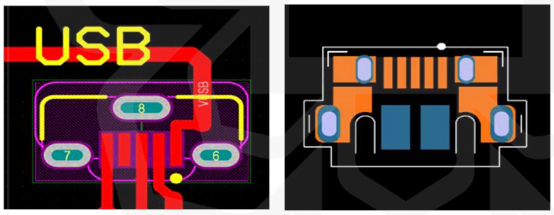 Incorrect (left) and correct (right) PCB footprint	Pin 6 of the schematic design should be connected to ground and pin 6,7,8 in PCB design also should be connected to ground. But for this type of USB, the right schematic and footprint of the component is the photo shown at the bottom part of the old schematic and PCB design.
8.	Short circuit 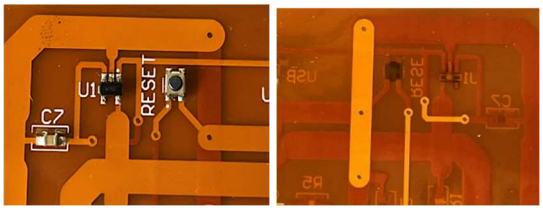 Front (left) and back (right) view of PCB	There is a short circuit in the connection of the board causing the board not powering up. Once the short circuit was stopped by cutting off the connection, some components appear to be burnt with smoking smell.

APPENDIX F: ISSUES IN THE SECOND POTENTIOSTAT DESIGN.

Issues encountered with the second potentiostat design.

No.	Components	Issues and Solution
1.	USB and PWR LED 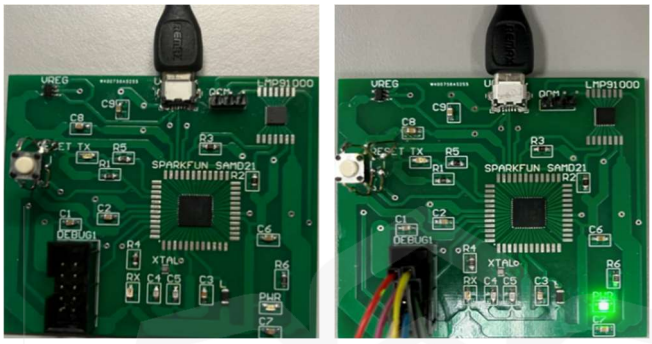 Before (left) and after (right) soldering process	Issue: The power diode does not light up when connected with power supply. Solution: Components from both boards were resoldered and the power diode finally lights up.
2.	DEBUG1 connector 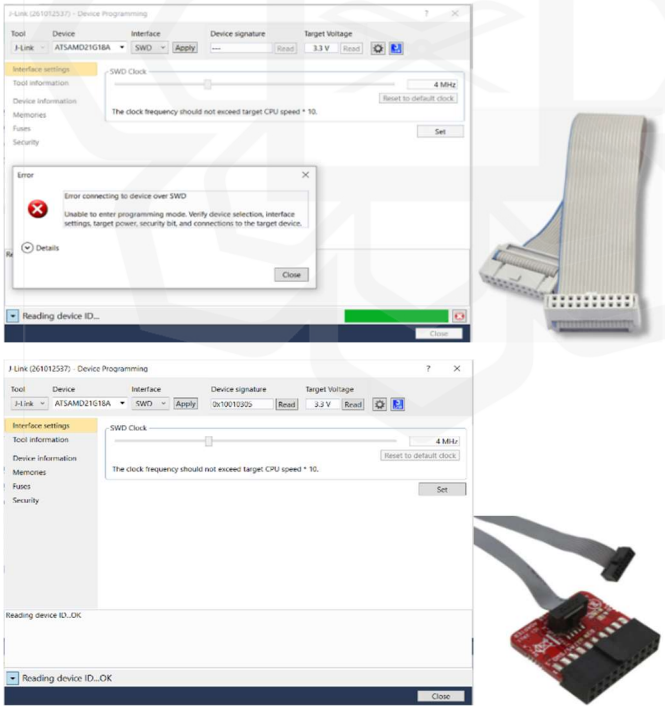 Before (top) and after (bottom) debugger wire replacement	Issue: Unable to bootload the board for coding upload. Solution: Replacing the debugger wire from using the 20-pin ribbon cable to 20 ARM JTAG cable.

APPENDIX G: CHEMICAL PREPARATION

Chemical lists for surface bio-functionalization process.

No.	Items	Suppliers	Qty
1.	455989-25G: Potassium Hexacyanoferrate (II) Trihydrate, 99.95 %	Sigma–Aldrich	25 g
2.	450561-5G: 11-Mercaptoundecanoic acid (11-MUA), 95 %	Sigma–Aldrich	5 g
3.	451088-5ML: 6-Mercaptohexanol (6-MCH), 97 %	Sigma–Aldrich	5 mL
4.	39391-10ML: N-(3-Dimethylaminopropyl)-N′-ethylcarbodiimide (EDC), 97 %	Sigma–Aldrich	10 mL
5.	AB145608-500MG: N-Hydroxysulfosuccinimide (Sulfo-NHS), 95 %	Sigma–Aldrich	500 mg
6.	AB41616-1ML: Mouse monoclonal [DN3] to Dengue Virus NS1 glycoprotein (NS1 Antibody)	Abcam	1 mL
7.	E9508-100ML: Ethanolamine (ETA), 98 %	Sigma–Aldrich	100 mL
8.	C0349-500G: Glycine (Aminoacetic acid)	Progressive Scientific	500 g
9.	AB64456-100µG: Recombinant Dengue Virus 2 NS1 glycoprotein (NS1 Antigen)	Abcam	100 µg
10.	459836-100ML: Anhydrous ethanol, 99.5 %	Sigma–Aldrich	100 mL

1. Baseline solution

Potassium Hexacyanoferrate (II) Trihydrate ($K_4Fe(CN)_6 \cdot 3H_2O$) - Powder

Desired final volume: 0.02 L

Desired final concentration: 0.5 mM

Molar mass: 422.39 g/mol

Preparation of baseline solution was done using Potassium Hexacyanoferrate (II) Trihydrate ($K_4Fe(CN)_6 \cdot 3H_2O$) in 10mM Phosphate Buffered Saline (PBS) solution with pH 7.4 for EIS measurement using bare gold electrode. 0.0422 g of the $K_4Fe(CN)_6 \cdot 3H_2O$ powder was mixed in 0.02 L PBS solution until it was ready.

2. 11-Mercaptoundecanoic acid (11-MUA) and 6-Mercaptohexanol (6-MCH) (SAM) – Step (b)

11-Mercaptoundecanoic acid (11-MUA) - Powder

Desired final volume: 0.01 L

Desired final concentration: 2.5 mM

Molar mass: 218.36 g/mol

6-Mercaptohexanol (6-MCH) - Liquid

Desired final volume: 0.01 L

Desired final concentration: 7.5 mM

Molar mass: 134.24 g/mol

The cleaned working electrode was placed inside the fluidic chamber and submerged for 24 hours at 4 °C in a mixture of 2.5 mM 11-mercaptoundecanoic acid (11-MUA) and 7.5 mM 6-mercaptohexanol (6-MCH) in absolute ethanol. 5.5 mg of 11-MUA was prepared in 10 mL absolute ethanol and 6-MCH was prepared about 10.58 mL in 9.99 mL absolute ethanol. Each solution was mixed together with ratio 1:1 until it was fully dissolved. After 24 hours, the modified SAM sensor was cleaned thoroughly using PBS.

3. N-(3-Dimethylaminopropyl)-N'-Ethylcarbodiimide (EDC) and N-Hydroxysulfosuccinimide (Sulfo-NHS) – Step (c)

N-(3-Dimethylaminopropyl)-N'-Ethylcarbodiimide (EDC) - Liquid

Desired final volume: 0.01 L

Desired final concentration: 2 mM

Molar mass: 155.24 g/mol

N-Hydroxysulfosuccinimide (Sulfo-NHS) - Powder

Desired final volume: 0.01 L

Desired final concentration: 5 mM

Molar mass: 217.13 g/mol

Aqueous solution containing 2 mM N-(3-Dimethylaminopropyl)-N'-Ethylcarbodiimide (EDC) and 5mM N-Hydroxysulfosuccinimide (Sulfo-NHS) immersed the modified SAM working electrode that was placed inside the fluidic chamber for 45 minutes at 4 °C. About 36.5 µL of EDC was prepared in 9.96 mL PBS and 10.86 mg of sulfo-NHS was prepared in PBS. Each solution was mixed together with a ratio 1:1 until it was ready. The modified SAM-EDC/Sulfo-NHS electrode was washed with PBS solution after incubation.

4. Anti-NS1 Antibody – Step (d)

Anti-NS1 antibody - Liquid

Desired final volume: 0.001 L

Desired final concentration: 1 µg/mL

1 µg/mL of anti-NS1 solution in PBS was incubated for 3 hours at 4 °C on the modified SAM-EDC/Sulfo-NHS working electrode surface placed inside the fluidic chamber. 0.1 mL of anti-NS1 antibody was diluted with 1 mL PBS solution at a ratio of 1:10 until fully mixed. The modified SAM-EDC/Sulfo-NHS-NS1Antibody electrode surface was cleaned using PBS solution after 3 hours.

5. Ethanolamine (ETA) – Step (e)

Ethanolamine (ETA) - Liquid

Desired final volume: 0.01 L

Desired final concentration: 1 M

Molar mass: 61.08 g/mol

Addition of 1 M ethanolamine (ETA) solution was modified for 1 hour at 4 °C on the modified SAM-EDC/Sulfo-NHS-NS1Antibody working electrode that was placed inside the fluidic chamber. About 0.62 mL of ETA was mixed in a 9.38 mL PBS solution until it was ready for use. The modified SAM-EDC/Sulfo-NHS-NS1Antibody-ETA surface was thoroughly rinsed with PBS after 1 hour of incubation.

6. Glycine solution – Step (f)

Glycine – Powder

Desired final volume: 0.1 L

Desired final concentration: 5 mM

Molar mass: 75.07 g/mol

The modified SAM-EDC/Sulfo-NHS-NS1Antibody-ETA electrode placed inside the fluidic chamber were immersed in 5 mM of glycine solution in PBS for 30 minutes at 4 °C. Glycine powder about 37.5 mg was dissolved in PBS solution and mixed thoroughly. PBS solution was used to clean the excess glycine on the modified SAM-EDC/Sulfo-NHS-NS1Antibody-ETA-Glycine surface.

7. NS1 Antigen – Step (g)

NS1 Antigen – Liquid

Desired final volume: 0.01 L

Desired final concentration: 10, 50, 100, 500, 1000 and 2000 ng/mL

Different NS1 antigen concentrations of 10, 50, 100, 500, 1000 and 2000 ng/mL were incubated on the modified SAM-EDC/Sulfo-NHS-NS1Antibody-ETA-Glycine electrode placed inside the fluidic chamber at 4 °C for 1 hour. 20 µL of NS1 antigen was diluted in 9.98 mL PBS solution and further dilution was done for 1000, 500, 100, 50, 10 ng/mL concentrations.